ELECTROMAGNETIC DESIGN AND SPACE MAPPING

John W. Bandler

P.O. Box 8083, Dundas, Ontario, Canada L9H 5E7
john@bandler.com www.bandler.com

Presented to Philips Components B.V., Roermond, The Netherlands
September 2-3, 1998

ELECTROMAGNETIC DESIGN AND SPACE MAPPING

John W. Bandler

BC-98-7-V

September 1998

ELECTROMAGNETIC DESIGN AND SPACE MAPPING

John W. Bandler

P.O. Box 8083, Dundas, Ontario, Canada L9H 5E7
john@bandler.com www.bandler.com

Presented to Philips Components B.V., Roermond, The Netherlands
September 2-3, 1998

Critical Issues of Automated EM Optimization

interfaces between gradient-based optimizers and discretized EM field solvers: interpolation and database

integration of EM analysis with circuit simulation, including harmonic balance simulation of nonlinear circuits

Geometry Capture™: user-defined optimizable structures of arbitrary geometry

Space Mapping™ optimization: intelligent correlation between engineering models: EM models, empirical models and equivalent circuit models

smoothness and continuity of response interpolation

robustness of optimization algorithms and uniqueness of the solutions

parallel and massively parallel EM analyses

Interface Between Optimizer and EM Solver
(*Bandler et al., 1993*)

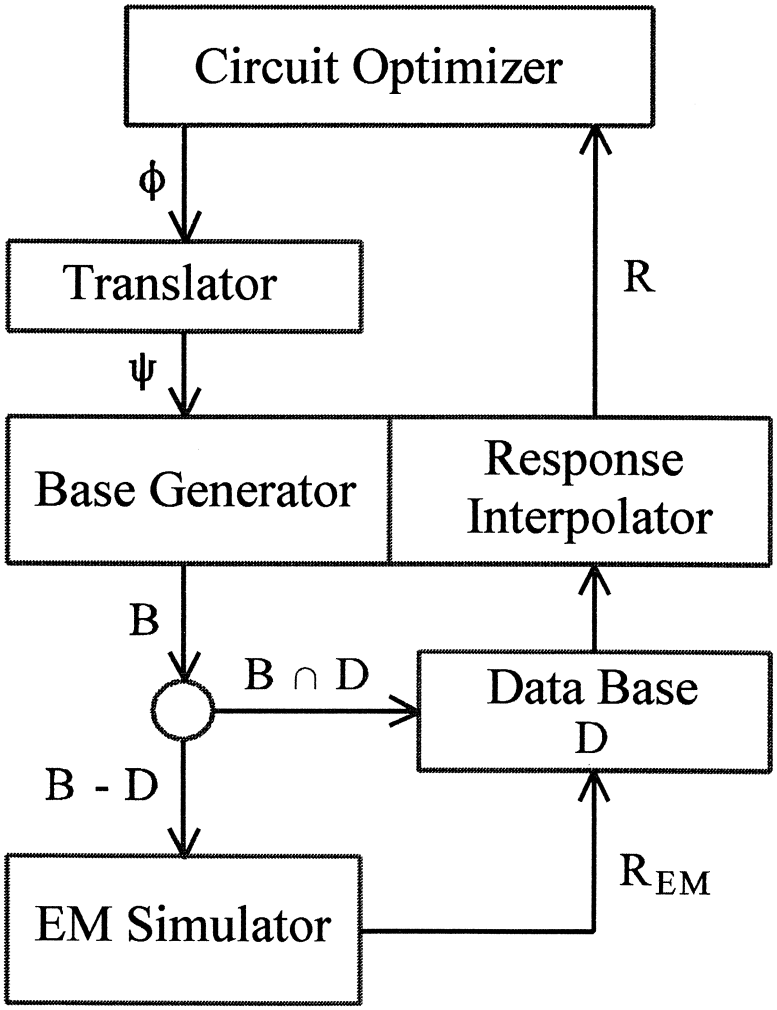

EM Optimization Environment

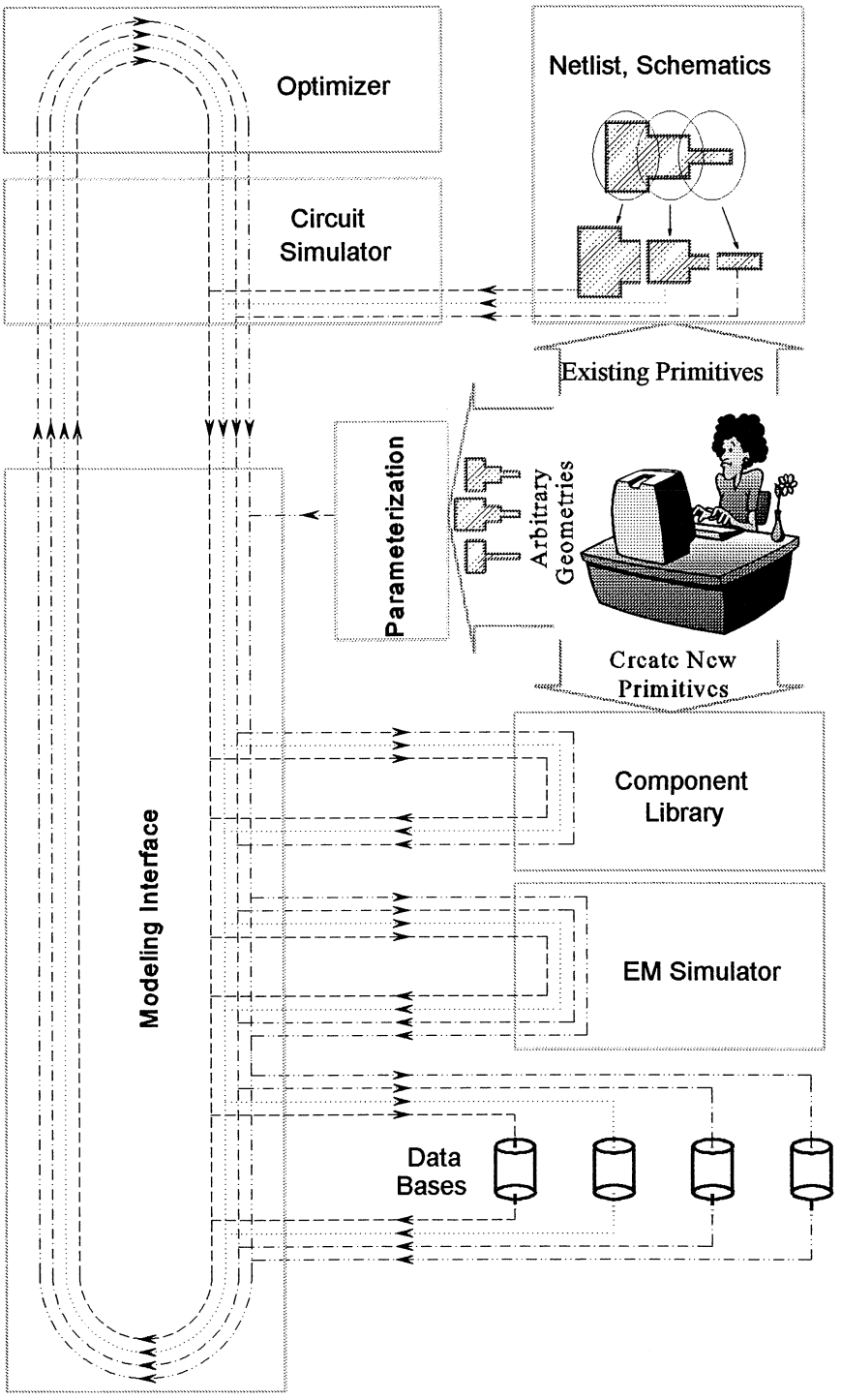

Simulation of Static Structures via Empipe™
(*OSA, 1992*)

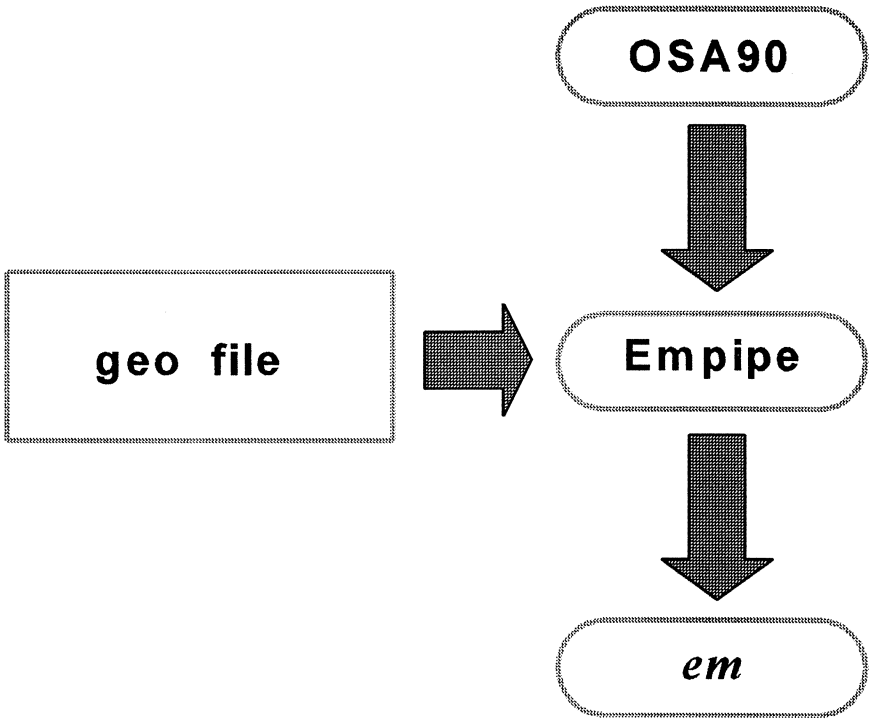

useful for analyzing circuits of mixed EM and empirical models

unsuitable for EM optimization

Empipe™ Optimizable Library Structures (*OSA, 1992*)

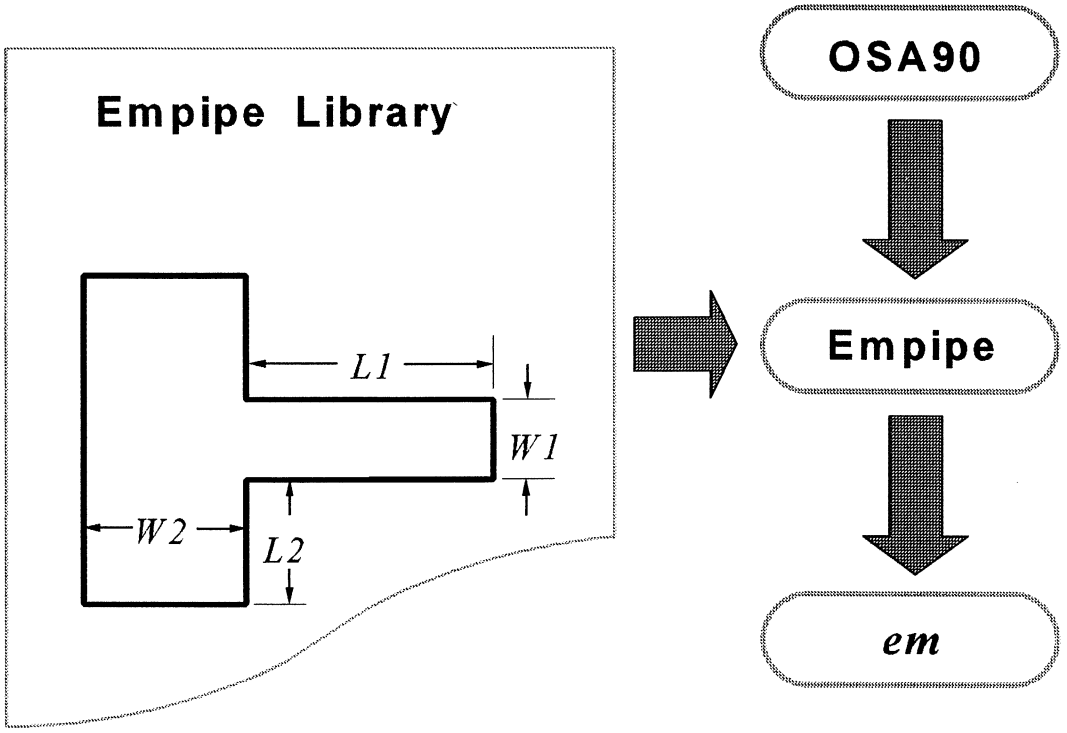

preprogrammed, ready to use

limited selection

complex structure decomposed into elementary structures connected by circuit theory, neglecting couplings between the elements

Empipe™ Library of Microstrip Structures

bend
cross junction
double patch capacitors
interdigital capacitors
line
mitered bend
open stub
overlay double patch capacitors
rectangular structure
spiral inductors
step junction
symmetrical and asymmetrical folded double stubs
symmetrical and asymmetrical gaps
symmetrical and asymmetrical double stubs
T junction

Geometry Capture™
(*OSA, 1994*)

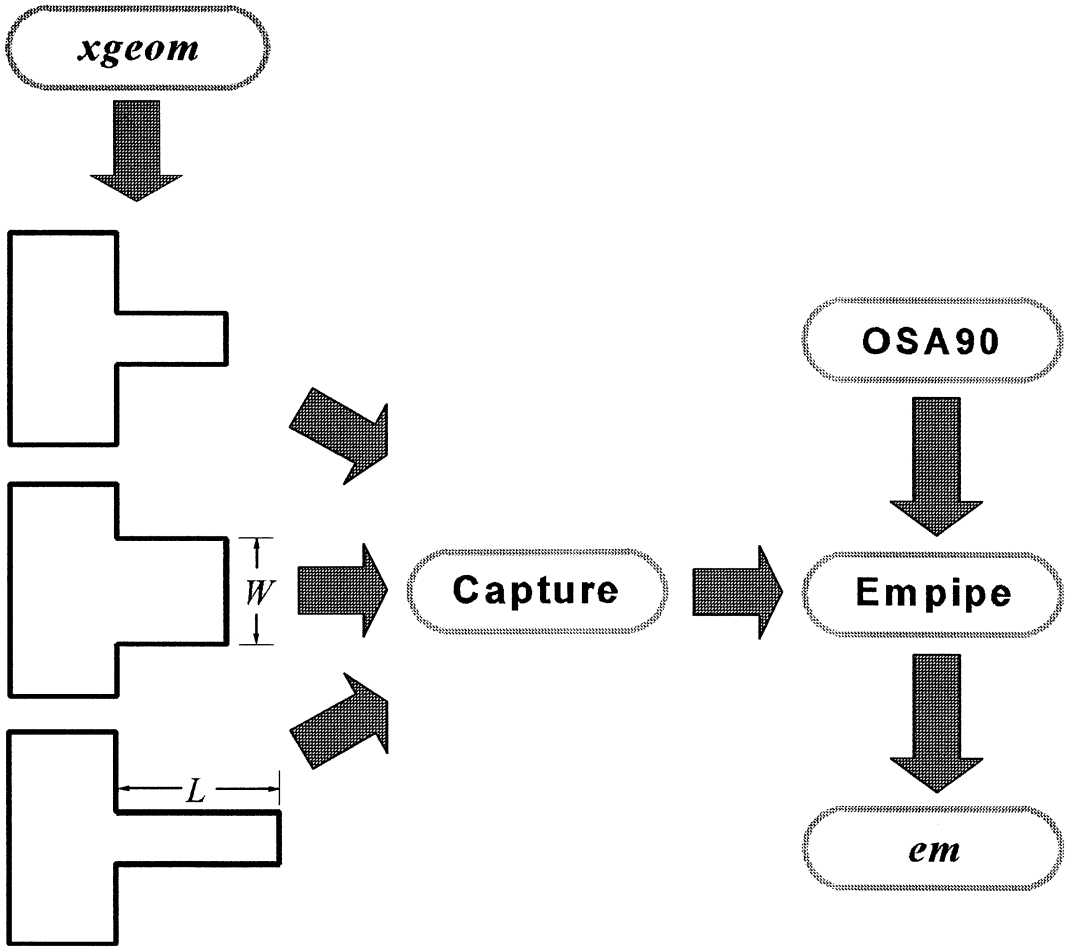

intuitive and totally flexible

graphical description of parameters and constraints

optimization not limited to geometrical dimensions but can also include substrate/metallization parameters

Microstrip Double Folded Stub Filter
(*Rautio, 1992*)

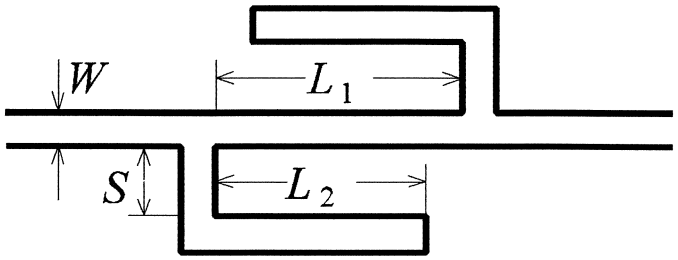

em™ driven by OSA90/hope™ through Empipe™

minimax optimization to move the center frequency of the stop band from 15 GHz to 13 GHz

W fixed at 4.8 mils

L_1, L_2 and S are variables

substrate thickness: 5 mils

relative dielectric constant: 9.9

design specifications

$|S_{21}| > -3$ dB for $f < 9.5$ GHz and $f > 16.5$ GHz

$|S_{21}| < -30$ dB for 12 GHz $< f <$ 14 GHz

EM Simulation of the Double Folded Stub Filter

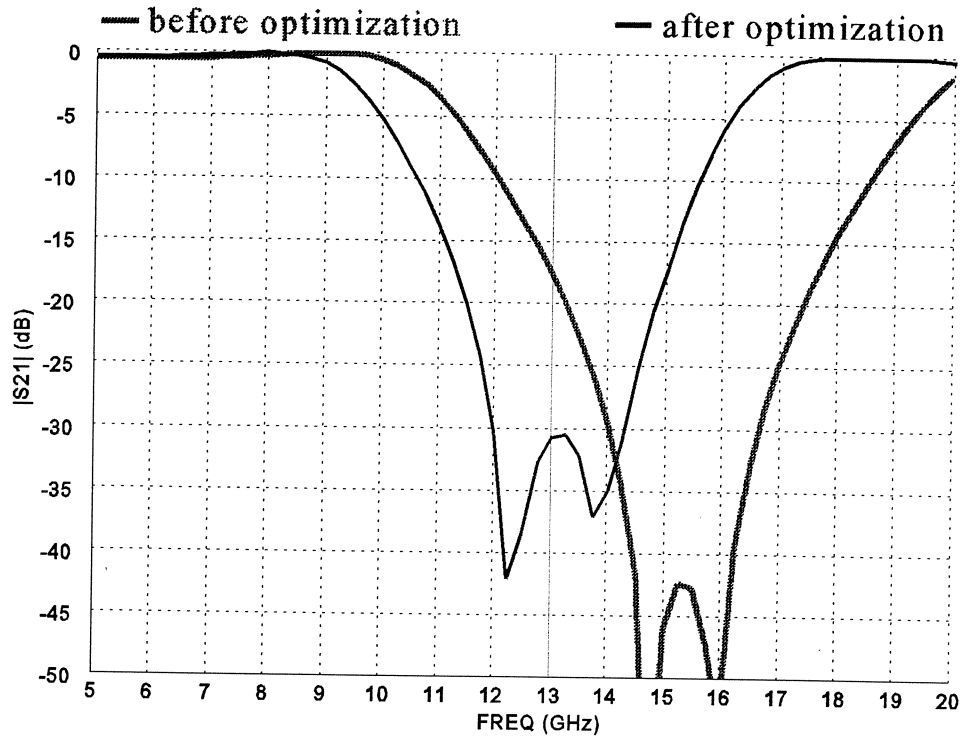

26-40 GHz Interdigital Bandpass Filter
(*Swanson, 1992*)

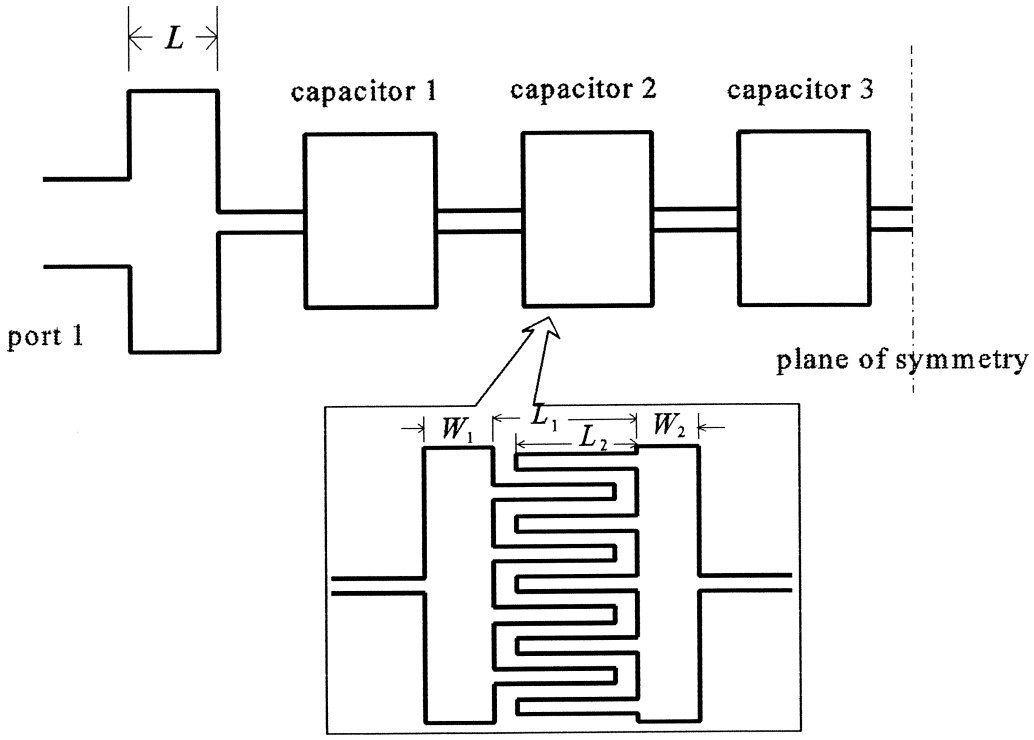

the initial design was obtained by matching a synthesized lumped ladder prototype at the center frequency using ***em***™

when the filter was simulated by ***em***™ in the whole frequency range, significant discrepancies w.r.t. the prototype necessitated manual adjustment and made a satisfactory design very difficult to achieve

EM Optimization of the Interdigital Bandpass Filter

a total of 13 designable parameters including the distance between the patches L_1, the finger length L_2 and two patch widths W_1 and W_2 for each of the three interdigital capacitors, and the length L of the end capacitor

the second half of the circuit, to the right of the plane of symmetry, is assumed identical to the first half, so it contains no additional variables

the transmission lines between the capacitors were fixed at the originally designed values

design specifications

$|S_{11}| < -20$ dB and $|S_{21}| > -0.04$ dB

for 26 GHz $< f <$ 40 GHz

substrate thickness: 10 mils

dielectric constant: 2.25

Simulation of the Interdigital Bandpass Filter After Optimization

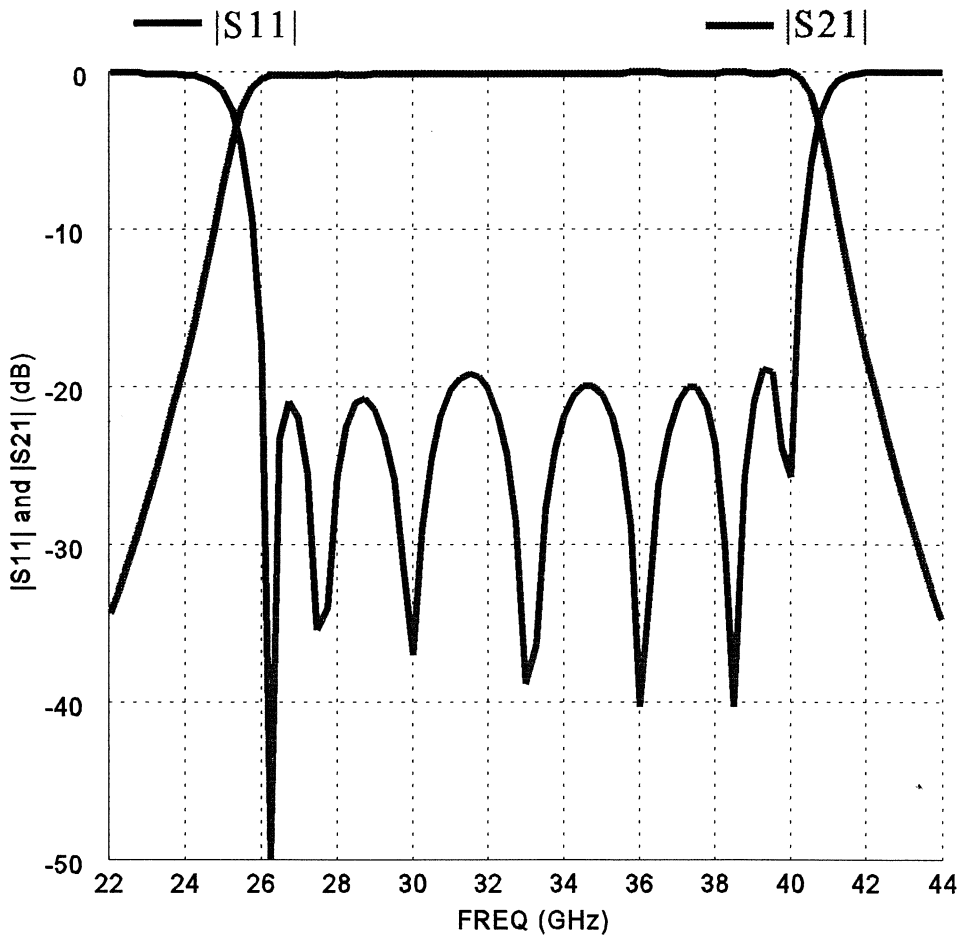

a typical minimax equal-ripple response of the filter was achieved after a series of consecutive optimizations with different subsets of optimization variables and frequency points

the resulting geometrical dimensions were rounded to 0.1 mil resolution

Nonlinear FET Class B Frequency Doubler
(*Microwave Engineering Europe, 1994*)

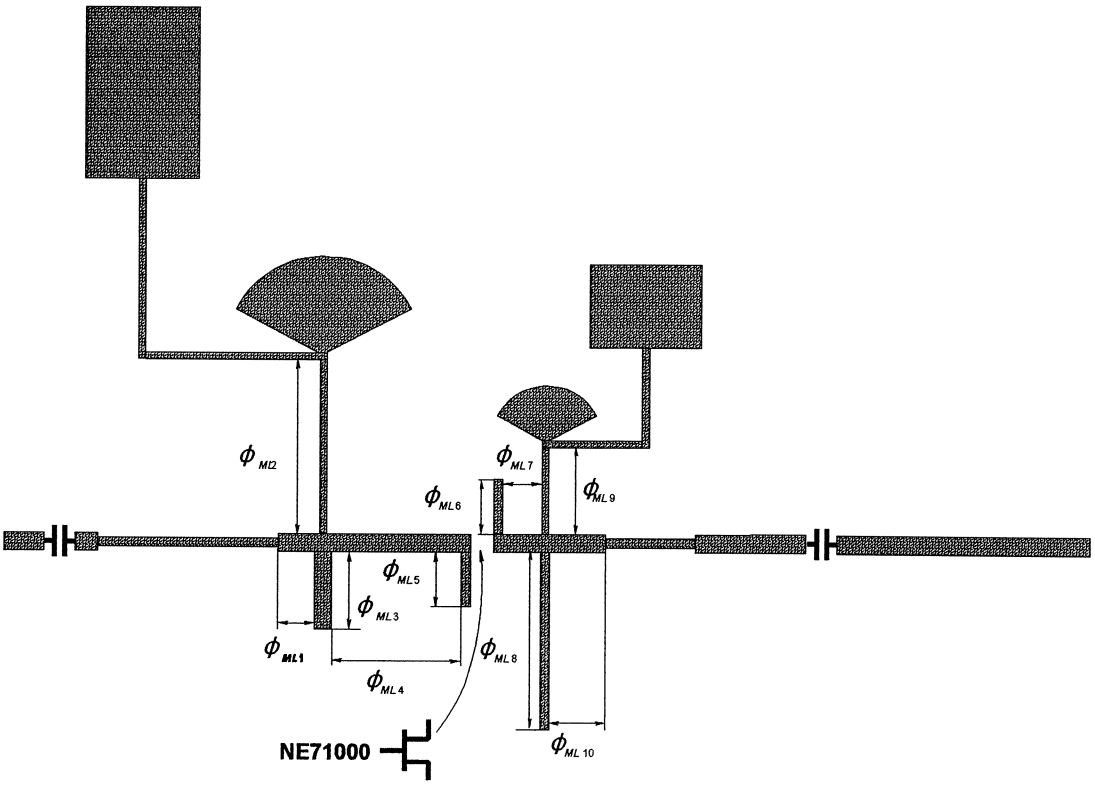

using Geometry Capture™, the linear subcircuit is defined as one optimizable structure with 10 variables

design specifications

conversion gain > 3 dB

spectral purity > 20 dB

at 7 GHz and 10 dBm input power

Conversion Gain Before and After Optimization

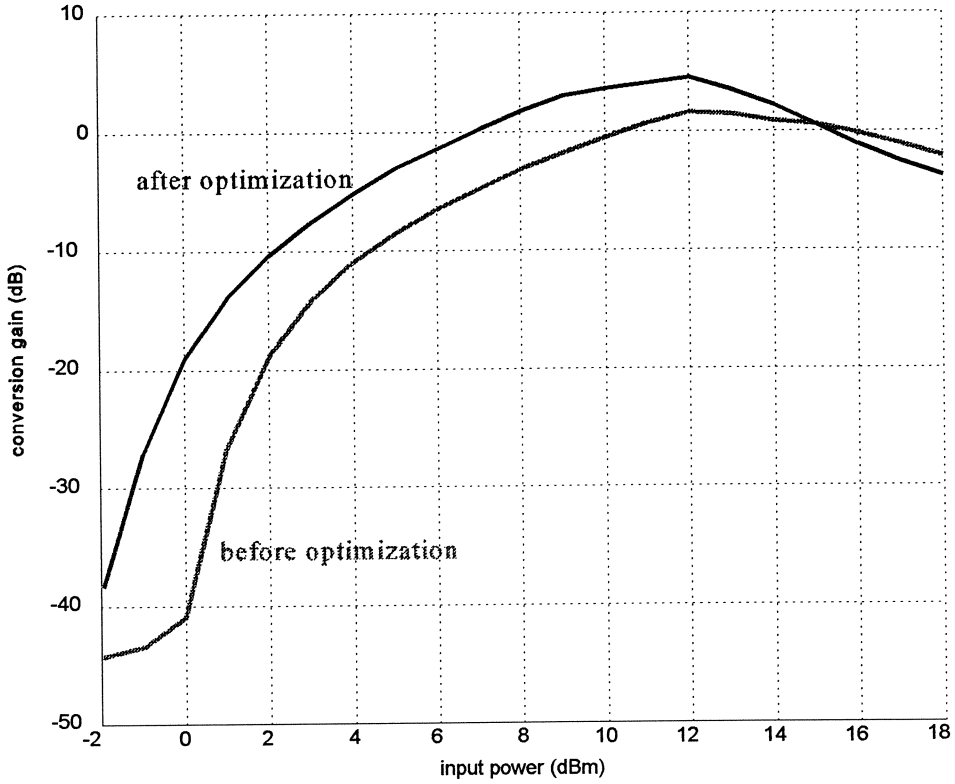

Conversion Gain Before and After Optimization

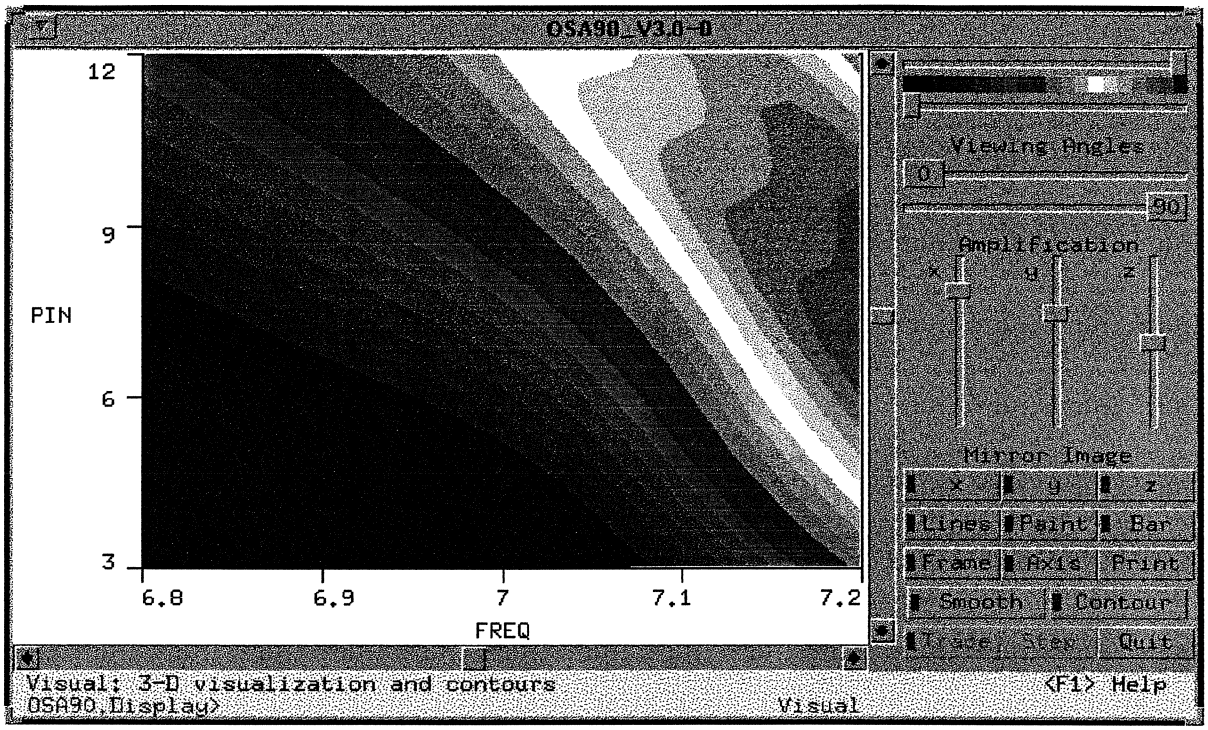

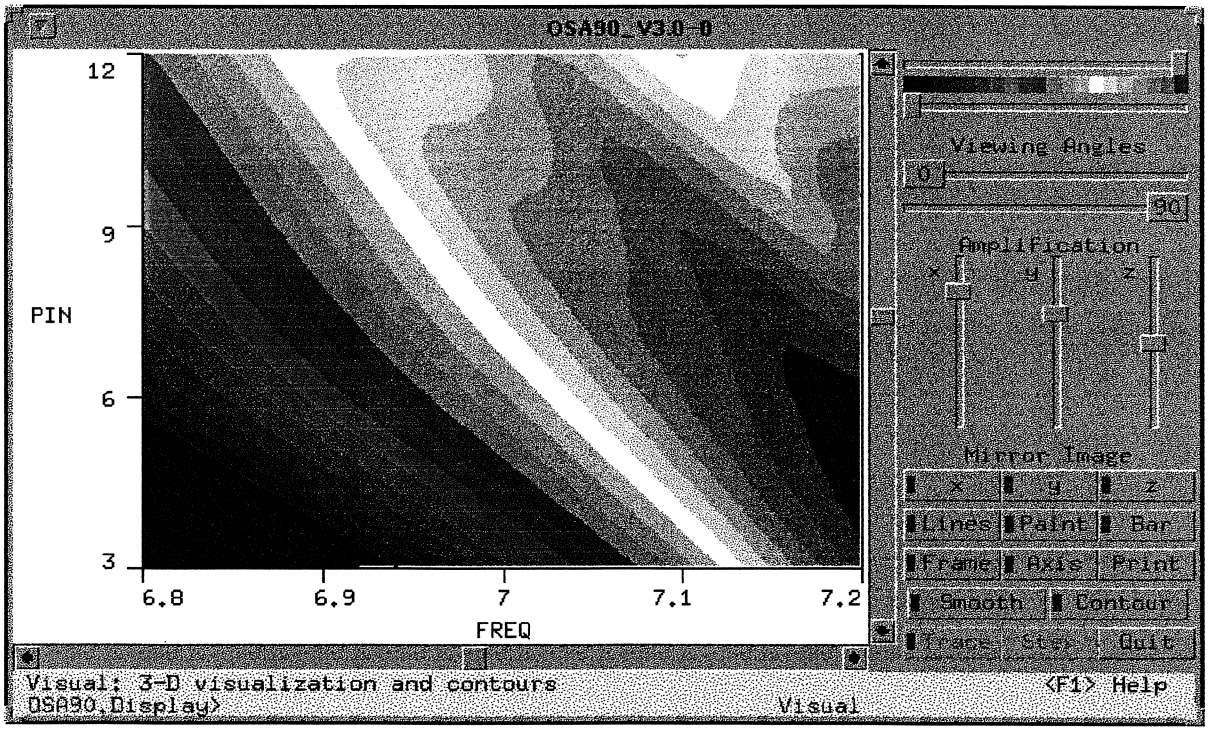

Spectral Purity Before and After Optimization

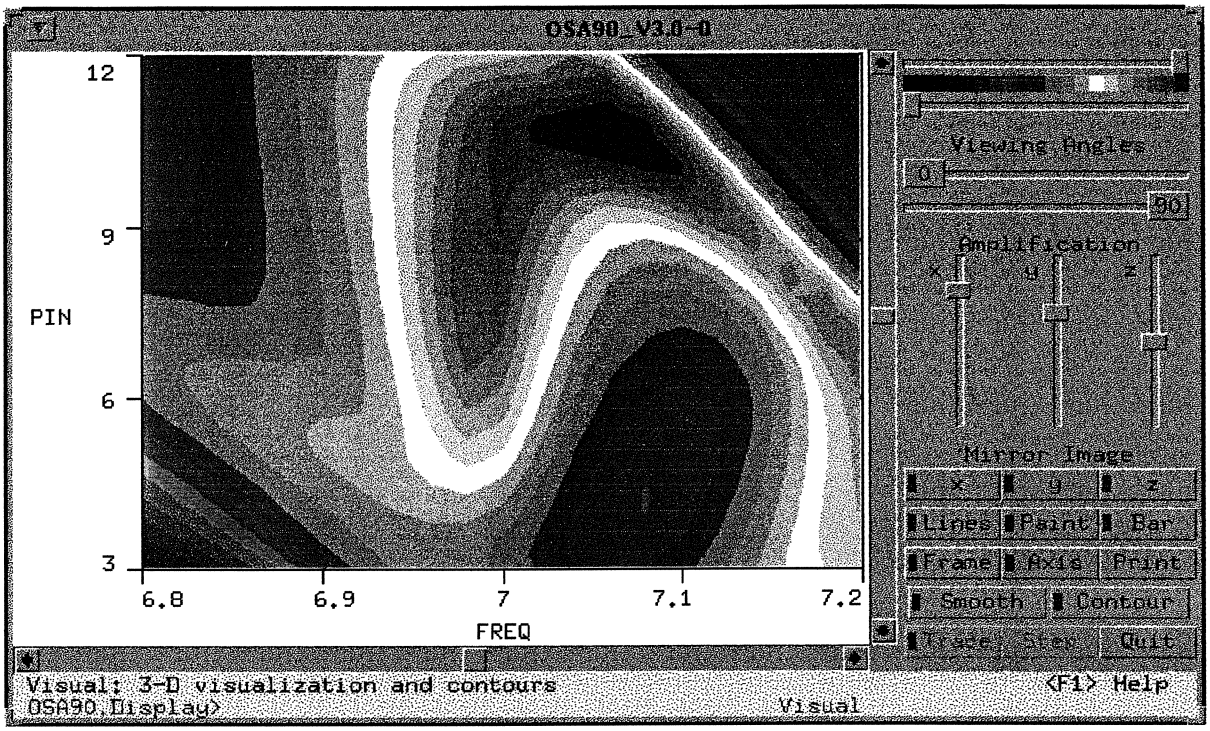

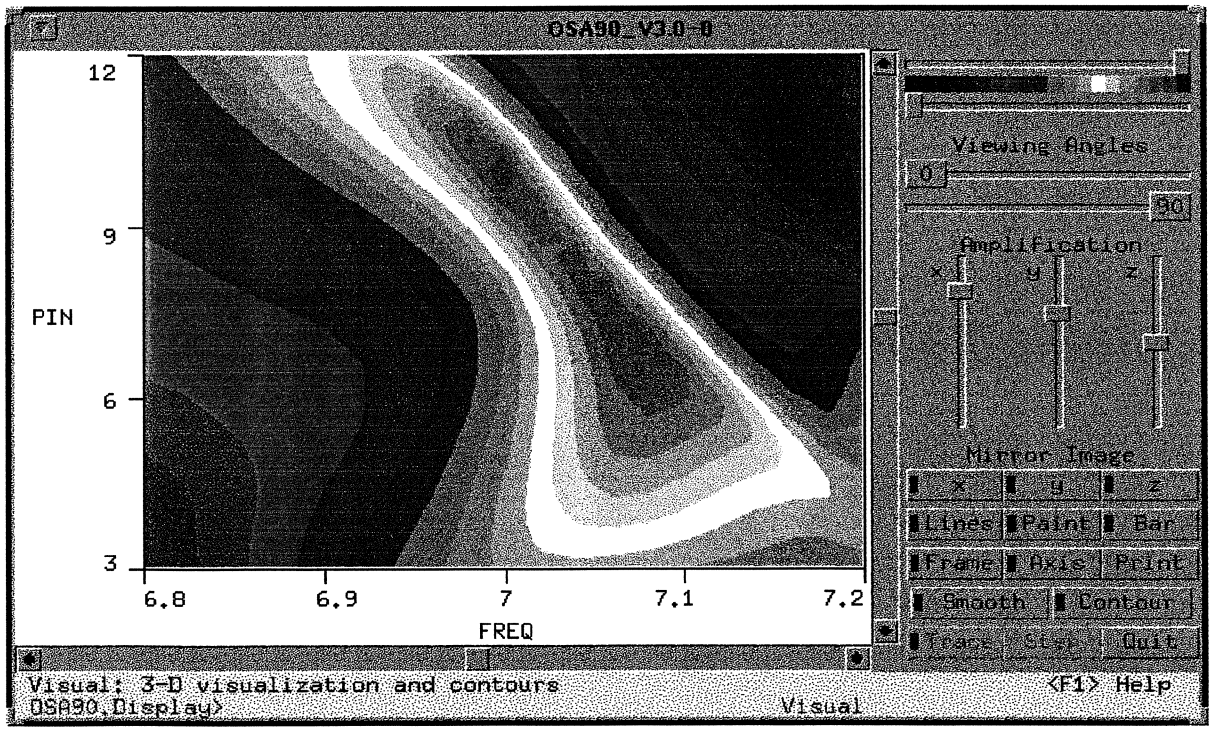

The HTS Quarter-Wave Parallel Coupled-Line Filter (*Westinghouse, 1993*)

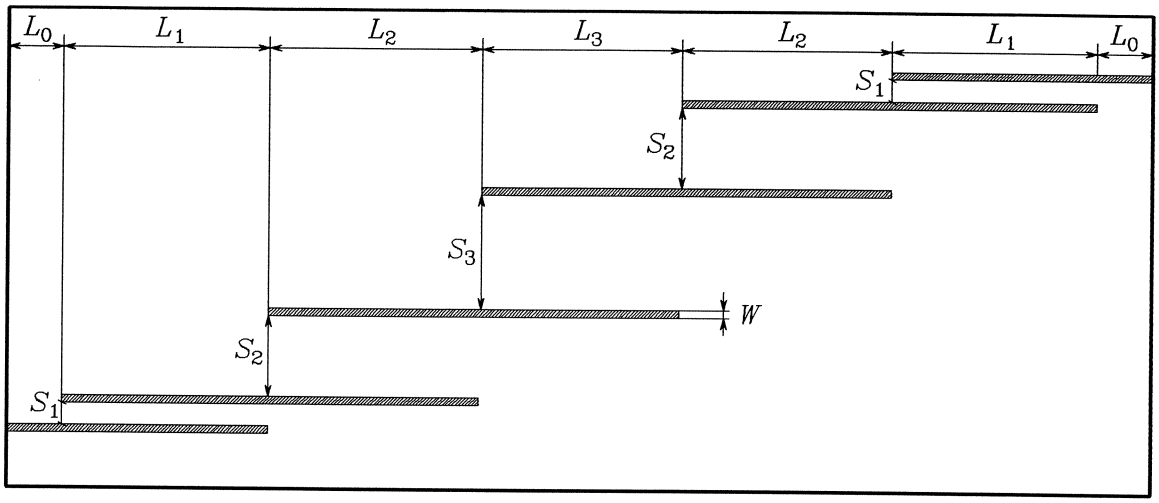

20 mil thick lanthanum aluminate substrate

the dielectric constant is 23.4

the x and y grid sizes for ***em*** simulation are 1.0 and 1.75 mil

100 elapsed minutes are needed for ***em*** analysis at a single frequency on a Sun SPARCstation 10

design specifications

$|S_{21}| < 0.05$ for $f < 3.967$ GHz and $f > 4.099$ GHz

$|S_{21}| > 0.95$ for 4.008 GHz $< f <$ 4.058 GHz

Starting Point of EM Optimization: Design Using Empirical Circuit Model

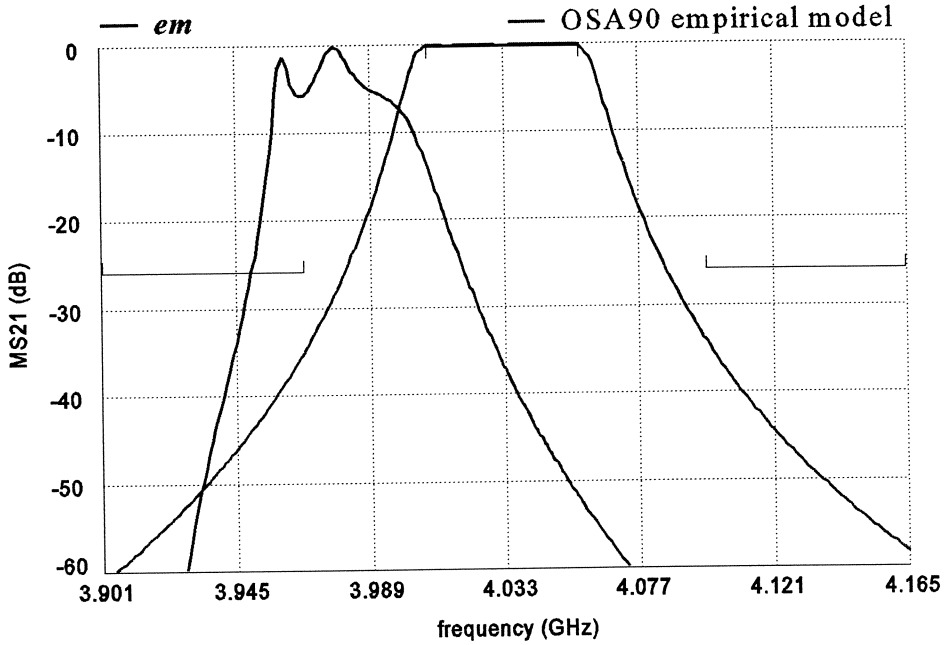

Solution by Aggressive Space Mapping: 4 Iterations Only

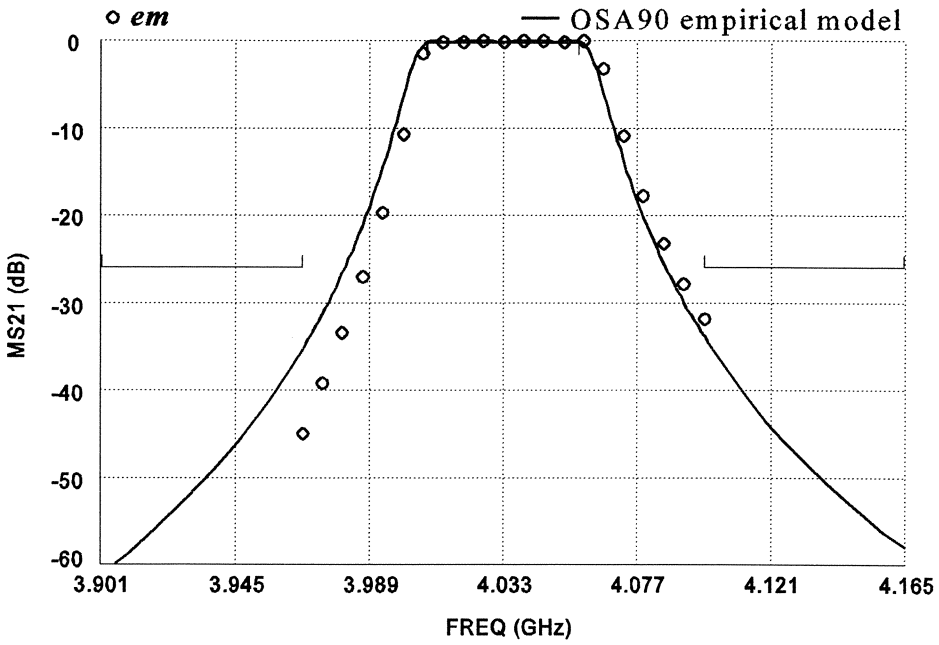

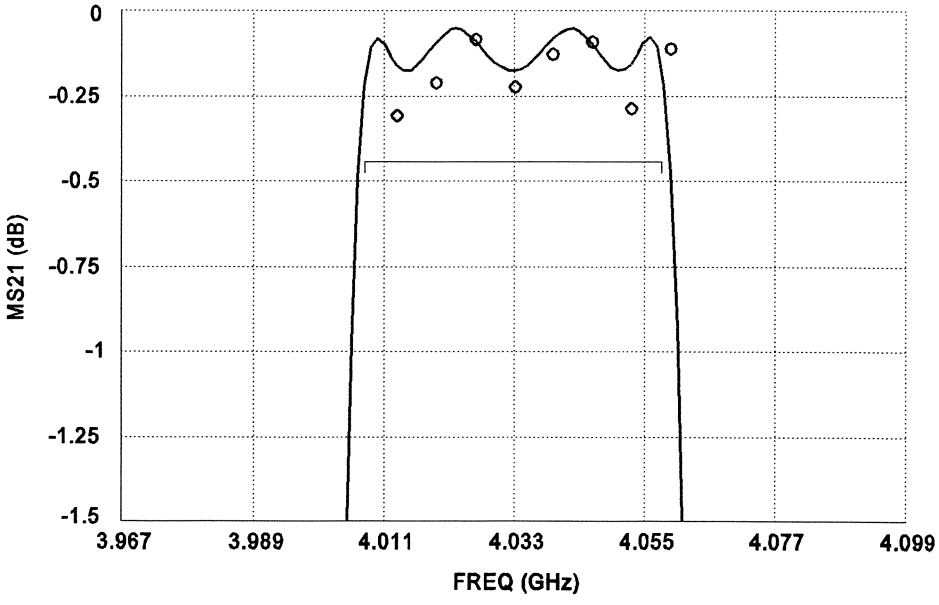

Solution Uniqueness Tested by Random Starting Points

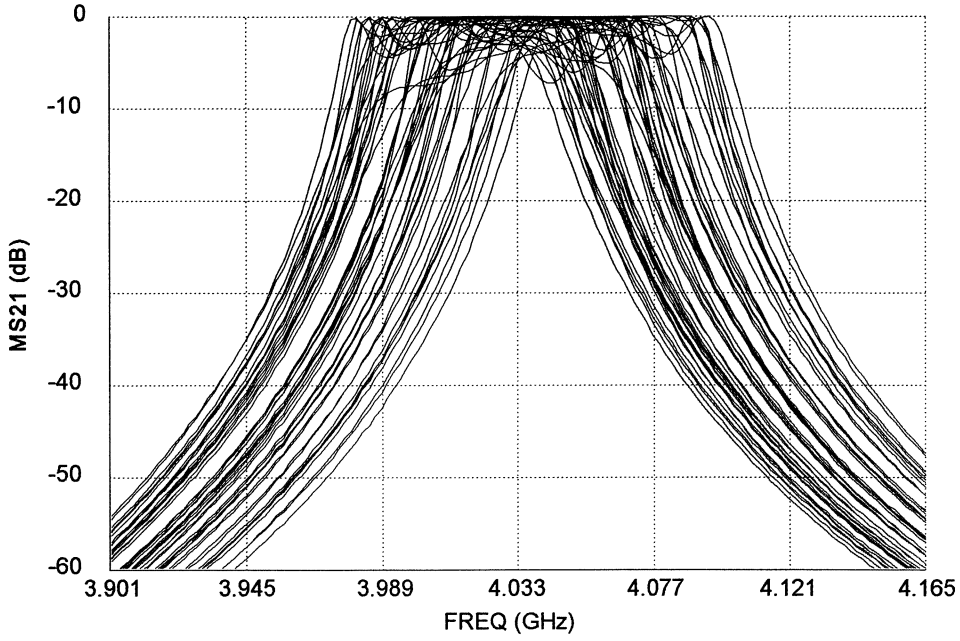

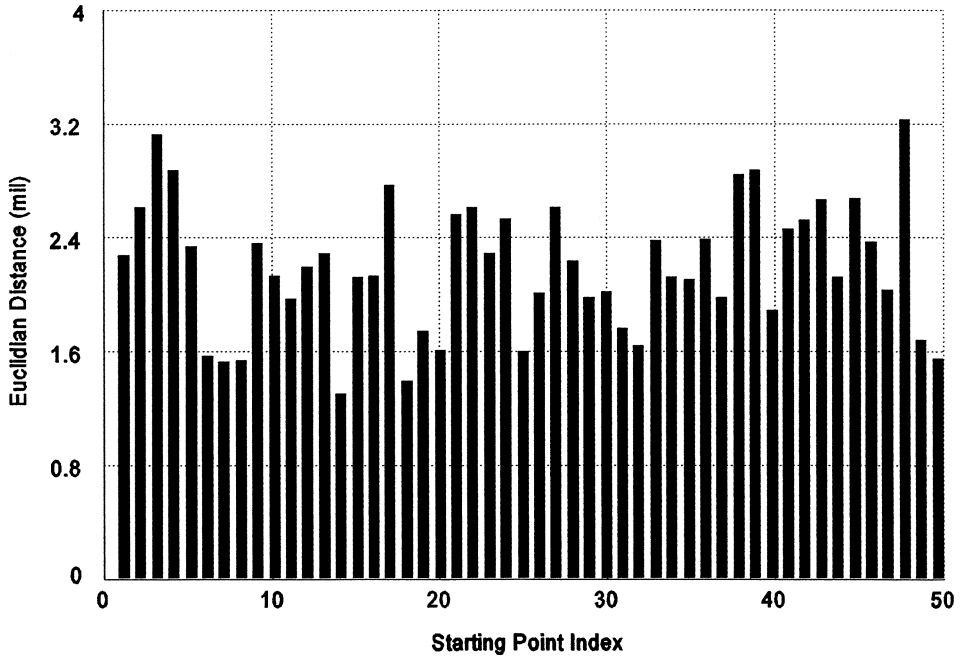

Solutions from the Random Starting Points

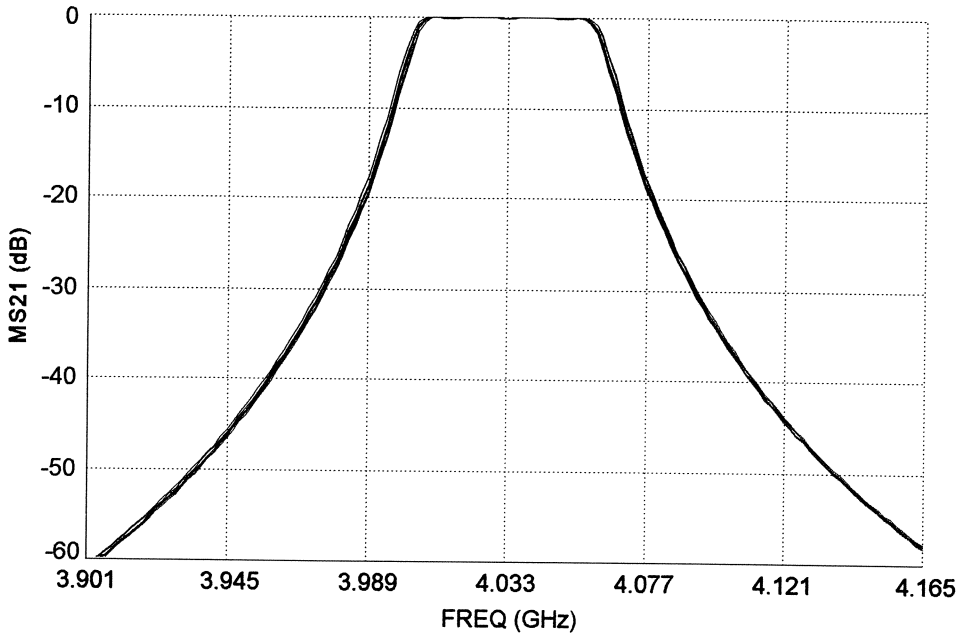

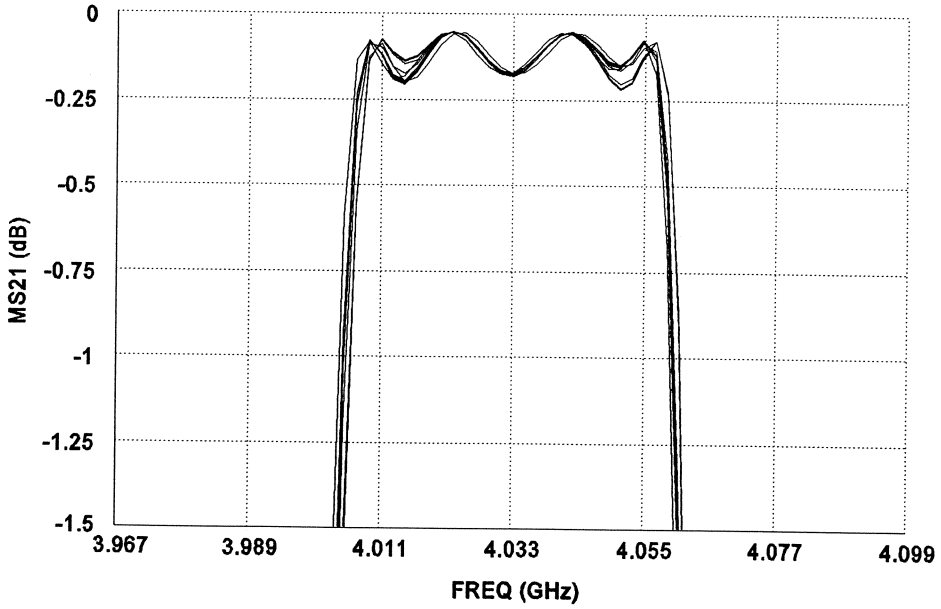

Two Distinct Solutions with Similar Responses

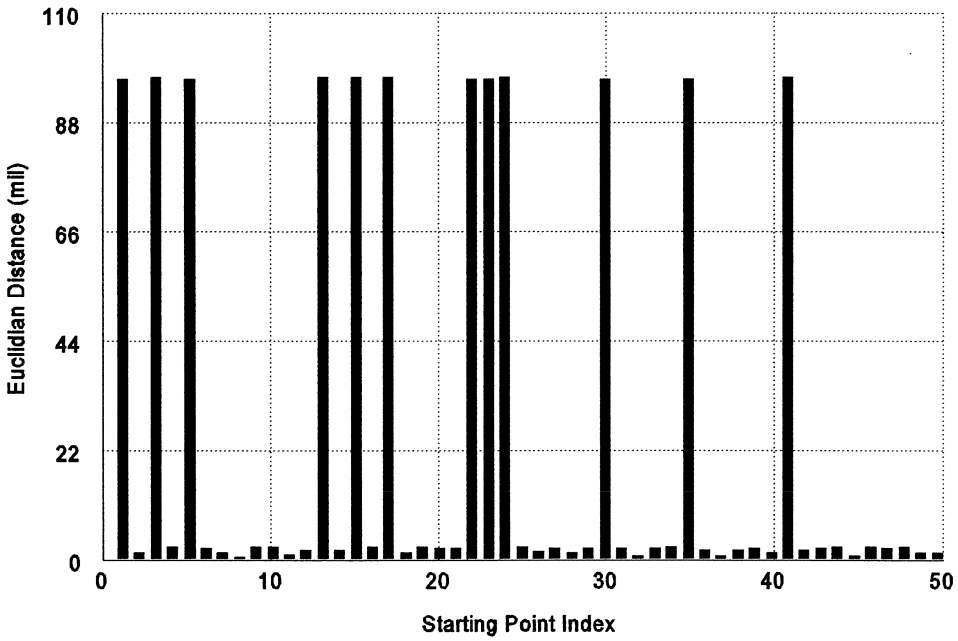

Truncation to the Nearest On-Grid Point

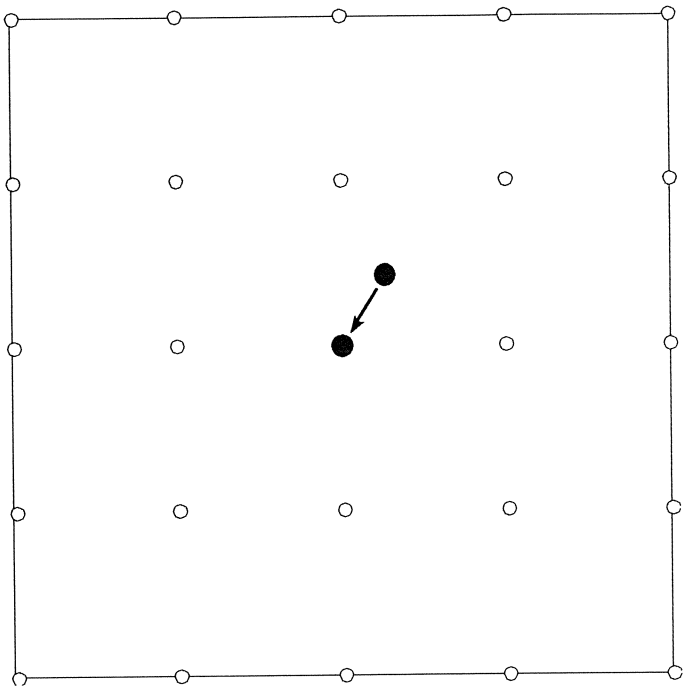

Linear Interpolation

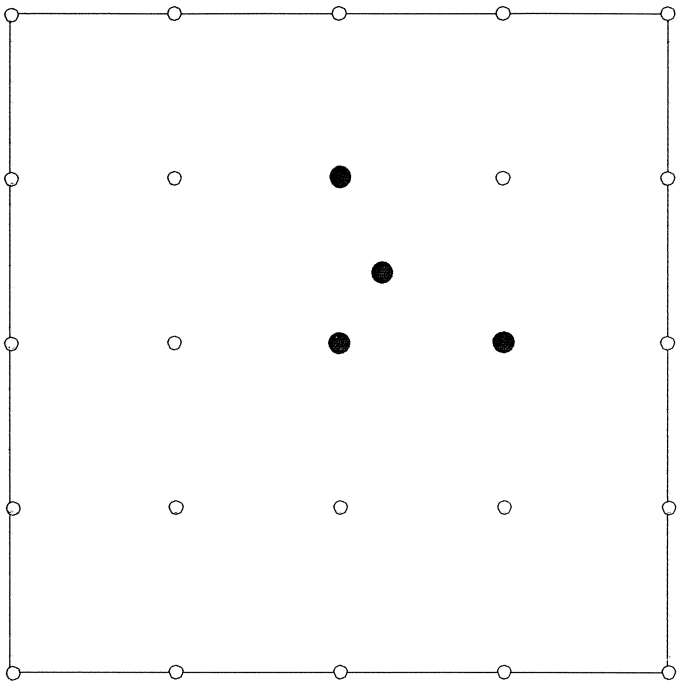

Quadratic Interpolation

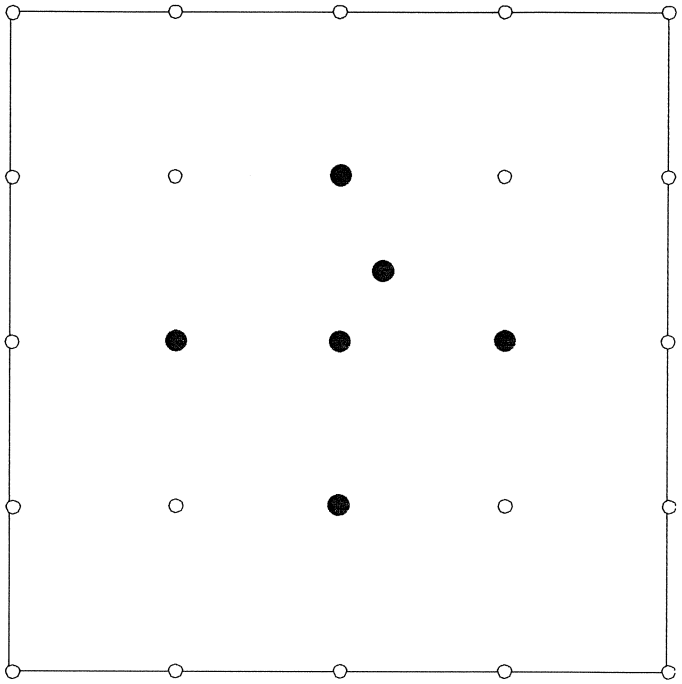

Potential Pitfalls Associated with Interpolation

interpolation may lead to distorted results especially for structures with resonance(s)

double stub test circuit

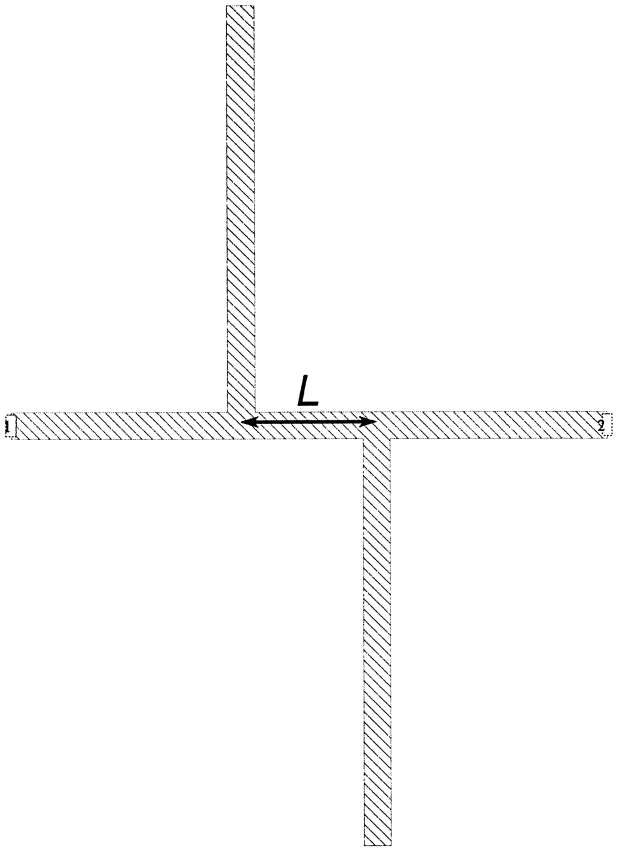

interpolate the parameter L between 30 mils and 35 mils (the grid size is 5 mils).

Linear Interpolation Based on *S* parameters

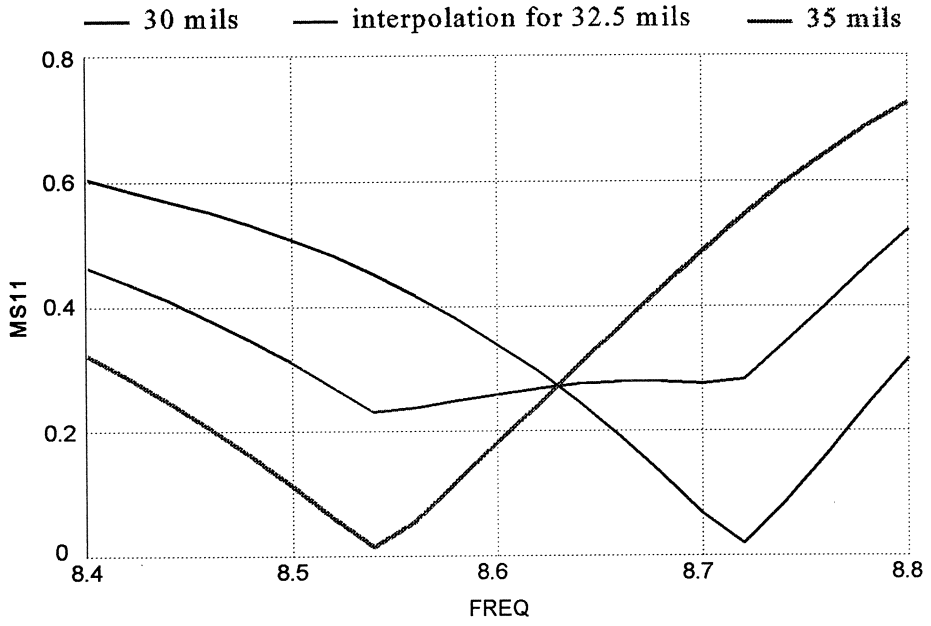

Linear Interpolation Based on *Y* Parameters

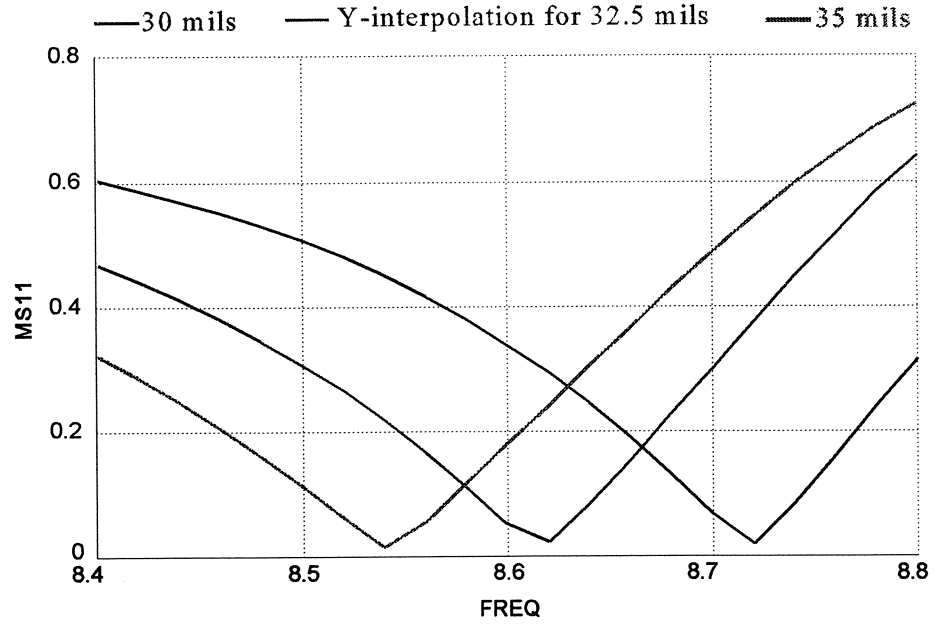

Y-Parameter-Interpolation May Also Have Problems

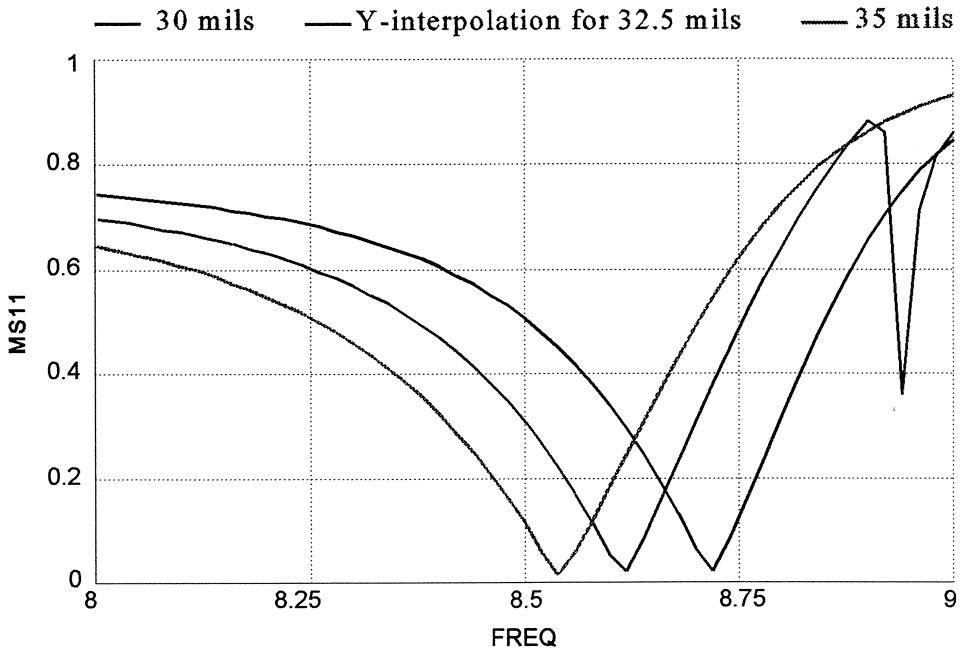

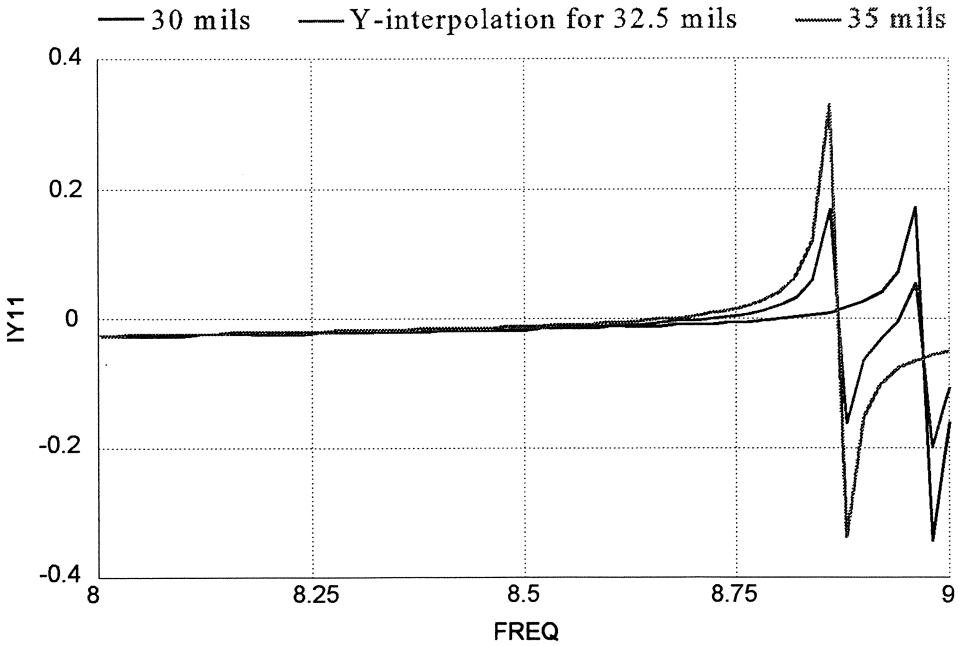

Empirical Circuit Model for Space Mapping

structure

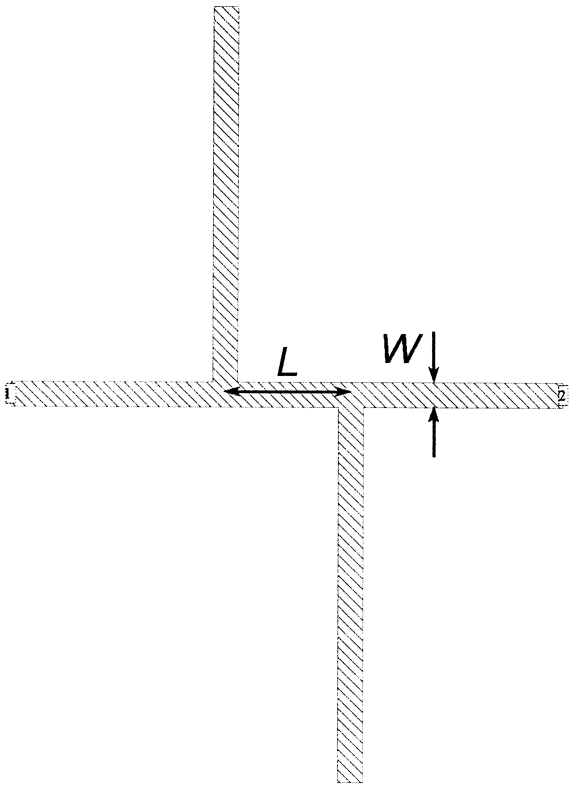

empirical circuit model

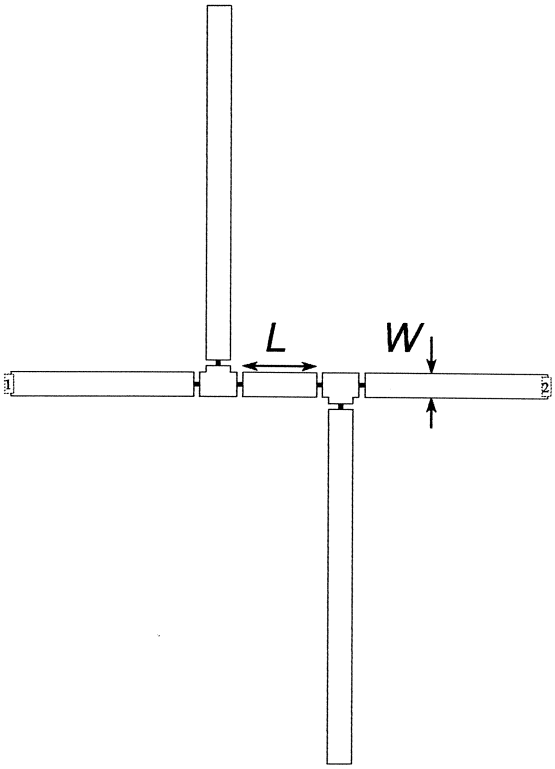

Parameter Extraction for Two On-Grid Points

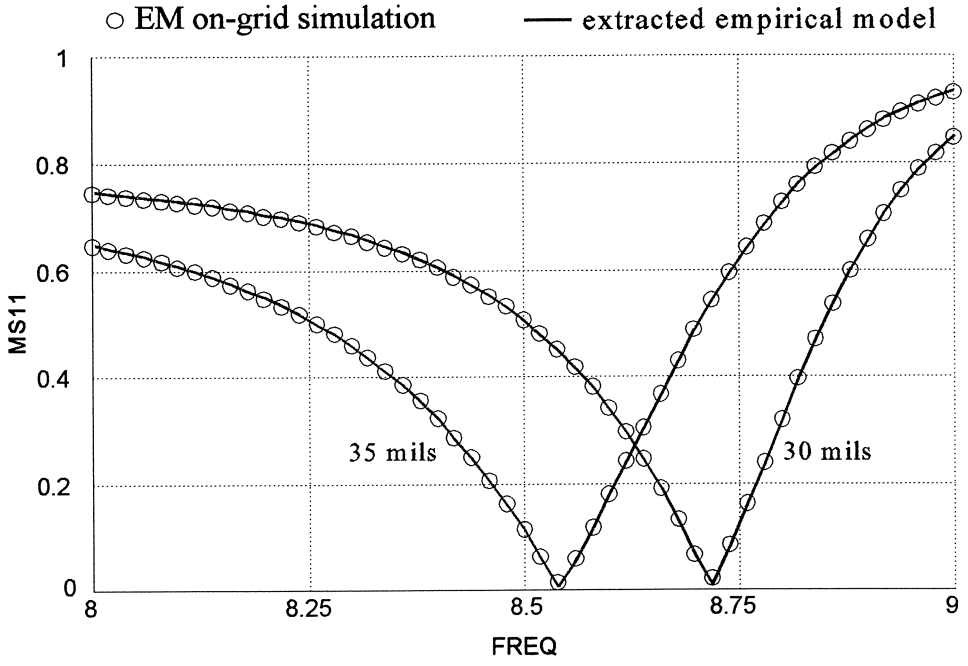

EM Parameters	
W	*L*
5 mils	30 mils
5 mils	35 mils

Empirical Model Parameters	
W	*L*
4.67 mils	32.1 mils
4.62 mils	37.2 mils

Space Mapping for Response Interpolation

$$\boldsymbol{x}_{em} \triangleq [\, L_{em} \,]$$

$$\boldsymbol{x}_{os} \triangleq [\, W_{os} \quad L_{os} \,]^T$$

W_{em} is considered a constant since the interpolation is with respect to L_{em}

Space Mapping: $\boldsymbol{x}_{os} = \boldsymbol{P}(\boldsymbol{x}_{em})$

parameter extraction: $\boldsymbol{R}_{os}(\boldsymbol{x}_{os}) \approx \boldsymbol{R}_{em}(\boldsymbol{x}_{em})$

base points: L_{em} = 30 mils and 35 mils

interpolation: $\boldsymbol{x}_{os}^{i} = \boldsymbol{P}(L_{em} = 32.5 mils)$

interpolated response: $\boldsymbol{R}_{os}(\boldsymbol{x}_{os}^{i})$

Space Mapping for Response Interpolation

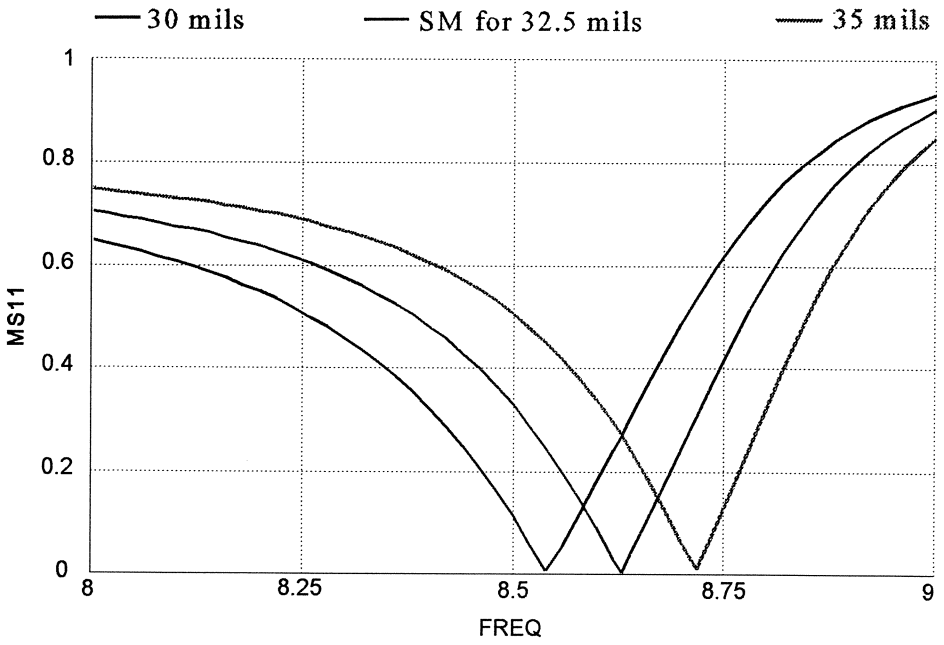

Increasing Sophistication of Design Methodology with Tolerances

DCTT: Design Centering, Tolerancing and Tuning using mathematical optimization (*1970s*)

deterministic (*Bandler et al., 1976*)

- performance-driven design
- fixed tolerance worst-case design
- variable tolerance worst-case design
- full DCTT

statistical (*see Bandler and Chen, 1988*)

- fixed tolerance yield-driven design
- correlated tolerances
- variable tolerance cost-driven design

CAD goal: first-pass success design, however...

role of tuning: tunable designs may be considered in which tunable variables are assigned possible ranges at the design stage; followed by postproduction testing and tuning

Yield Interpretation in the Parameter Space

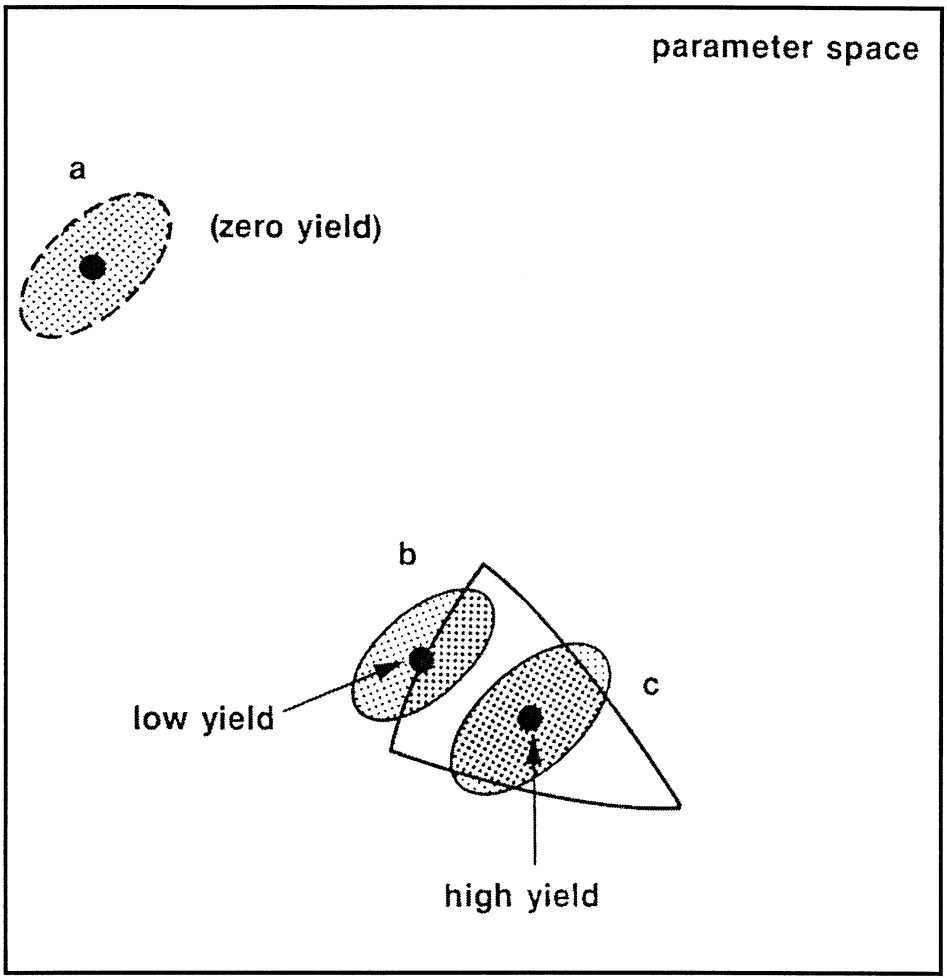

10 dB Distributed Attenuator Design

(*Bandler et al., 1995*)

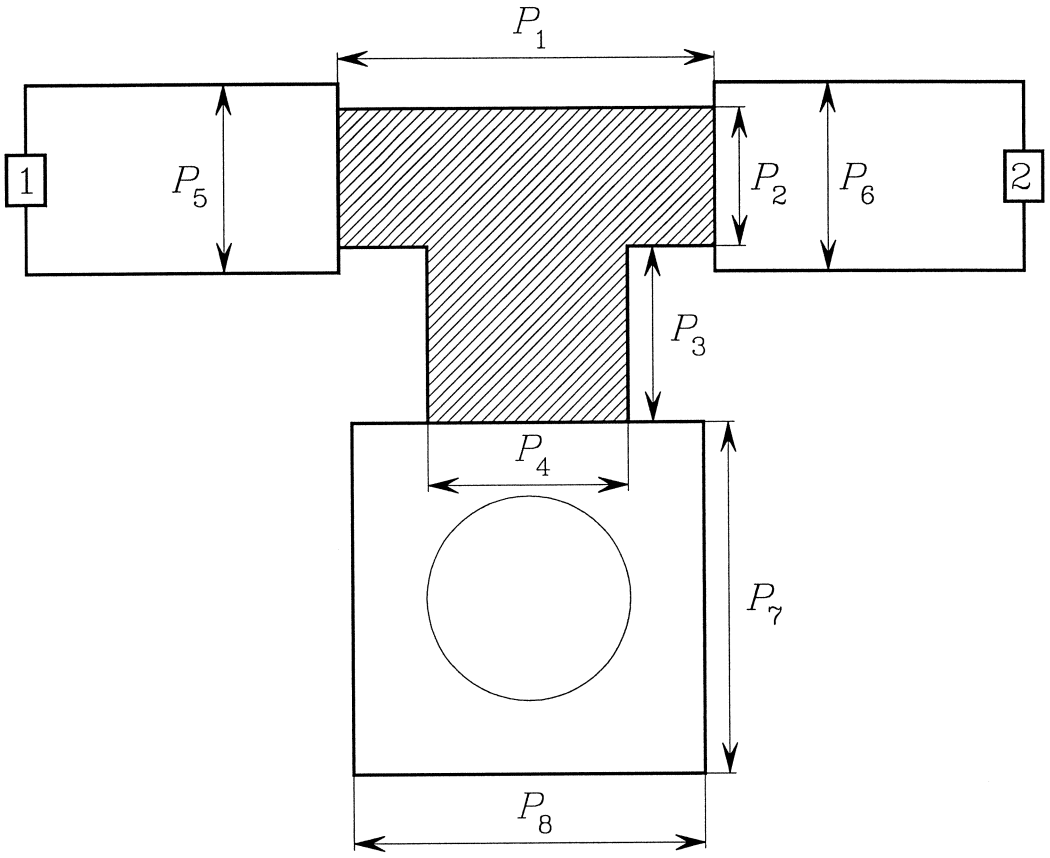

built on a 15 mil thick substrate with relative dielectric constant of 9.8

metallization of a high resistivity (50 Ω/sq)

the feed lines and the grounding pad are assumed lossless

Statistical Design of the Attenuator

design specifications (from 2 GHz to 18 GHz)

$$9.5\ \text{dB} \le \text{insertion loss} \le 10.5\ \text{dB}$$
$$\text{return loss} \ge 10\ \text{dB}$$

the structure, treated as a whole, has 8 geometrical parameters

designable: 4 parameters describing the resistive area

statistical: 8 parameters (with a standard deviation of 0.25 mil)

em simulation at a single frequency requires about 7 CPU minutes on a Sun SPARCstation 1+

Distributed (Parallel) Computing

nominal design: 30 ***em*** analyses with an average of 3.8 analyses run in parallel

about 168 minutes on the network of Sun SPARCstations 1+

time is reduced by 75%

statistical design: additional 113 ***em*** analyses with an average of 2.5 analyses run in parallel

time is reduced by 60%

Monte Carlo Sweeps of the Attenuator Responses

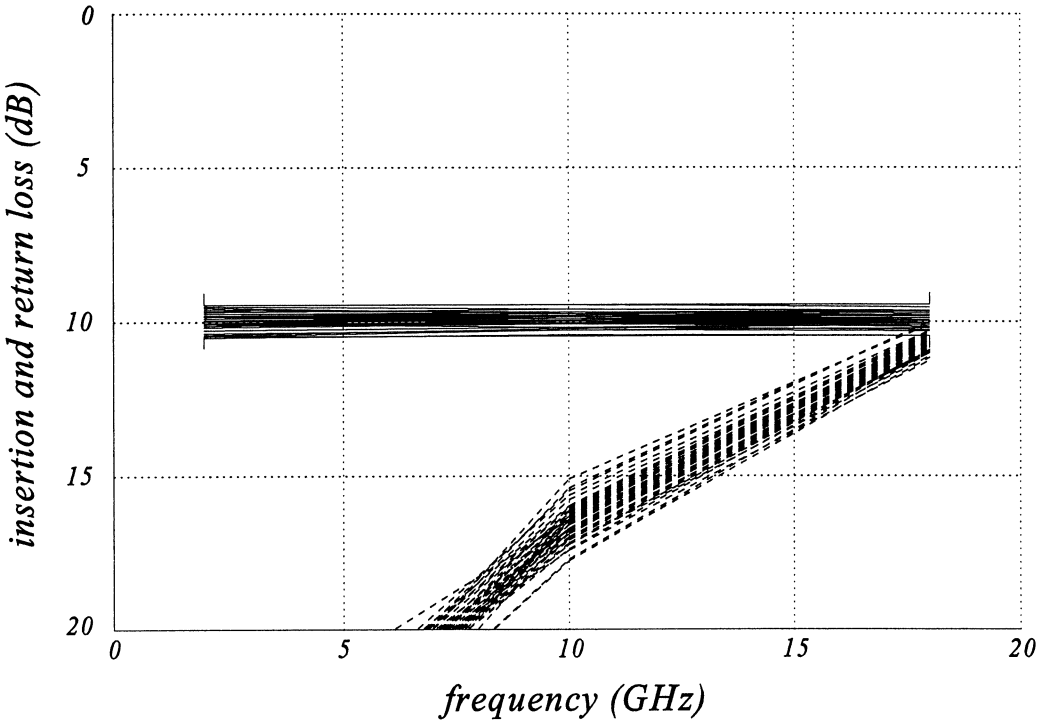

yield (estimated from 250 Monte Carlo outcomes) is increased from 82% to 97%

A Broadband Small-Signal Amplifier

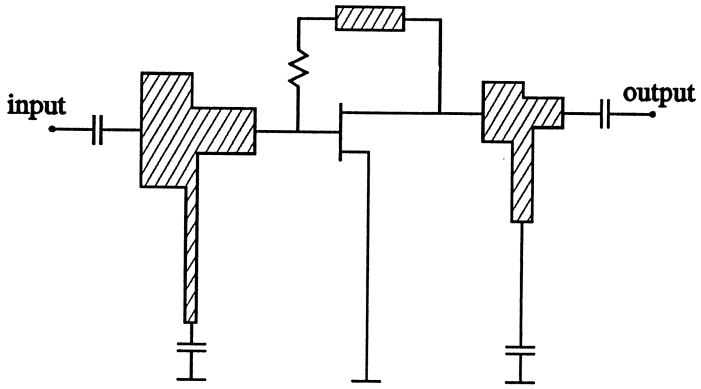

parameters of the feedback microstrip line and the microstrip T-structures

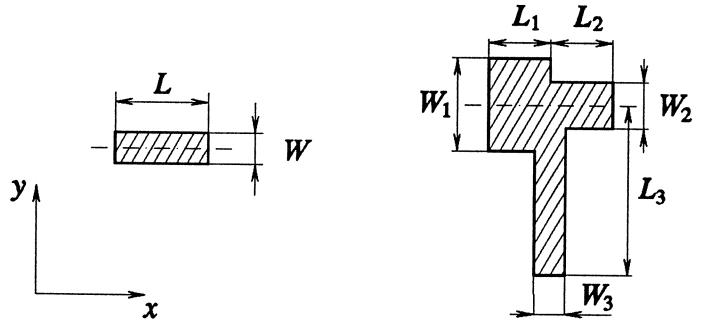

design specifications

$$7\ \text{dB} \le |S_{21}| \le 8\ \text{dB} \quad \text{for} \quad 6\ \text{GHz} \le f \le 18\ \text{GHz}$$

design variables

gate T-structure: $W_{g1}, L_{g1}, W_{g2}, L_{g2}$

drain T-structure: $W_{d1}, L_{d1}, W_{d2}, L_{d2}$

Combined *em*/SPICE Yield-Driven Design
(*Bandler et al., 1997*)

the MESFET simulated by SPICE

microstrip components accurately simulated by Sonnet's ***em***

> the line and the *T*-structure primitives of the Empipe library are invoked

circuit-level simulation and optimization carried out by OSA90/hope

uniform distribution within a 0.5 mil tolerance for all geometrical parameters

yield at the nominal minimax solution is 43%

yield is increased to 74% after yield optimization

50 outcomes used for yield optimization

Run Charts Before and After Yield Optimization

$|S_{21}|$ at 18 GHz

250 outcomes

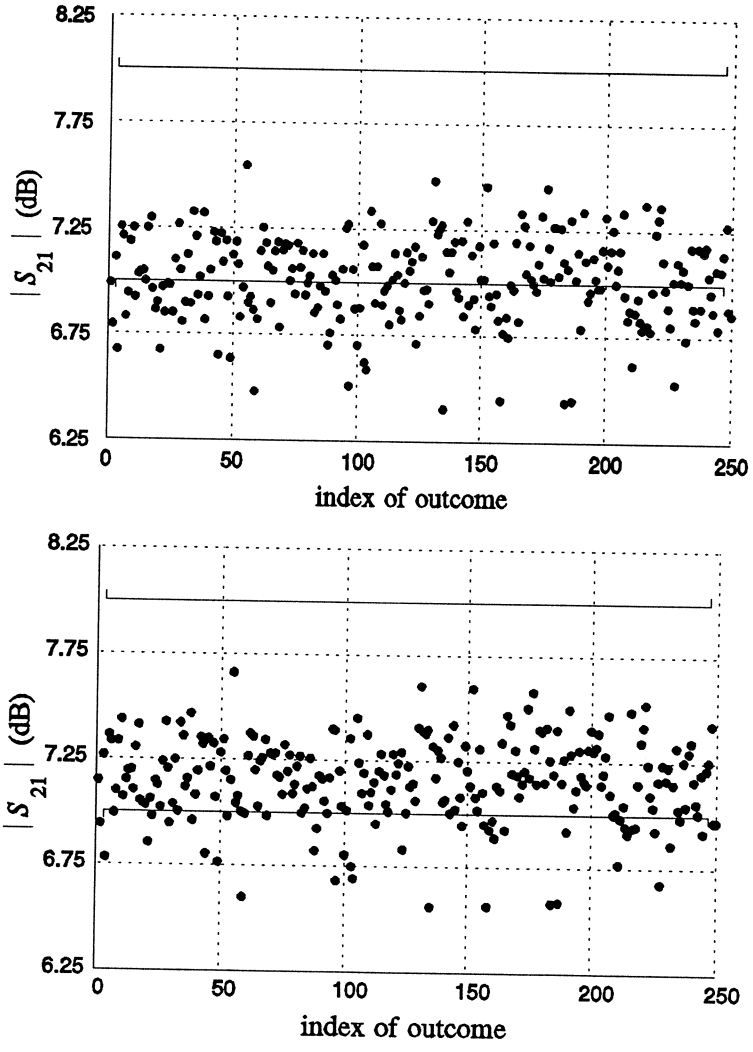

clearly, many more outcomes meet the specification after yield optimization

Space Mapping
(*Bandler et al., 1994*)

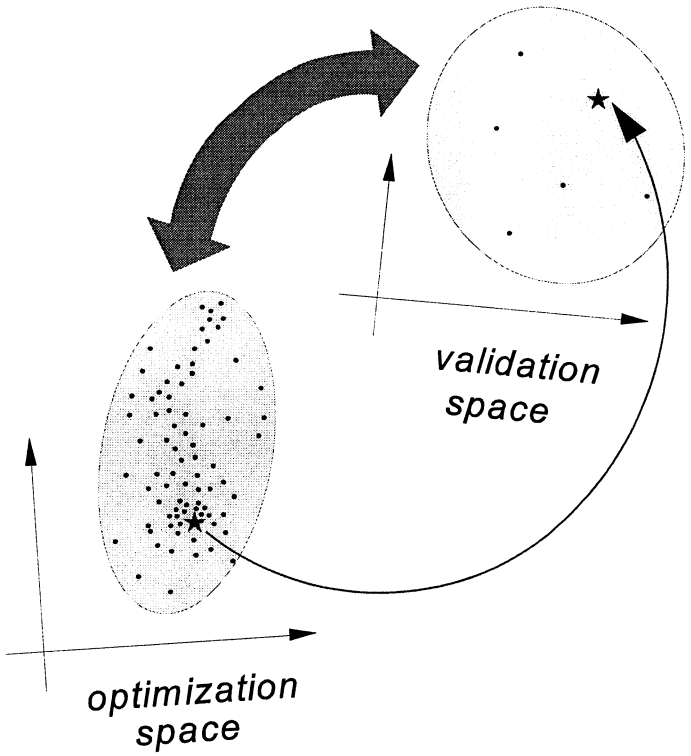

optimization or "coarse" model: $\boldsymbol{R}_{os}(\boldsymbol{x}_{os})$

EM, validation or "fine" model: $\boldsymbol{R}_{em}(\boldsymbol{x}_{em})$

Space Mapping: $\boldsymbol{x}_{os} = \boldsymbol{P}(\boldsymbol{x}_{em})$

such that $\boldsymbol{R}_{os}(\boldsymbol{P}(\boldsymbol{x}_{em})) \approx \boldsymbol{R}_{em}(\boldsymbol{x}_{em})$

Space Mapped solution: $\bar{\boldsymbol{x}}_{em} = \boldsymbol{P}^{-1}(\boldsymbol{x}^{*}_{os})$

fast response evaluation
for tolerance analysis: $\boldsymbol{R}_{os}(\boldsymbol{P}(\boldsymbol{x}_{em}))$

The Concept of Space Mapping

(*Bandler et al., 1994*)

we wish to find a mapping $\boldsymbol{P}(\boldsymbol{x}_{em})$ from the EM space $\boldsymbol{X}_{em}$ to the optimization space $\boldsymbol{X}_{os}$ such that

$$\| \boldsymbol{R}_{os}(\boldsymbol{P}(\boldsymbol{x}_{em})) - \boldsymbol{R}_{em}(\boldsymbol{x}_{em}) \| \leq \varepsilon$$

where $\boldsymbol{R}_{os}$ and $\boldsymbol{R}_{em}$ are the circuit responses simulated by the OS and EM simulators, respectively

starting from the optimal design $\boldsymbol{x}^*_{os}$ (in $\boldsymbol{X}_{os}$) we use SM to find the mapped solution in $\boldsymbol{X}_{em}$ as

$$\bar{\boldsymbol{x}}_{em} = \boldsymbol{P}^{-1}(\boldsymbol{x}^*_{os})$$

assuming that $\boldsymbol{P}$ is invertible

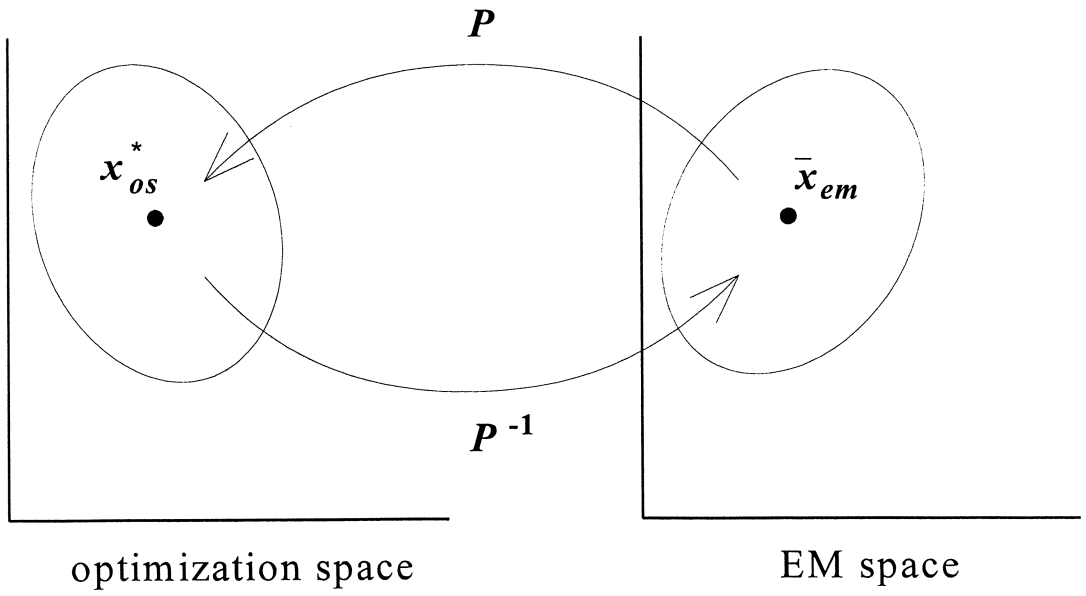

Aggressive Space Mapping
(*Bandler et al., 1995*)

new algorithm aggressively exploits *every* EM simulation

avoids upfront EM analyses at many base points

applies the classical Broyden update to the mapping

quasi-Newton iteration

$$\boldsymbol{x}_{em}^{(i+1)} = \boldsymbol{x}_{em}^{(i)} - \boldsymbol{B}^{(i)^{-1}} \left(\boldsymbol{P}^{(i)} \left(\boldsymbol{x}_{em}^{(i)} \right) - \boldsymbol{x}_{os}^{*} \right)$$

Broyden update:

$$\boldsymbol{B}^{(i+1)} = \boldsymbol{B}^{(i)} + \frac{\left(\boldsymbol{P}^{(i+1)} \left(\boldsymbol{x}_{em}^{(i+1)} \right) - \boldsymbol{x}_{os}^{*} \right) \boldsymbol{h}^{(i)^{T}}}{\boldsymbol{h}^{(i)^{T}} \boldsymbol{h}^{(i)}}$$

where

$$\boldsymbol{h}^{(i)} = \boldsymbol{x}_{em}^{(i+1)} - \boldsymbol{x}_{em}^{(i)}$$

Illustration of Aggressive Space Mapping Optimization

Step 0

find the optimal design x_{os}^* in Optimization Space

Step 1

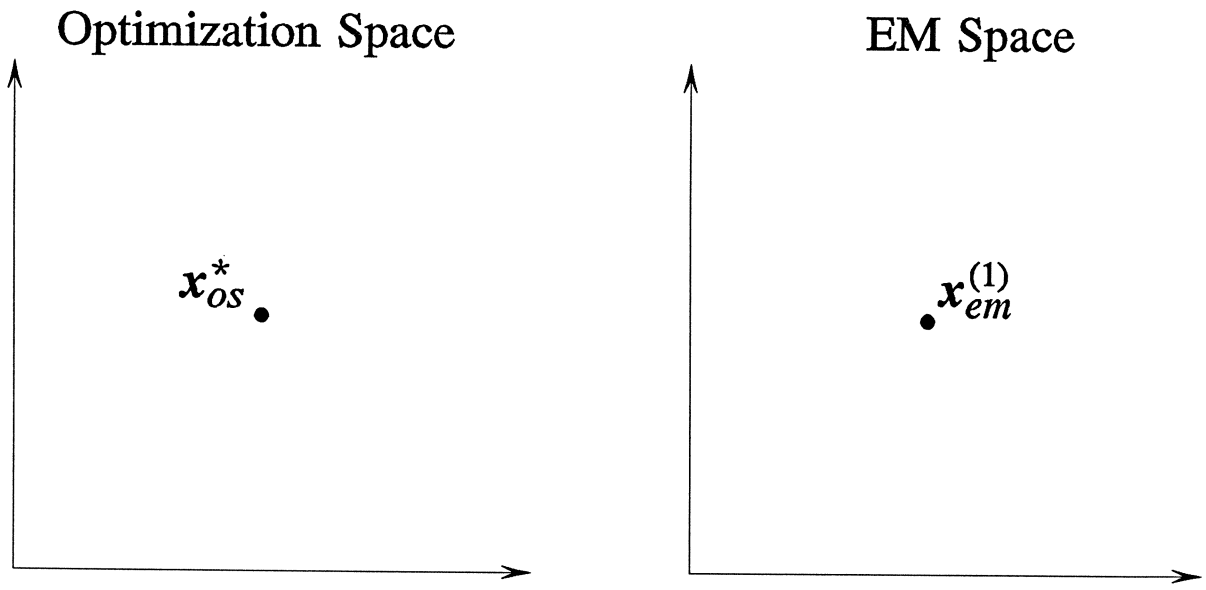

set $x_{em}^{(1)} = x_{os}^*$ assuming x_{em} and x_{os} represent the same physical parameters

Illustration of Aggressive Space Mapping Optimization

Step 2

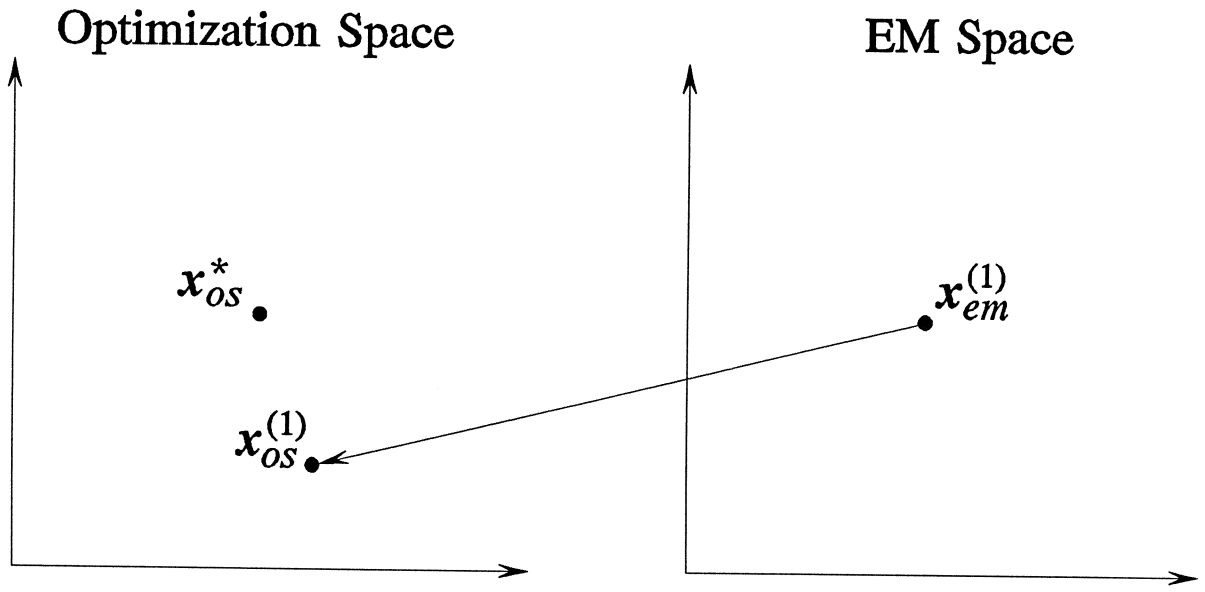

perform X_{os}-space model parameter extraction

Illustration of Aggressive Space Mapping Optimization

Step 3

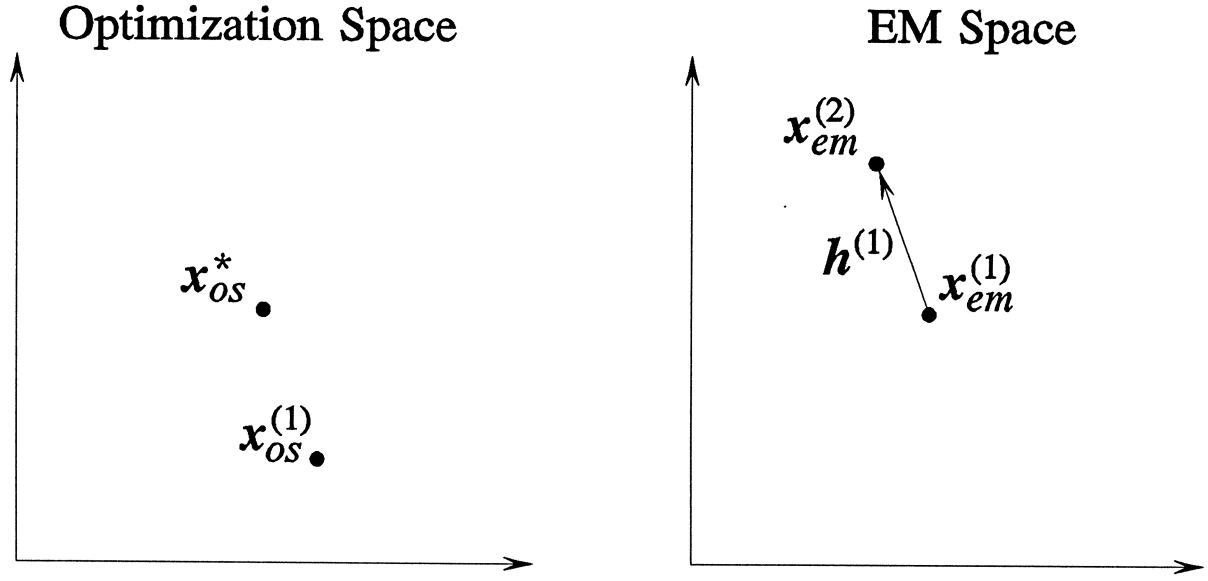

initialize Jacobian approximation $B^{(1)} = \mathbf{1}$

obtain $x_{em}^{(2)}$ by solving

$$B^{(1)} h^{(1)} = -f^{(1)}$$

where

$$f^{(1)} = x_{os}^{(1)} - x_{os}^{*}$$

Illustration of Aggressive Space Mapping Optimization

Step 4

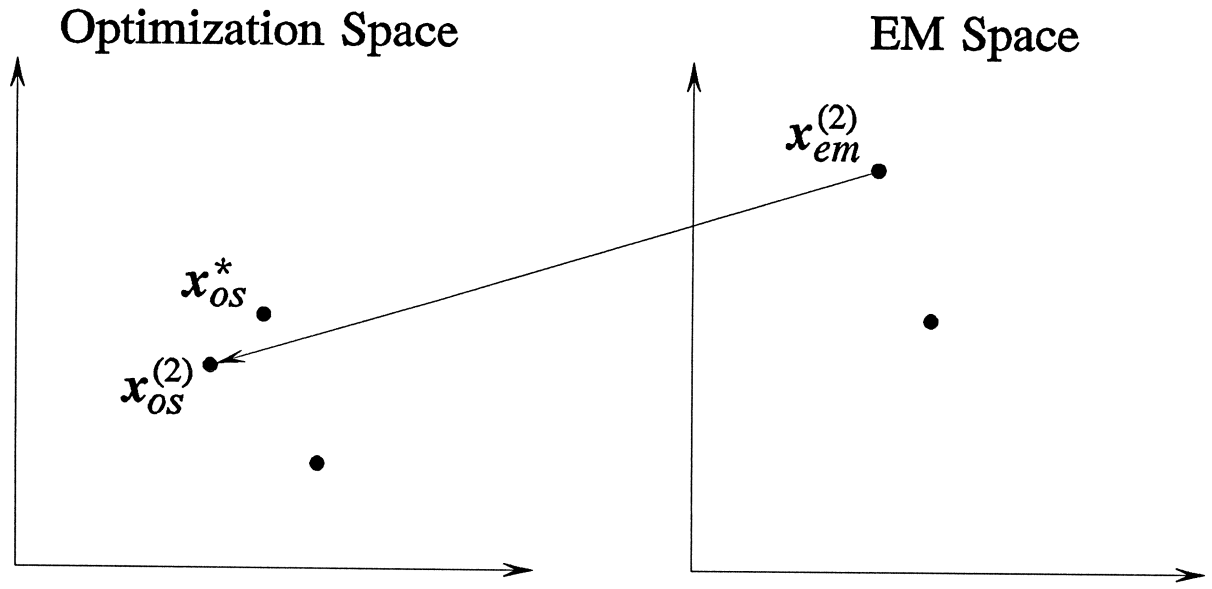

perform X_{os}-space model parameter extraction

Illustration of Aggressive Space Mapping Optimization

Step 5

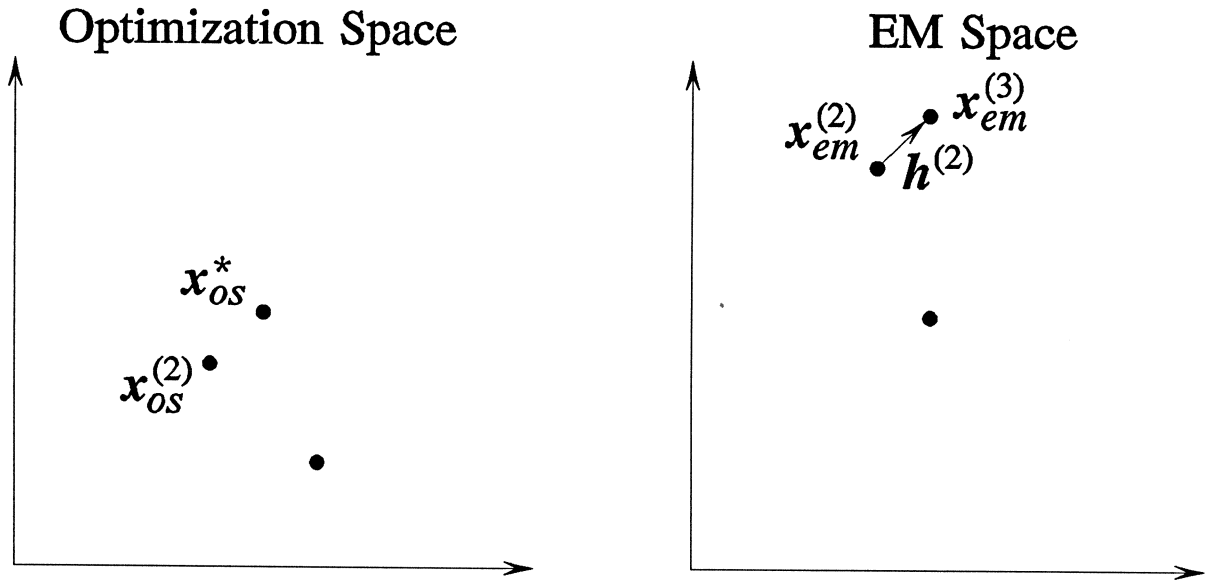

update Jacobian approximation from $B^{(1)}$ to $B^{(2)}$

obtain $x_{em}^{(3)}$ by solving

$$B^{(2)}h^{(2)} = -f^{(2)}$$

where

$$f^{(2)} = x_{os}^{(2)} - x_{os}^{*}$$

Illustration of Aggressive Space Mapping Optimization

Step 6

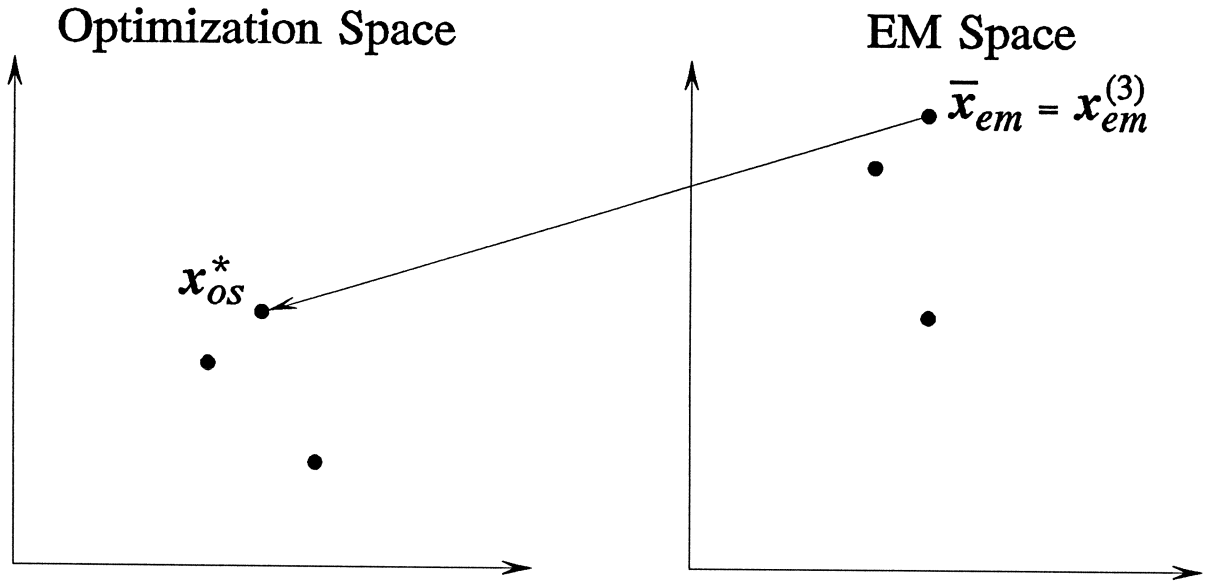

perform X_{os}-space model parameter extraction

if $\| x_{os}^{(3)} - x_{os}^* \| \leq \epsilon$ then $\bar{x}_{em} = x_{em}^{(3)}$ is considered as the SM solution

Space Mapping Optimization

to avoid direct optimization of computationally intensive models

the multi-simulator approach is particularly relevant and suitable for Space Mapping

automatic alignment of two distinct models of different accuracy and computational efficiency

such models would normally be facilitated by two disjoint simulators

two different EM simulators are used here

> EM space or "fine" model - 3D FEM-based field simulator Maxwell Eminence (*Ansoft Corporation*)
>
> optimization space (OS) or "coarse" model - the RWGMM library of waveguide mode-matching (MM) models connected by network theory (*Fritz Arndt*)

Space Mapping Using MM/Network Theory and FEM (*Bandler et al., 1997*)

flow diagram of Space Mapping concurrently exploiting the hybrid MM/network theory and FEM simulation techniques

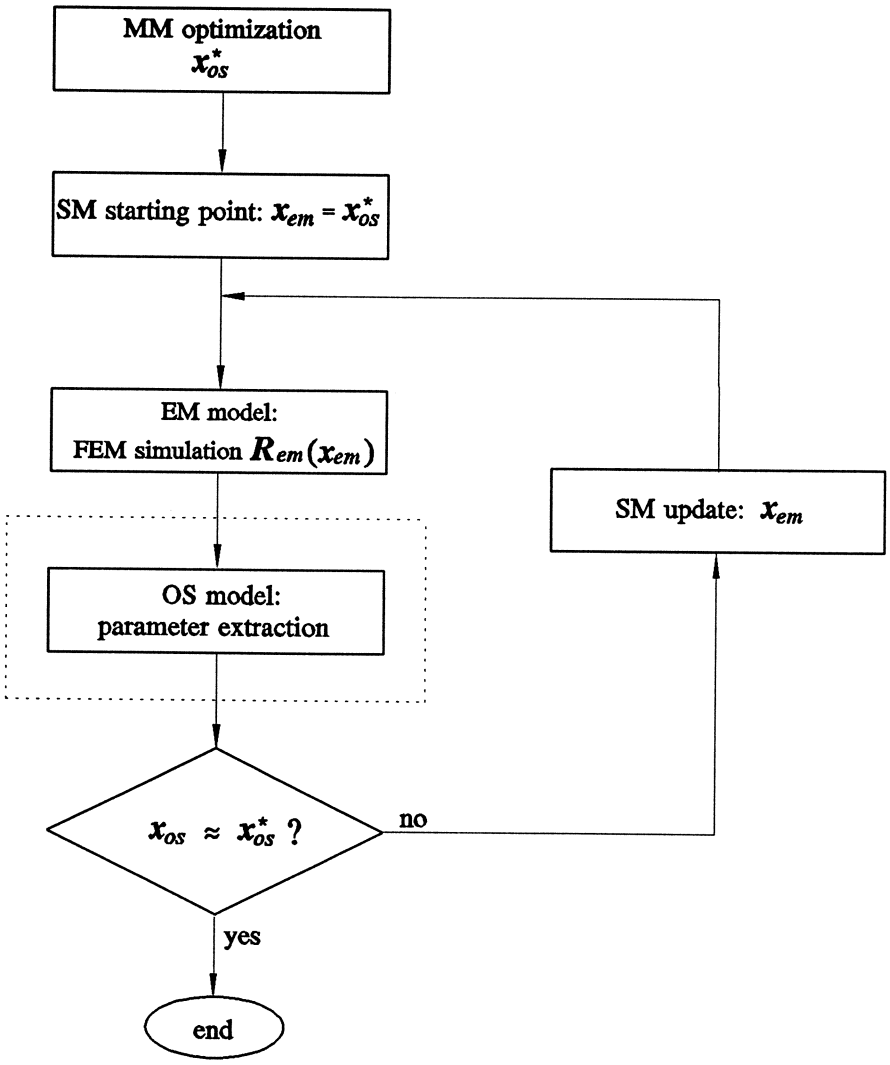

two-level Datapipe architecture

Optimization of an H-Plane Resonator Filter

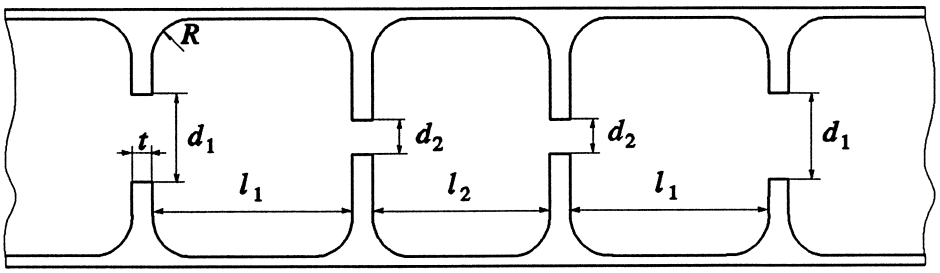

the waveguide cross-section: 15.8×7.9 mm

iris and corner radius: $t = 0.4$ mm, $R = 1$ mm

design variables

d_1, d_2, l_1 and l_2

design specifications

$|S_{21}| <$ -35 dB for $13.5 \le f \le 13.6$ GHz
$|S_{11}| <$ -20 dB for $14.0 \le f \le 14.2$ GHz
$|S_{21}| <$ -35 dB for $14.6 \le f \le 14.8$ GHz

FEM analysis - fine (or EM) model for Space Mapping

capable of analyzing arbitrary shapes

computationally very intensive

Coarse Model for Space Mapping Optimization

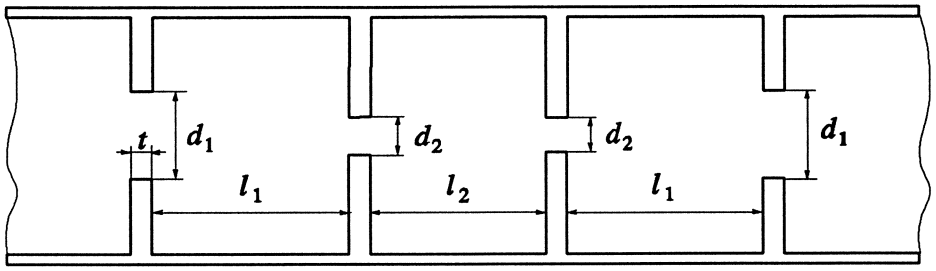

OS model (coarse model) for Space Mapping

sharp corners

hybrid MM/network theory simulation

- computationally efficient
- accurately treats a variety of predefined geometries
- ideally suited for modeling complex waveguide structures decomposable into available library building blocks

minimax optimization of the OS model gives the starting point for Space Mapping

Responses at the Starting Point

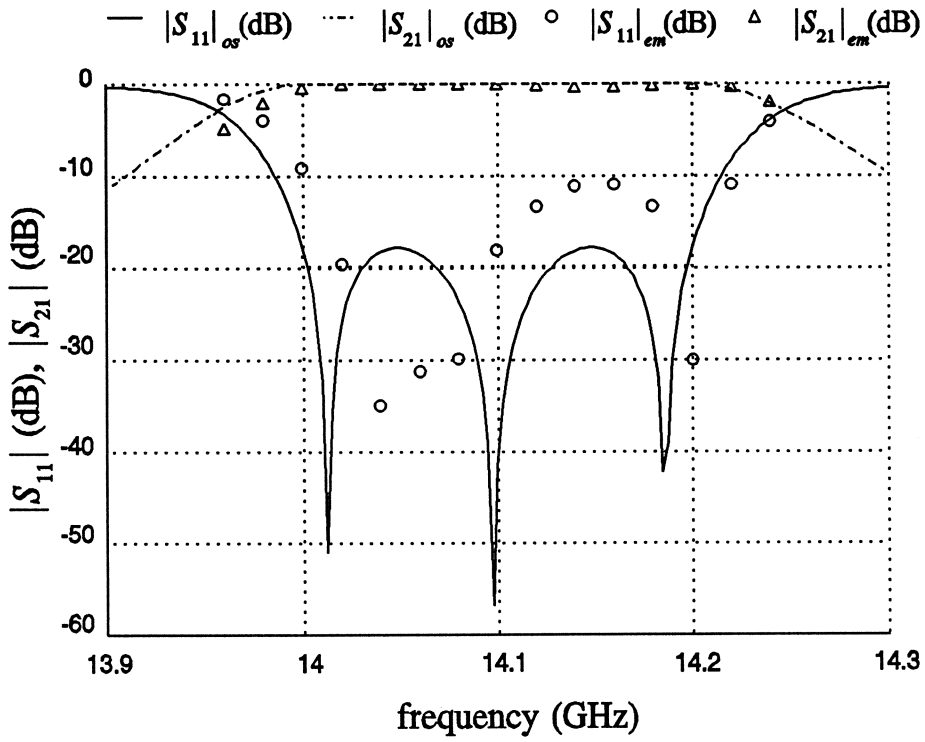

focus on the passband: 13.96 to 14.24 GHz

RWGMM (curves) and Maxwell Eminence (points)

discrepancy is evident

$d_1 = 6.04541, d_2 = 3.21811, l_1 = 13.0688$ and $l_2 = 13.8841$

the minimax solution in the OS space, x_{os}^*, yields the target response for Space Mapping

SM Optimized FEM Responses

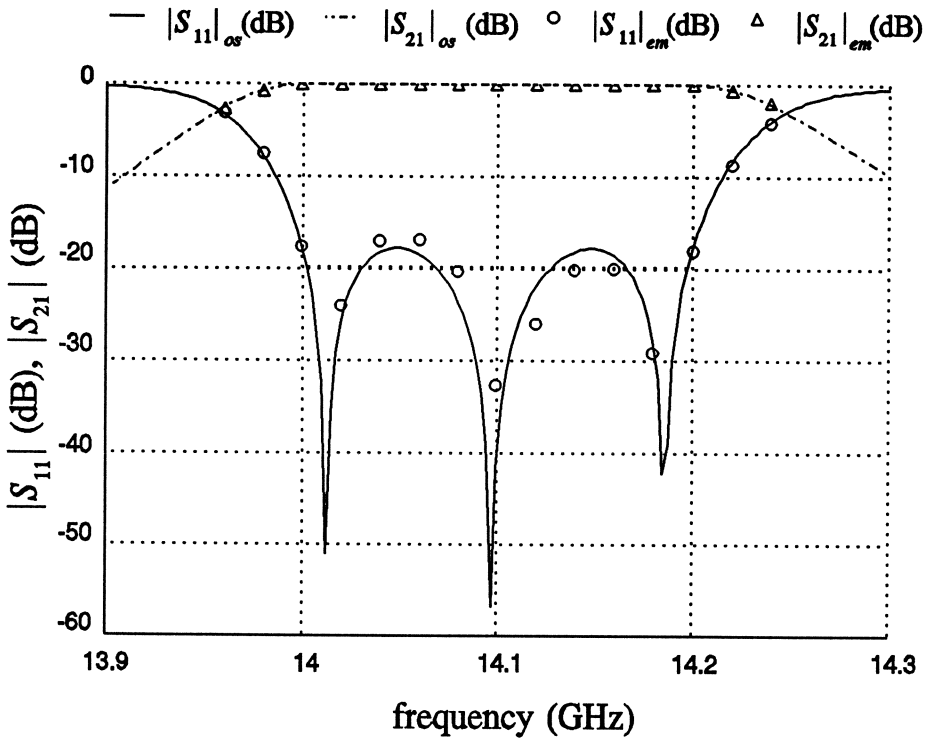

only 4 Maxwell Eminence simulations

RWGMM (curves) and Maxwell Eminence (points)

very good match

$d_1 = 6.17557, d_2 = 3.29058, l_1 = 13.0282$ and $l_2 = 13.8841$

direct optimization using Empipe3D confirms that the Space Mapping solution is indeed optimal

Tolerance Simulation Using SM

first, the mapping is established during nominal SM optimization

statistical outcomes in the EM space are mapped to the corresponding points in the OS space

we are able to rapidly estimate the effects of manufacturing tolerances, benefitting from

the accuracy of the FEM model

the speed of the hybrid MM/network theory simulations

the CPU time required for the Monte Carlo analysis is comparable to just a single full FEM simulation

Monte Carlo Analysis of the H-Plane Filter

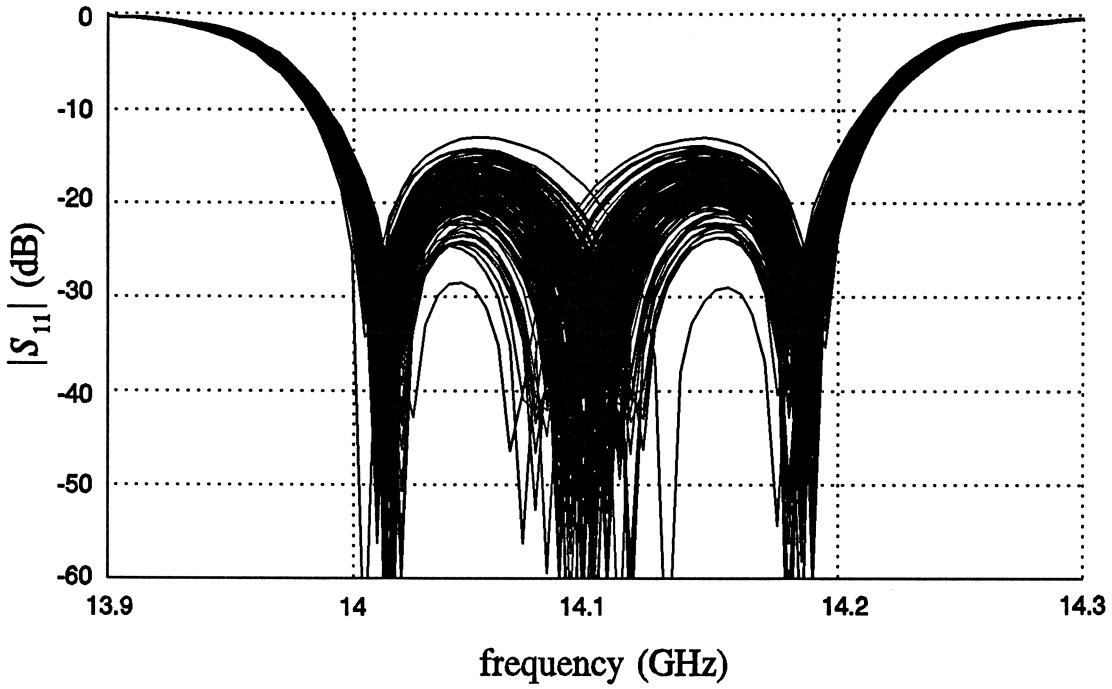

the statistical outcomes were randomly generated from normal distribution with a standard deviation of 0.0333%

the yield estimated from 200 outcomes is 88.5% w.r.t. the specification of $|S_{11}| <$ -15 dB in the passband

increasing the standard deviation to 0.1% results in yield dropping to 19% for 200 outcomes

Trust Region Aggressive Space Mapping Algorithm
(*Bakr et al., 1998*)

using $\boldsymbol{f}^{(i)} = \boldsymbol{P}(\boldsymbol{x}_{em}^{(i)}) - \boldsymbol{x}_{os}^{*}$
solve $(\boldsymbol{B}^{(i)T}\boldsymbol{B}^{(i)} + \lambda \boldsymbol{I})\,\boldsymbol{h}^{(i)} = -\boldsymbol{B}^{(i)T}\boldsymbol{f}^{(i)}$ for $\boldsymbol{h}^{(i)}$

this corresponds to minimizing $\left\|\boldsymbol{f}^{(i)}+\boldsymbol{B}^{(i)}\boldsymbol{h}^{(i)}\right\|_2^2$ subject to $\left\|\boldsymbol{h}^{(i)}\right\|_2 \le \delta$ where δ is the size of the trust region

λ, which correlates to δ, can be determined (*Moré et al., 1983)*

single point parameter extraction is performed at the new point $\boldsymbol{x}_{em}^{(i+1)} = \boldsymbol{x}_{em}^{(i)} + \boldsymbol{h}^{(i)}$ to get $\boldsymbol{f}^{(i+1)}$

if $\boldsymbol{f}^{(i+1)}$ satisfies a certain success criterion for the reduction in the l_2 norm of the vector $\boldsymbol{f}$, the point $\boldsymbol{x}_{em}^{(i+1)}$ is accepted and the matrix $\boldsymbol{B}^{(i)}$ is updated using Broyden's update

otherwise a temporary point is generated using $\boldsymbol{x}_{em}^{(i+1)}$ and $\boldsymbol{f}^{(i+1)}$ and is added to the set of points to be used for multi-point parameter extraction

a new $\boldsymbol{f}^{(i+1)}$ is obtained through multi-point parameter extraction

Trust Region Aggressive Space Mapping Algorithm
(*Bakr et al., 1998*)

the last three steps are repeated until a success criterion is satisfied or the step is declared a failure

step failure has two forms

(1) $\boldsymbol{f}$ may approach a limiting value without satisfying the success criterion or
(2) the number of fine model points simulated since the last successful step reaches n+1

Case (1): the parameter extraction is trusted but the linearization used is suspect; the size of the trust region is decreased and a new point $\boldsymbol{x}_{em}^{(i+1)}$ is obtained

Case (2): sufficient information is available for an approximation to the Jacobian of the fine model responses w.r.t. the fine model parameters used to predict the new point $\boldsymbol{x}_{em}^{(i+1)}$

the mapping between the two spaces is exploited in the parameter extraction step by solving

$$\underset{\boldsymbol{x}_{os}}{minimize} \left\| \boldsymbol{R}_{os}(\boldsymbol{x}_{os} + \boldsymbol{B}^{(i)}(\boldsymbol{x} - \boldsymbol{x}_{em}^{(i+1)})) - \boldsymbol{R}_{em}(\boldsymbol{x}) \right\|$$

simultaneously for a set of points $\boldsymbol{x}$

Three-Section Waveguide Transformer, Rounded Corners

(*Empipe3D manual, 1997*)

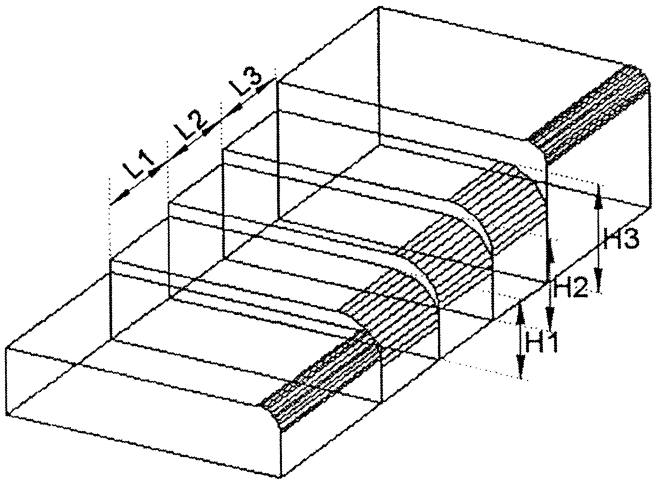

impedance matching between WR-75 half height and WR-75 full height waveguides

designable variables: the height and length of each section

fine (EM) model: HP HFSS

coarse model: ideal analytical model (*Bandler, 1969*)

the optimal design was obtained in 3 iterations, requiring 7 fine model simulations by HP HFSS

design specifications

$$|S_{11}| \leq -30\,\text{dB} \quad \text{for} \quad 9.5\ \text{GHz} \leq f \leq 15\ \text{GHz}$$

Three-Section Waveguide Transformer, Rounded Corners

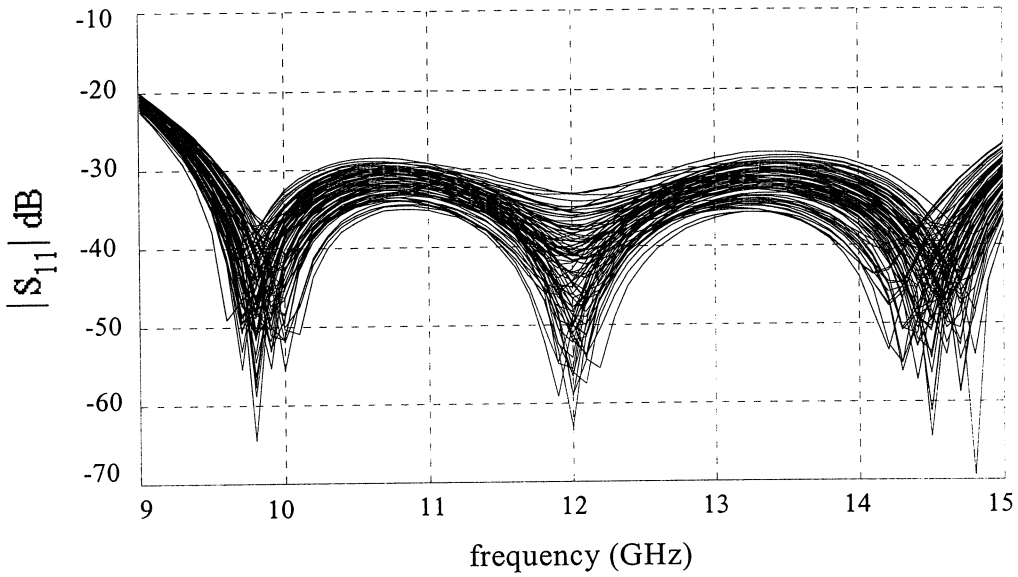

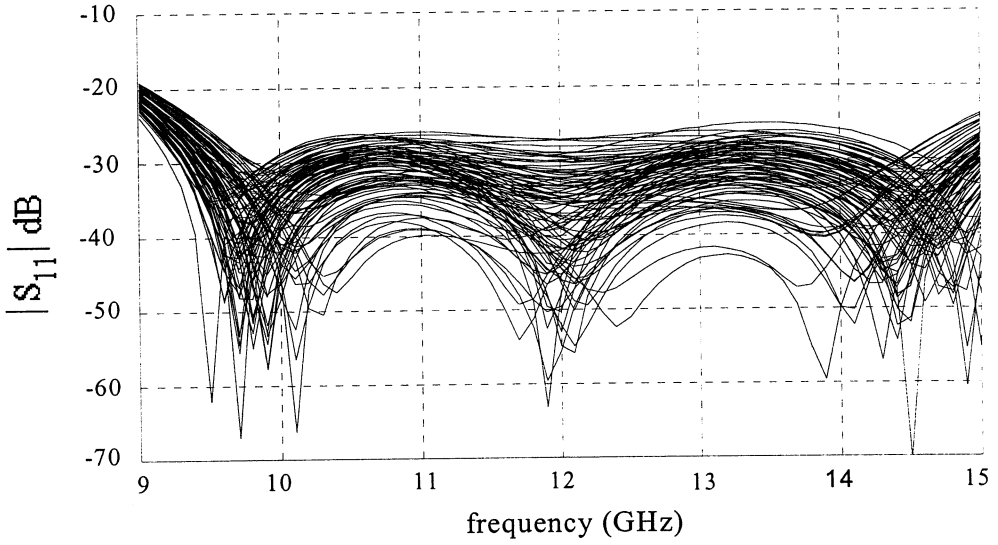

parameters uniformly distributed with tolerances of 1% and 2%

Monte Carlo analysis uses 100 coarse model simulations only

yield is 39% and 4%, respectively

The Advantages of Space Mapping

the aim is to avoid direct optimization in the CPU-intensive X_{em} space

the bulk of the computation involved in optimization is carried out in the X_{os} space

the optimal solution is mapped from the X_{os} space to the X_{em} space using the inverse mapping P^{-1}

we expect to obtain a rapidly improved design after each fine model simulation

significantly more efficient than the "brute force" direct EM optimization

a fundamentally new concept in engineering-oriented optimization practice

Background

assume that X_{os} (optimization space) and X_{em} (EM space) have the same dimensionality, i.e.,

$$x_{os} \in \mathbb{R}^n \quad \text{and} \quad x_{em} \in \mathbb{R}^n,$$

but may not represent the same parameters

the X_{os}-space model can be comprised of empirical models, or an efficient coarse-grid EM model

the X_{em}-space model is typically a fine-grid EM model but, ultimately, can represent actual hardware prototypes

we assume that the X_{os}-space model responses, $R_{os}(x_{os})$, are much faster to calculate but less accurate than the X_{em}-space model responses, $R_{em}(x_{em})$

we initially perform optimization in X_{os} to obtain the optimal design x_{os}^*, for instance in the minimax sense

subsequently, apply SM to find the mapped solution $\bar{x}_{em}$ in X_{em} to reproduce the optimal performance predicted by the empirical model

The Concept of Space Mapping
(*Bandler, Biernacki, Chen, Grobelny and Hemmers, 1994*)

our aim is to find an appropriate mapping, P, from the X_{em}-space to the X_{os}-space, i.e.,

$$x_{os} = P(x_{em})$$

such that

$$R_{os}(P(x_{em})) \approx R_{em}(x_{em})$$

we assume that such a mapping exists and is one-to-one within some local modeling region encompassing our SM solution

once the mapping is established, the SM solution is

$$\bar{x}_{em} = P^{-1}(x^*_{os})$$

Original Space Mapping Method

the mapping is established through an iterative process

to obtain the initial approximation to the mapping, $P^{(0)}$, we perform EM analyses at a preselected set of base points in X_{em} around the starting point

as the first base point we may select the starting point, i.e.,

$$x_{em}^{(1)} = x_{os}^{*}$$

assuming x_{em} and x_{os} represent the same physical parameters, followed by additional base points chosen by perturbation as

$$x_{em}^{(i)} = x_{em}^{(1)} + \Delta x_{em}^{(i-1)}, \quad i = 2, 3, ..., m$$

this is followed by parameter extraction optimization in X_{os} to obtain the set of corresponding base points $x_{os}^{(i)}$ according to

$$\underset{x_{os}^{(i)}}{\text{minimize}} \; \| R_{os}(x_{os}^{(i)}) - R_{em}(x_{em}^{(i)}) \|$$

for $i = 1, 2, ..., m$, where $\| \cdot \|$ indicates a suitable norm

Original Space Mapping Method (continued)

at the jth iteration, both sets may be expanded to contain m_j points which are used to establish the updated mapping $P^{(j)}$

the current approximation $P^{(j)}$ is used to estimate $\bar{x}_{em}$ as

$$x_{em}^{(m_j+1)} = P^{(j)^{-1}}(x_{os}^*)$$

the process continues until the termination condition

$$\| R_{os}(x_{os}^*) - R_{em}(x_{em}^{(m_j+1)}) \| \leq \epsilon$$

is satisfied, where ϵ is a small positive constant, then $P^{(j)}$ is our desired P

if not, the set of base points in X_{em} is augmented by $x_{em}^{(m_j+1)}$ and correspondingly, $x_{os}^{(m_j+1)}$ determined by parameter extraction augments the set of base points in X_{os}

upon termination, we set $\bar{x}_{em} = x_{em}^{(m_j+1)} = P^{(j)^{-1}}(x_{os}^*)$ as the SM solution

Aggressive Approach to Space Mapping
(*Bandler, Biernacki, Chen, Hemmers and Madsen, 1995*)

at the SM solution, $R_{em}(x_{em}^{(M)})$ will closely match $R_{os}(x_{os}^{*})$,

$$\| R_{os}(x_{os}^{*}) - R_{em}(x_{em}^{(M)}) \| \leq \epsilon$$

where M is the number of iterations needed to converge to an SM solution

hence, after an additional parameter extraction optimization in X_{os}, the resulting point

$$x_{os}^{(M)} = P(x_{em}^{(M)})$$

approaches the point x_{os}^{*} (optimal solution in X_{os}), or

$$\| x_{os}^{(M)} - x_{os}^{*} \| \leq \eta \text{ as } j \rightarrow M$$

where η is a small positive constant

by setting η to 0, we consider the set of n nonlinear equations

$$f(x_{em}) = \mathbf{0}$$

of the form

$$f(x_{em}) = P(x_{em}) - x_{os}^{*}$$

where x_{os}^{*} is a given vector

Aggressive Space Mapping - Quasi-Newton Iteration

let $\boldsymbol{x}_{em}^{(j)}$ be the jth approximation to the solution and $\boldsymbol{f}^{(j)}$ written for $\boldsymbol{f}(\boldsymbol{x}_{em}^{(j)})$

the next iterate is found by a quasi-Newton iteration

$$\boldsymbol{x}_{em}^{(j+1)} = \boldsymbol{x}_{em}^{(j)} + \boldsymbol{h}^{(j)}$$

by solving the linear system

$$\boldsymbol{B}^{(j)}\boldsymbol{h}^{(j)} = -\boldsymbol{f}^{(j)}$$

$\boldsymbol{B}^{(j)}$ is an approximation to the Jacobian matrix

$$\boldsymbol{J}(\boldsymbol{x}_{em}^{(j)}) = \left(\frac{\partial \boldsymbol{f}^{T}(\boldsymbol{x}_{em})}{\partial \boldsymbol{x}_{em}} \right)^{T} \Bigg|_{\boldsymbol{x}_{em} = \boldsymbol{x}_{em}^{(j)}}$$

in our implementation, $\boldsymbol{B}^{(1)}$ is set to the identity matrix

the approximation to the Jacobian matrix is updated by the classic Broyden formula (*Broyden, 1965*)

$$\boldsymbol{B}^{(j+1)} = \boldsymbol{B}^{(j)} + \frac{\boldsymbol{f}(\boldsymbol{x}_{em}^{(j)} + \boldsymbol{h}^{(j)}) - \boldsymbol{f}(\boldsymbol{x}_{em}^{(j)}) - \boldsymbol{B}^{(j)}\boldsymbol{h}^{(j)}}{\boldsymbol{h}^{(j)^{T}}\boldsymbol{h}^{(j)}} \boldsymbol{h}^{(j)^{T}}$$

Aggressive Space Mapping - Implementation

begin with a point, $x_{os}^* \triangleq arg\,min\,\{H(x_{os})\}$, representing the optimal design in X_{os} where $H(x_{os})$ is some appropriate objective function

Step 0 initialize $x_{em}^{(1)} = x_{os}^*$, $B^{(1)} = \mathbf{1}$, $f^{(1)} = P(x_{em}^{(1)}) - x_{os}^*$, $j = 1$; stop if $\| f^{(1)} \| \leq \eta$

Step 1 solve $B^{(j)} h^{(j)} = -f^{(j)}$ for $h^{(j)}$

Step 2 set $x_{em}^{(j+1)} = x_{em}^{(j)} + h^{(j)}$

Step 3 evaluate $P(x_{em}^{(j+1)})$

Step 4 compute $f^{(j+1)} = P(x_{em}^{(j+1)}) - x_{os}^*$; if $\| f^{(j+1)} \| \leq \eta$, stop

Step 5 update $B^{(j)}$ to $B^{(j+1)}$

Step 6 set $j = j + 1$; go to *Step* 1

Fully Automated Space Mapping Optimization

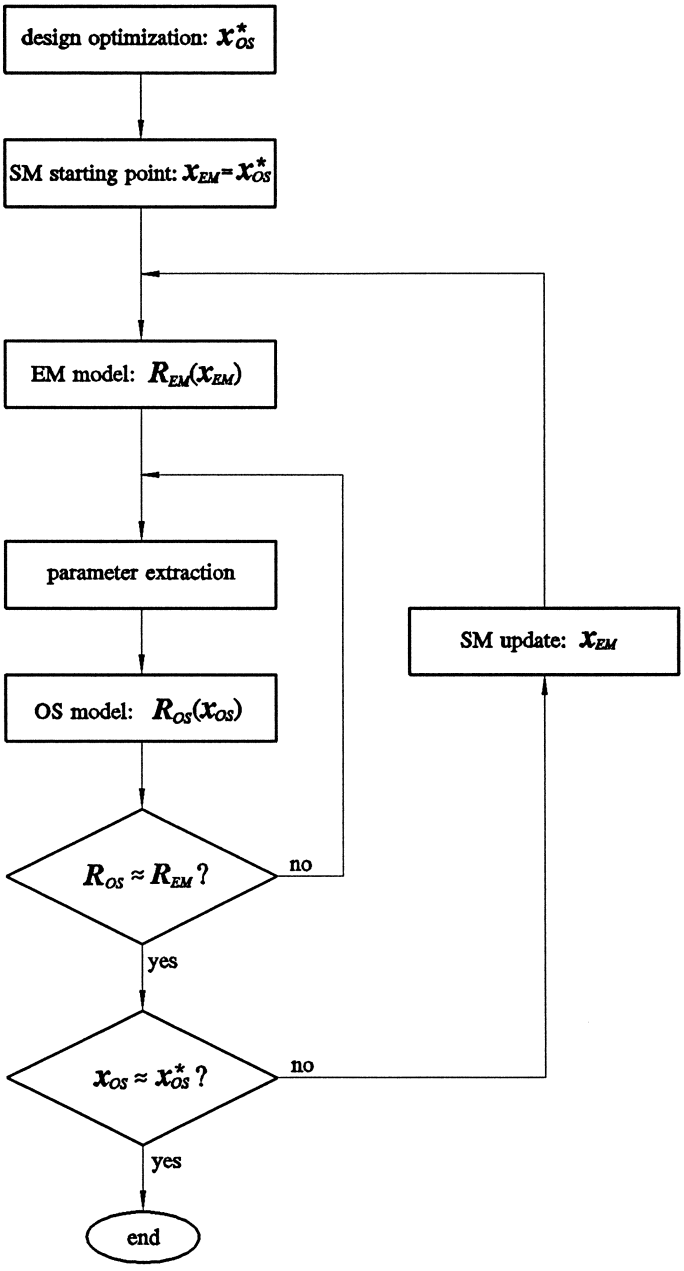

two-level Datapipe architecture

Frequency Space Mapping for Parameter Extraction

parameter extraction can be a serious challenge, especially at the starting point, if the model responses are misaligned

$\mathrm{Re}\{S_{11}\}$ using OSA90/hope (—) and *em* (---) at x_{os}^{*}

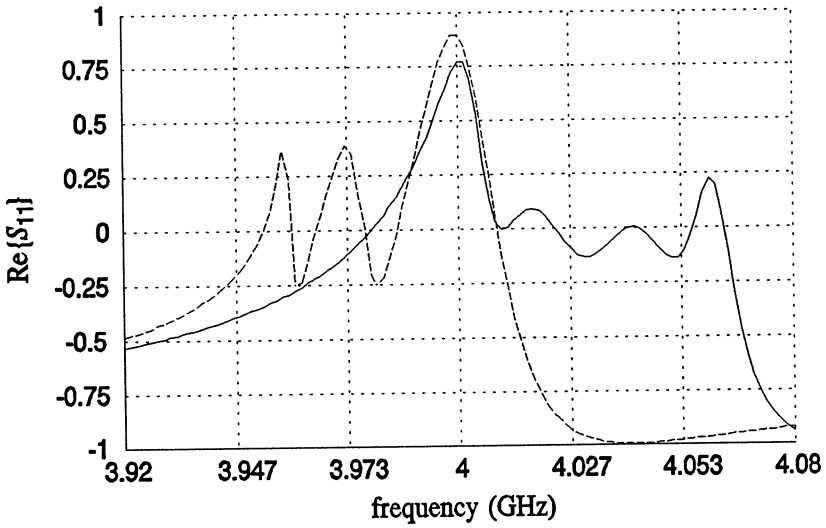

straightforward optimization from such a starting point can lead to a local minimum

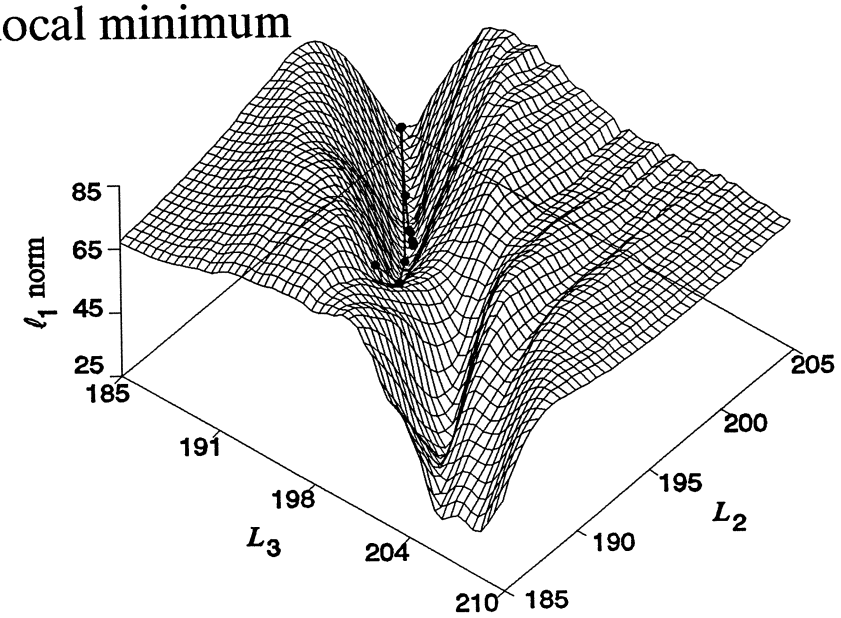

Frequency Space Mapping - Mapping and Alignment

to better condition the parameter extraction subproblem

first, we align R_{os} and R_{em} along the frequency axis using

$$\omega_{os} = P_{\omega}(\omega)$$

this frequency space mapping can be as simple as

$$\omega_{os} = \sigma\omega + \delta$$

at the starting point, we determine σ_0 and δ_0 by

$$\underset{\sigma_0,\, \delta_0}{\text{minimize}} \; \| R_{os}(x_{os}, \sigma_0, \delta_0) - R_{em}(x_{em}) \|$$

where x_{os} and x_{em} are fixed and $x_{os} = x_{em}$

resulting alignment between OSA90/hope (—) and *em* (---):

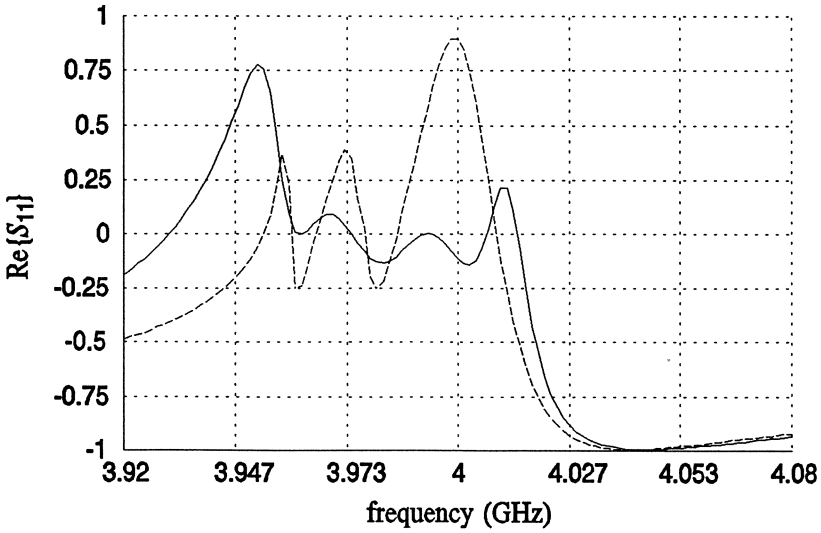

Frequency Space Mapping:
Sequential FSM (SFSM) Algorithm

we perform a sequence of optimizations to gradually achieve the identity Frequency Space Mapping

we optimize x_{os} to match R_{os} and R_{em}:

$$\underset{x_{os}^{(j)}}{\text{minimize}} \; \| R_{os}(x_{os}^{(j)}, \sigma^{(j)}, \delta^{(j)}) - R_{em}(x_{em}) \|$$

the values $\sigma^{(j)}$ and $\delta^{(j)}$ are updated according to

$$\sigma^{(j)} = 1 + (\sigma_0 - 1)\frac{(K - j)}{K}$$

and

$$\delta^{(j)} = \delta_0 \frac{(K - j)}{K},$$

respectively, for $j = 0, 1, ..., K$

K determines the number of steps in the sequence

larger values of K increase the probability of success in the parameter extraction subproblem at the expense of longer optimization time

Frequency Space Mapping:
Exact Penalty Function (EPF) Algorithm

we perform only one optimization to achieve the identity Frequency Space Mapping and optimize x_{os} to match R_{os} to R_{em}

the ℓ_1 norm version of the EPF formulation is given by

$$\underset{x_{os},\, \sigma,\, \delta}{\text{minimize}} \quad \{ \| R_{os}(x_{os}, \sigma, \delta) - R_{em}(x_{em}) \|_1 + \alpha_1 | \sigma - 1 | + \alpha_2 | \delta | \}$$

the minimax version is given by

$$\underset{x_{os},\, \sigma,\, \delta}{\text{minimize}} \left\{ \max_{1 \le i \le 4} \left[U(x_{os}, \sigma, \delta),\ U(x_{os}, \sigma, \delta) - \alpha_i g_i \right] \right\}$$

where

$$U(x_{os}, \sigma, \delta) = \| R_{os}(x_{os}, \sigma, \delta) - R_{em}(x_{em}) \|$$

and

$$g(\sigma, \delta) = \begin{bmatrix} \sigma - 1 \\ 1 - \sigma \\ \delta \\ -\delta \end{bmatrix}$$

in both EPF formulations, α_i are kept fixed and must be sufficiently large to obtain the identity mapping and hence the solution to the parameter extraction problem

Frequency Space Mapping - Results

Re$\{S_{11}\}$ using OSA90/hope (—) and *em* (---)

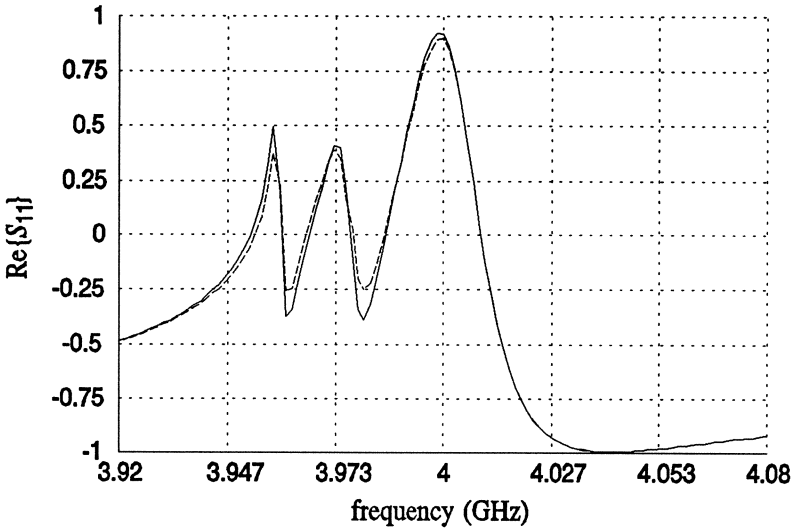

resulting match after applying the FSM algorithm

Decomposition
(Bandler, Biernacki, Chen and Huang, 1997)

partitions a complex structure into a few smaller substructures

each substructure is analyzed separately

the results are combined to obtain the response of the overall structure

2D analytical methods or even empirical formulas can be used for some non-critical regions

full-wave 3D models are adopted for the analysis of the key substructures

A Five-Pole C-Band Interdigital Filter

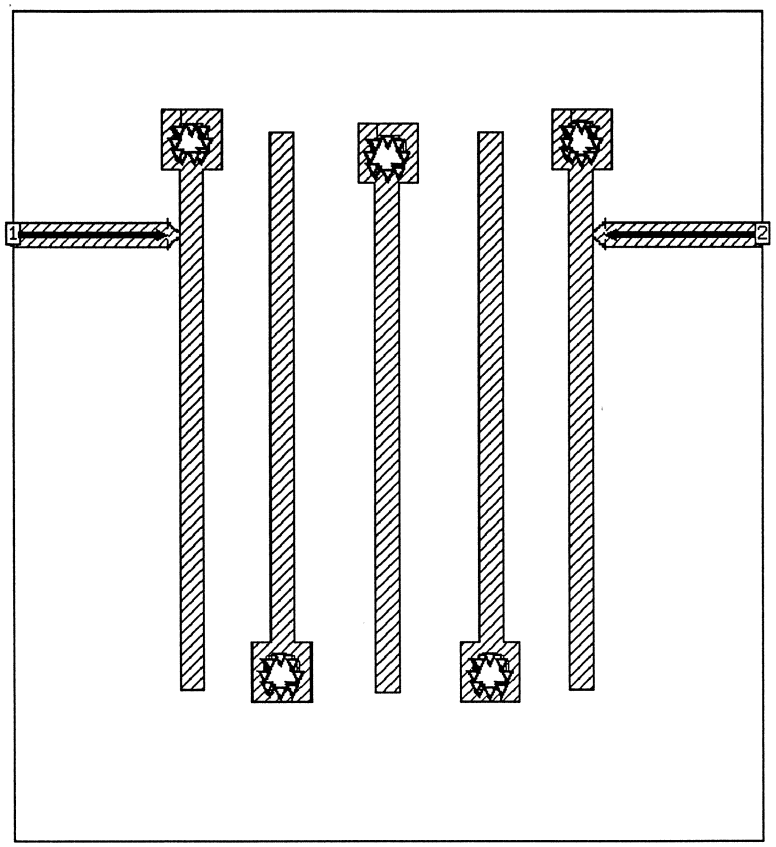

15 mil thick alumina substrate with ε_r = 9.8.

the width of each microstrip is chosen to be 10 mil

quarter wavelength resonators

Interdigital Filter Design

specifications

passband cutoff	$f_1 = 4.9$ GHz, $f_2 = 5.3$ GHz
passband ripple	$r = 0.1$ dB
isolation bandwidth	$BWI = 0.95$ GHz
isolation	$DBI = 30$ dB

the order of the filter is determined as 5

all other dimensions including the gaps and the positions of the tapped lines are obtained by synthesis (*Matthaei et al., 1964*)

design variables include two gaps between the resonators and four lengths of microstrip lines from an appropriate position of each resonator to its ends

the size of the vias is fixed

The Fine Model of the Interdigital Filter

full-wave EM simulations of the whole structure using Sonnet's *em*

for good accuracy the grid size has to be sufficiently small

selected grid size: 1×1 mil

about 1.5 CPU hours per frequency point on a Sun SPARCstation 10

much longer if losses are included

this translates into considerable EM simulation time for fine frequency sweeps

direct optimization would require many EM analyses and consequently excessive CPU time

Dimensions and Material Parameters of the Filter

FILTER MATERIAL PARAMETERS AND GEOMETRICAL DIMENSIONS

Parameter	Value
substrate dielectric constant	9.8
substrate thickness (mil)	15
conducting metal thickness (mil)	0
substrate dielectric loss tangent	0/0.001*
conductivity of the metal	$\infty/5.8\times10^{7}$*
shielding cover height (mil)	75
width of input/output lines (mil)	10
width of each resonator (mil)	10
via diameter (mil)	13
via pad dimensions (mil $\times$ mil)	25 $\times$ 25

* loss tangent and conductivity for simulations without and with losses, respectively

Decomposition of the Interdigital Filter

the coarse model is constructed using decomposition

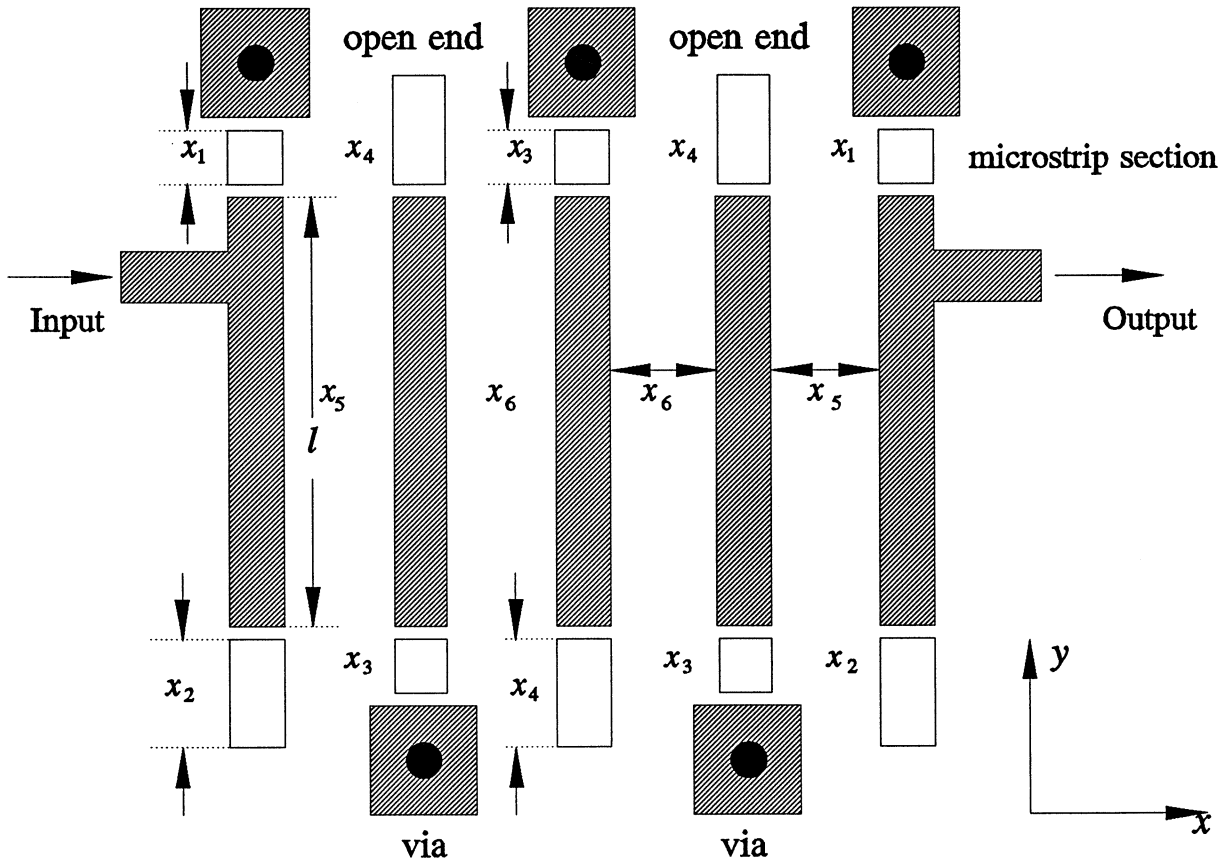

the substructures are analyzed separately using either EM models with a coarse grid or empirical models

the partial results are then combined through circuit theory to obtain the response of the overall filter

The Coarse Model of the Interdigital Filter

the center shaded 12-port network is analyzed by *em* with a very coarse grid: 5 × 10 mil

the vias have fixed dimensions - one via is analyzed by *em* with a grid of 1 × 1 mil only once; in subsequent simulations all vias are represented by their reflection coefficient

all other parts including the microstrip line sections and the open ends are analyzed using the empirical models of OSA90/hope

less than 1 CPU minute per frequency point on a Sun SPARCstation 10

off-grid responses, when needed during optimization, are obtained by interpolation

the coarse model retains most of the adjacent and non-adjacent couplings, thus it provides reasonably accurate results at dramatically faster speed

Design Procedure

first, we optimize the filter using the coarse model

minimax solution x_{os}^* is obtained

we check this coarse model solution using the fine model at a few selected frequencies

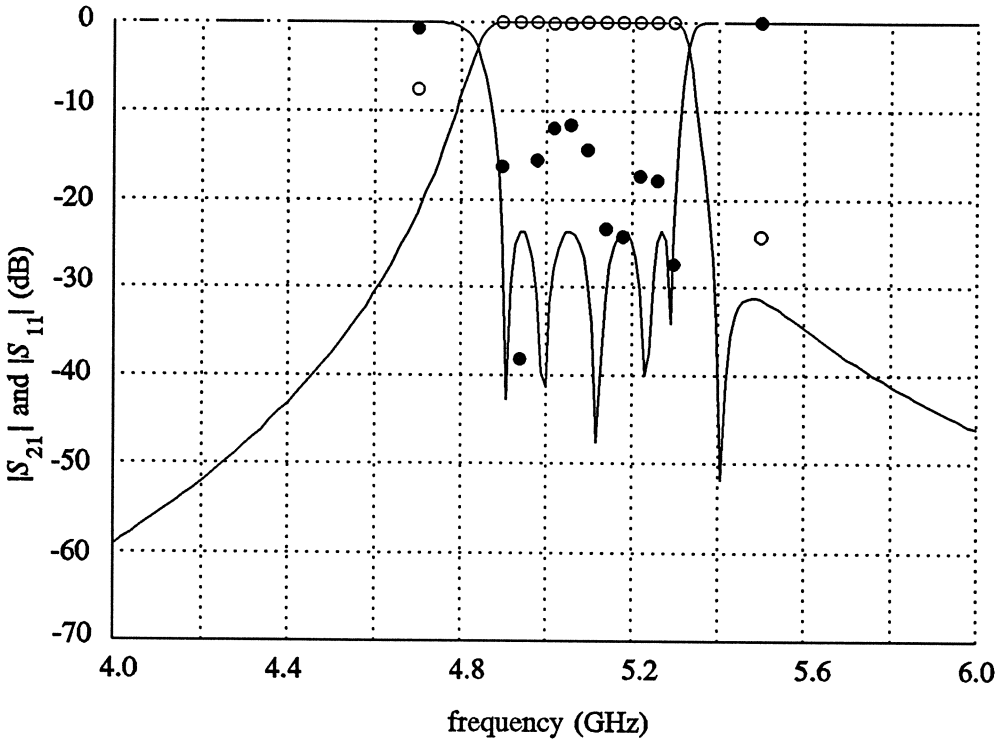

solid curves — optimized $|S_{11}|$ and $|S_{21}|$ responses of the coarse model at the optimal point x_{os}^*

circles — fine model responses at x_{os}^*

Results of EM Validation

the fine model responses deviate significantly from the optimized coarse model responses

the passband return loss is only about 11 dB and the bandwidth is wider than specified

discrepancies may be due to the coarse grid and some couplings not taken into account by the coarse model

WHAT'S NEXT?

typically, engineers manually tune the design and try to meet design specifications

we offer an automated approach using Space Mapping

Space Mapping Optimization of the Interdigital Filter

SM optimization starts with $x_{em}^{(1)} = x_{os}^{*}$

after the first iteration, a new point $x_{em}^{(2)}$ in the X_{em} space is obtained

the fine model responses of this new point are compared with the coarse model optimal responses

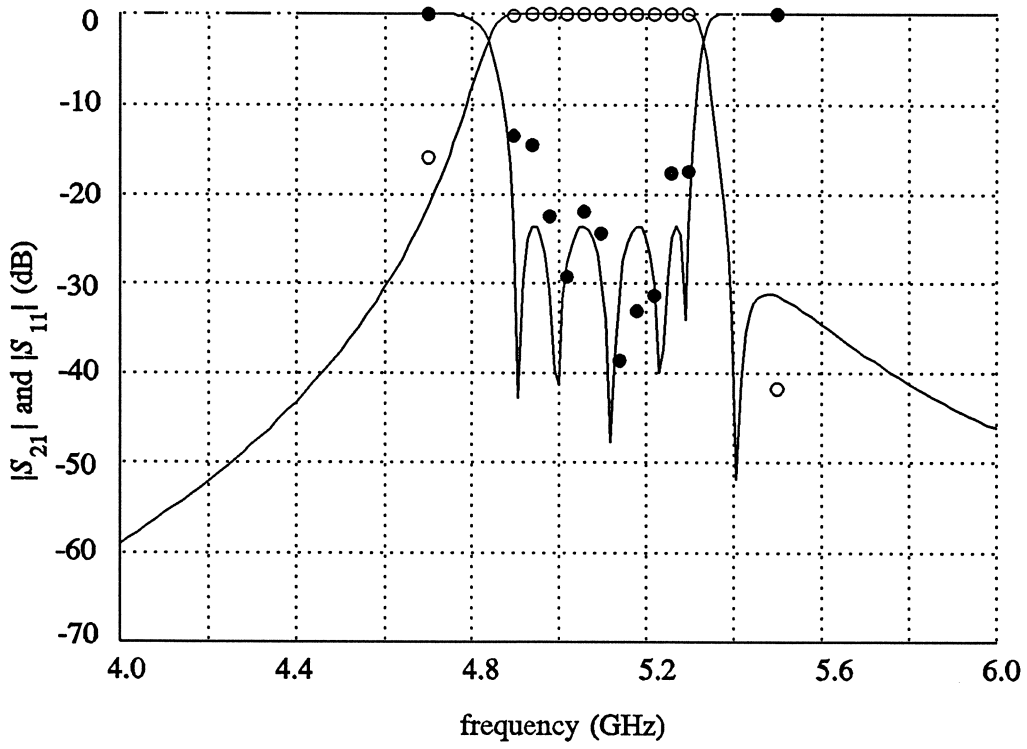

return loss is improved and the bandwidth is reduced at the lower frequency end

Second Iteration of Space Mapping

another iteration of SM produces $x_{em}^{(3)}$

the fine model responses at $x_{em}^{(3)}$ at 13 frequency points are compared with the coarse model optimal responses

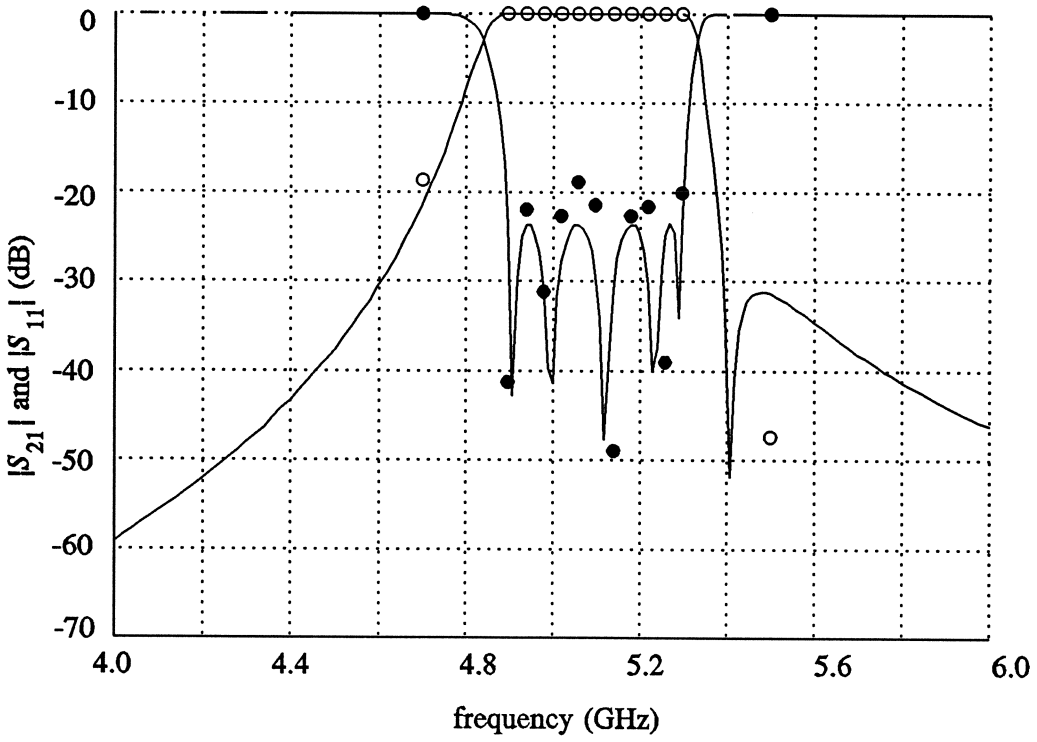

only three EM simulations of the fine model were needed

Final EM Validation

a dense frequency sweep is desired

here, simulation includes the conductor and dielectric losses

the fine model responses at $x_{em}^{(3)}$

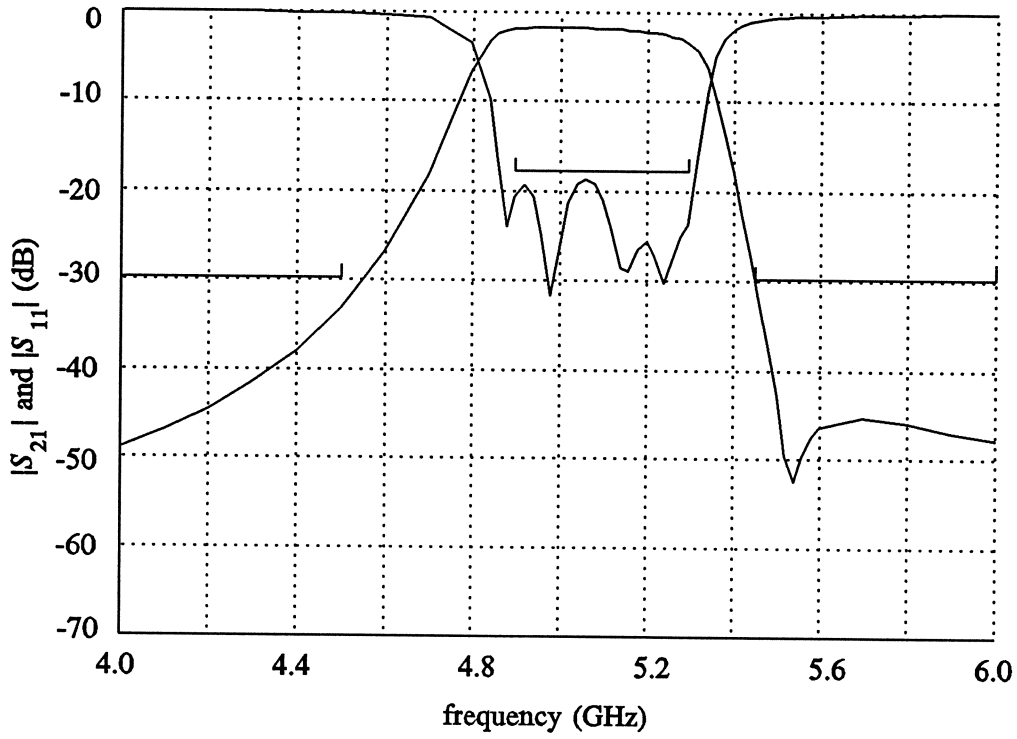

the passband return loss is better than 18.5 dB

Trust Region Aggressive Space Mapping Algorithm
(Bakr, Bandler, Biernacki, Chen and Madsen, 1998)

using $\boldsymbol{f}^{(i)} = \boldsymbol{P}(\boldsymbol{x}_{em}^{(i)}) - \boldsymbol{x}_{os}^{*}$
solve $(\boldsymbol{B}^{(i)T}\boldsymbol{B}^{(i)} + \lambda \boldsymbol{I})\,\boldsymbol{h}^{(i)} = -\boldsymbol{B}^{(i)T}\boldsymbol{f}^{(i)}$ for $\boldsymbol{h}^{(i)}$

this corresponds to minimizing $\left\|\boldsymbol{f}^{(i)} + \boldsymbol{B}^{(i)}\boldsymbol{h}^{(i)}\right\|_2^2$ subject to $\left\|\boldsymbol{h}^{(i)}\right\|_2 \le \delta$ where δ is the size of the trust region

λ, which correlates to δ, can be determined *(Moré et al., 1983)*

single point parameter extraction is performed at the new point $\boldsymbol{x}_{em}^{(i+1)} = \boldsymbol{x}_{em}^{(i)} + \boldsymbol{h}^{(i)}$ to get $\boldsymbol{f}^{(i+1)}$

if $\boldsymbol{f}^{(i+1)}$ satisfies a certain success criterion for the reduction in the l_2 norm of the vector $\boldsymbol{f}$, the point $\boldsymbol{x}_{em}^{(i+1)}$ is accepted and the matrix $\boldsymbol{B}^{(i)}$ is updated using Broyden's update

otherwise a temporary point is generated using $\boldsymbol{x}_{em}^{(i+1)}$ and $\boldsymbol{f}^{(i+1)}$ and is added to the set of points to be used for multi-point parameter extraction

a new $\boldsymbol{f}^{(i+1)}$ is obtained through multi-point parameter extraction

Trust Region Aggressive Space Mapping Algorithm

the last three steps are repeated until a success criterion is satisfied or the step is declared a failure

step failure has two forms

(1) f may approach a limiting value without satisfying the success criterion or
(2) the number of fine model points simulated since the last successful step reaches n+1

Case (1): the parameter extraction is trusted but the linearization used is suspect; the size of the trust region is decreased and a new point $\boldsymbol{x}_{em}^{(i+1)}$ is obtained

Case (2): sufficient information is available for an approximation to the Jacobian of the fine model responses w.r.t. the fine model parameters used to predict the new point $\boldsymbol{x}_{em}^{(i+1)}$

the mapping between the two spaces is exploited in the parameter extraction step by solving

$$\underset{\boldsymbol{x}_{os}}{minimize} \left\| \boldsymbol{R}_{os}(\boldsymbol{x}_{os} + \boldsymbol{B}^{(i)}(\boldsymbol{x} - \boldsymbol{x}_{em}^{(i+1)})) - \boldsymbol{R}_{em}(\boldsymbol{x}) \right\|$$

simultaneously for a set of points $\boldsymbol{x}$

Flow Chart

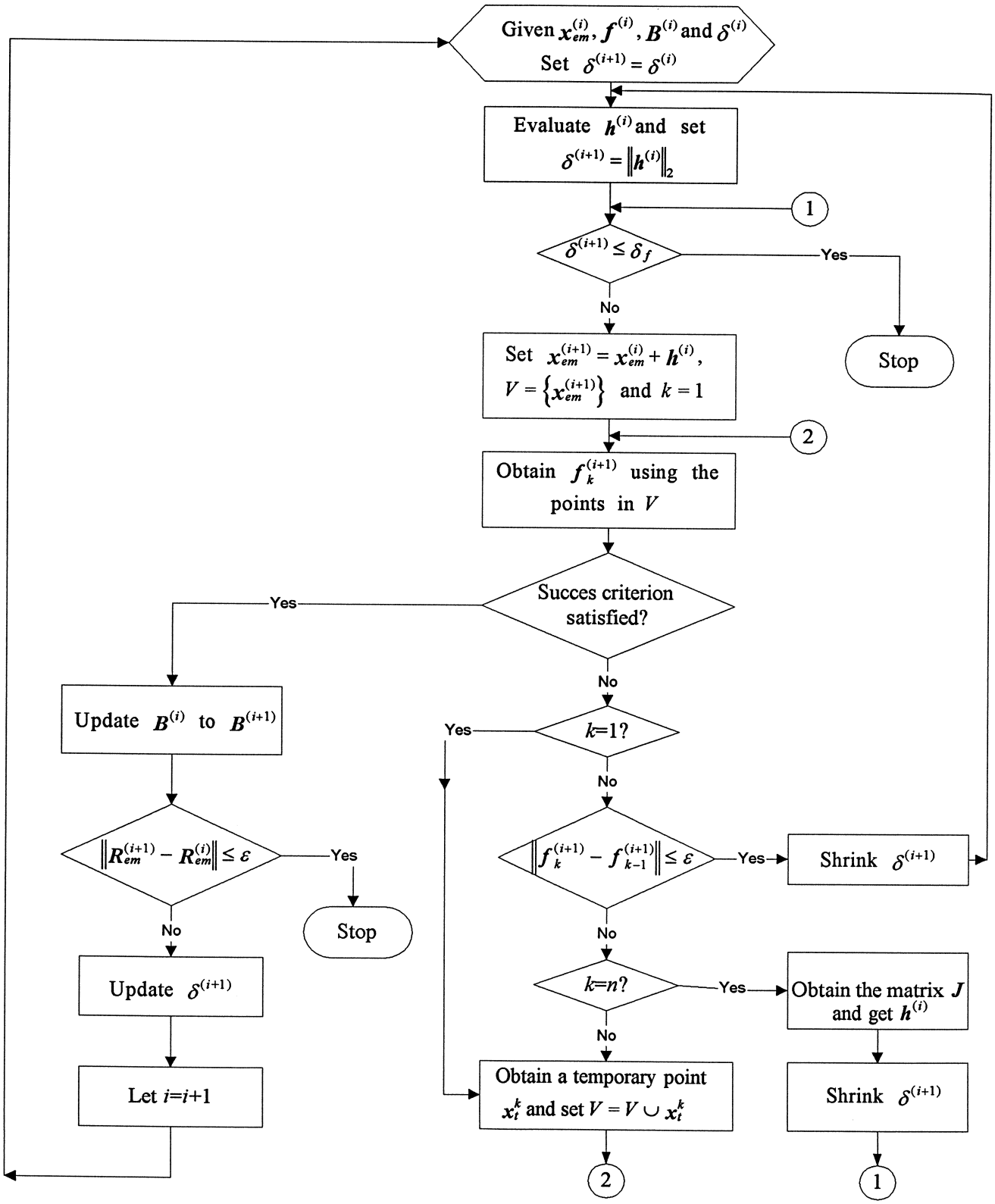

98-14-33

The Current Implementation

The algorithm is currently implemented in MATLAB

OSA90 is used as a platform for the multi-point parameter extraction and for the fine model simulations

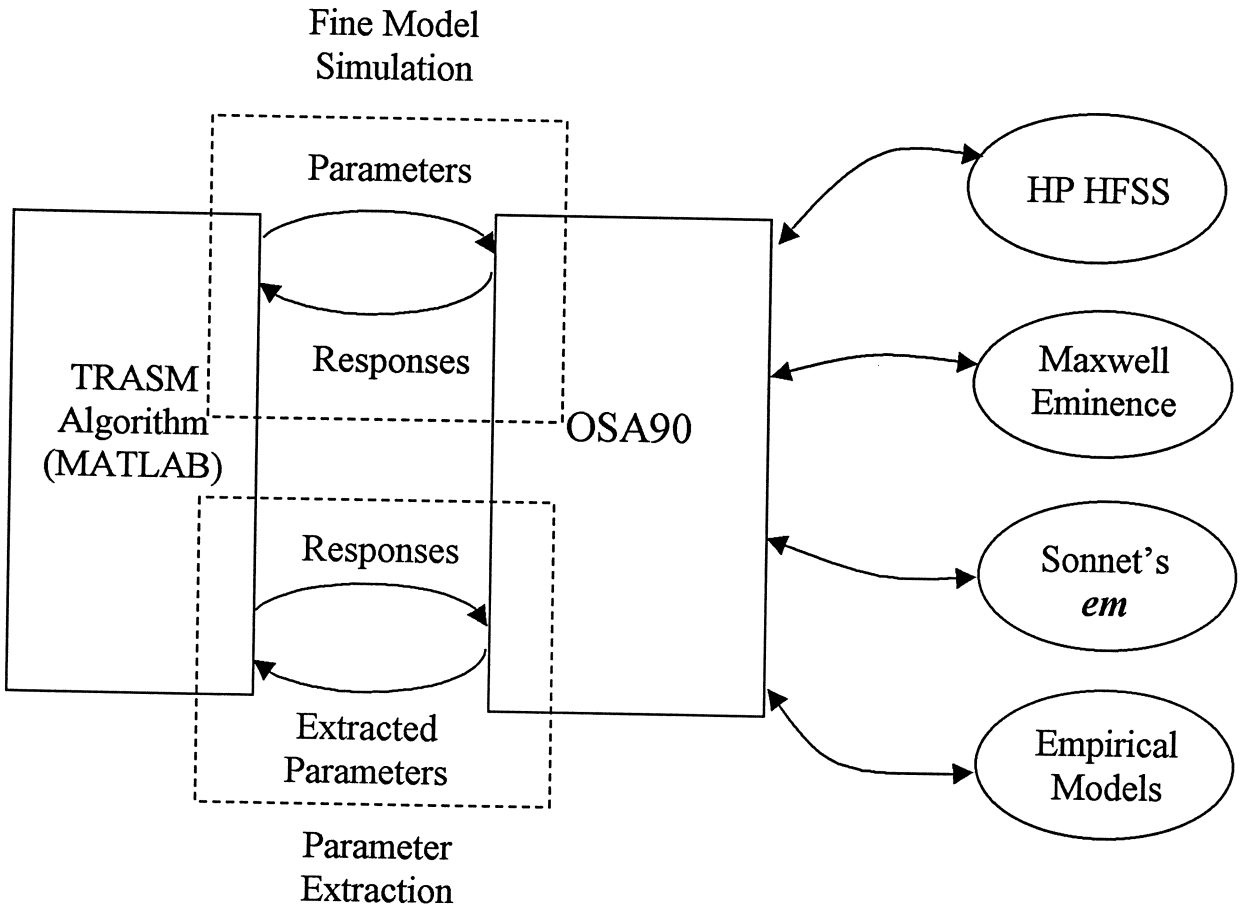

TRASM : Trust Region Aggressive Space Mapping

High-Temperature Superconducting Filter
(*Westinghouse, 1993*)

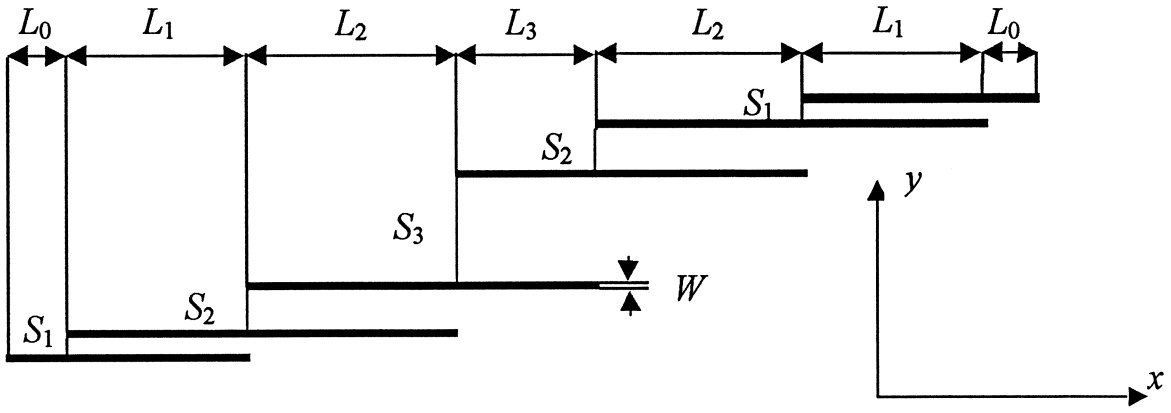

20 mil thick substrate

the dielectric constant is 23.4

passband specifications: $|S_{21}| \geq 0.95$ for 4.008 GHz $\leq f \leq$4.058 GHz

stopband specifications: $|S_{21}| \leq 0.05$ for $f \leq$ 3.967 GHz and 4.099 GHz $\leq f$

designable parameters L_1, L_2, L_3, S_1, S_2 and S_3; L_0 and W are kept fixed

coarse model exploits the empirical models of microstrip lines, coupled lines and open stubs available in OSA90/hope

High-Temperature Superconducting Filter Fine Model

the fine model employs a fine-grid Sonnet ***em*** simulation

the *x* and *y* grid sizes for ***em*** are 1.0 and 1.75 mil

100 elapsed minutes are needed for ***em*** analysis at single frequency on a Sun SPARCstation 10

final design is obtained in 5 TRASM iterations, requiring 8 ***em*** simulations

15 frequency points are used per ***em*** simulation

High-Temperature Superconducting Filter Responses

the optimal coarse model (—) response and the fine model response (o) at the initial and final designs

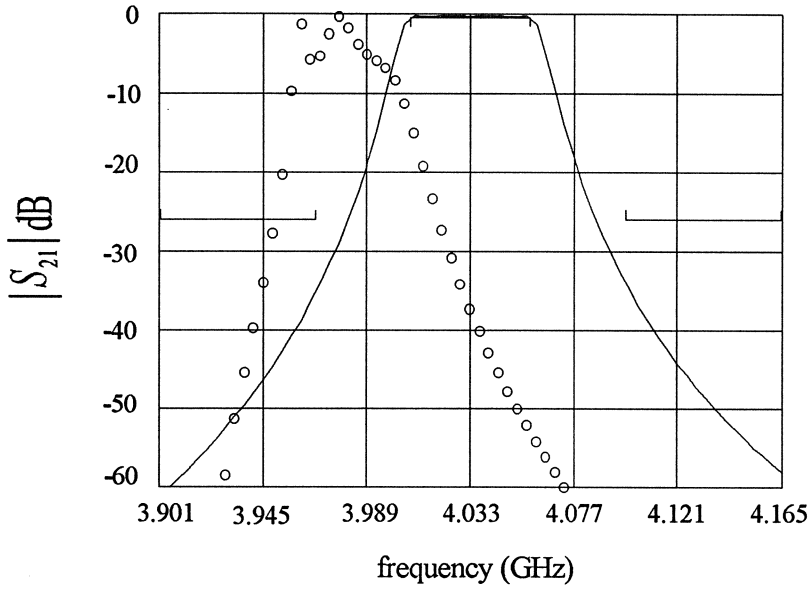

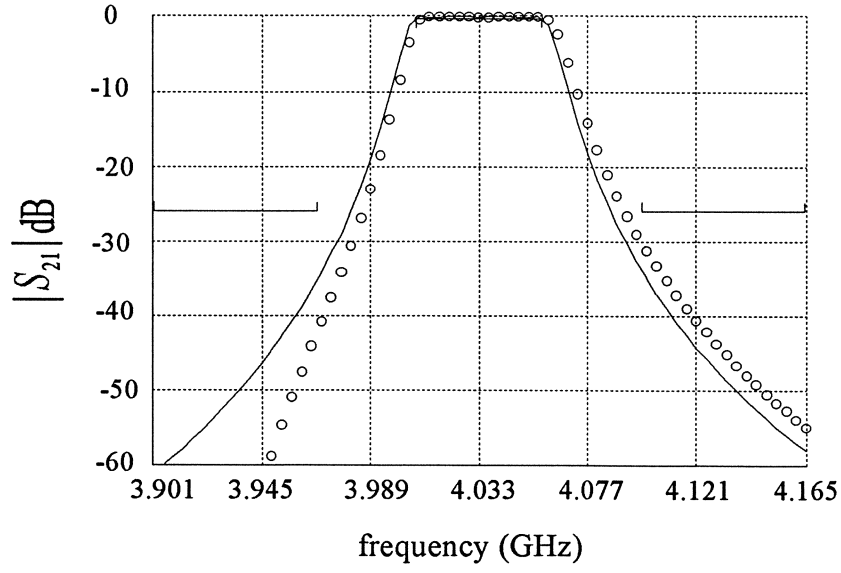

Passband Details for the High-Temperature Superconducting Filter

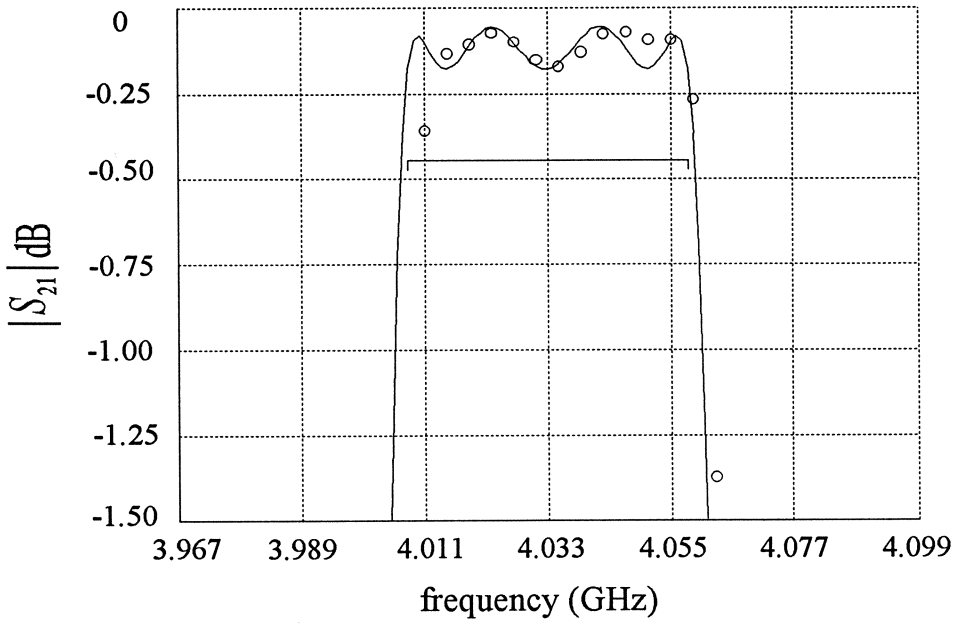

Discussion

Space Mapping is very broadly defined in terms of "coarse" and "fine" models

recent variants of "space mapping" techniques include:

A.M. Pavio, "The electromagnetic analysis and optimization of a broad class of problems using companion models," *Workshop on Automated Circuit Design using Electromagnetic Simulators, IEEE MTT-S Int. Microwave Symp.* (Orlando, FL, 1995).

M.-Q. Lee and S. Nam, "Efficient coupling patterns design of miniaturized dielectric filter using EM simulator and EPO technique," *IEEE MTT-S Int. Microwave Symp. Dig.* (San Francisco, CA, 1996), pp. 737-739.

S. Ye and R.R. Mansour, "An innovative CAD technique for microstrip filter design," *IEEE Trans. Microwave Theory Tech.*, vol. 45, 1997, pp. 780-786.

S. Moreau, S. Gendraud, R. Comte, D. Chaimbault, S. Bila, D. Baillargeat, S. Verdeyme, M. Aubourg and P. Guillon, "Analysis and optimization of microwave filters by the finite element method," *Workshop on State-of-the-art Filter Design using EM and Circuit Simulation Techniques, IEEE MTT-S Int. Microwave Symp.* (Denver, CO, 1997).

S. Bila, D. Baillargeat, S. Verdeyme and P. Guillon, "Automated design of microwave devices using full EM optimization method," *IEEE MTT-S Int. Microwave Symp. Dig.* (Baltimore, MD, 1998), pp. 1771-1774.

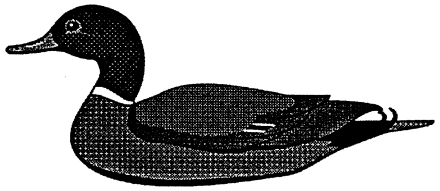

Conclusions

SM promises the accuracy of EM and physical simulation and the speed of circuit-level optimization

accurate but computationally intensive fine model calibrates computationally efficient coarse models

our approach has broad applicability and can profoundly change the way the EM simulators are perceived and used as a CAD tool

a coherent framework combines the power of aggressive SM with decomposition

decomposition further accelerates the coarse model simulation

we present a novel Trust Region Aggressive Space Mapping algorithm for the optimization of microwave circuits

TRASM integrates a trust region methodology with the Aggressive Space Mapping technique

a recursive multi-point parameter extraction step is exploited to improve the uniqueness of the parameter extraction step

multi-point parameter extraction exploits the available information about the mapping between the two spaces to improve the uniqueness of the step

References

J.W. Bandler, R.M. Biernacki, S.H. Chen, P.A. Grobelny and R.H. Hemmers, "Space mapping technique for electromagnetic optimization," *IEEE Trans. Microwave Theory Tech.*, vol. 42, 1994, pp. 2536-2544.

J.W. Bandler, R.M. Biernacki, S.H. Chen, R.H. Hemmers and K. Madsen, "Electromagnetic optimization exploiting aggressive space mapping," *IEEE Trans. Microwave Theory Tech.*, vol. 43, 1995, pp. 2874-2882.

J.W. Bandler, R.M. Biernacki and S.H. Chen, "Fully automated space mapping optimization of 3D structures," *IEEE MTT-S Int. Microwave Symp. Dig.* (San Francisco, CA, 1996), pp. 753-756.

J.W. Bandler, R.M. Biernacki, S.H. Chen and Y.F. Huang, "Design optimization of interdigital filters using aggressive space mapping and decomposition," *IEEE Trans. Microwave Theory Tech.*, vol. 45, 1997, pp. 761-769.

J.W. Bandler, R.M. Biernacki, S.H. Chen and P.A. Grobelny, "Optimization technology for nonlinear microwave circuits integrating electromagnetic simulations," *Int. J. Microwave and mm-Wave CAE*, vol. 7, 1997, pp. 6-28.

J.W. Bandler, R.M. Biernacki, S.H. Chen and D. Omeragić, "Space mapping optimization of waveguide filters using finite element and mode-matching electromagnetic simulators," *IEEE MTT-S Int. Microwave Symp. Dig.* (Denver, CO, 1997), pp. 635-638.

M.H. Bakr, J.W. Bandler, R.M. Biernacki, S.H. Chen and K. Madsen, "A trust region aggressive space mapping algorithm for EM optimization," *IEEE MTT-S Int. Microwave Symp. Dig.* (Baltimore, MD, 1998), pp 1759-1762.

Space Mapping Optimization of Waveguide Filters Using Finite Element and Mode-Matching Electromagnetic Simulators

John W. Bandler *

Simulation Optimization Systems Research Laboratory and Department of Electrical and Computer Engineering, McMaster University, Hamilton, Canada L8S 4L7

Radoslaw M. Biernacki and Shao Hua Chen

HP EEsof Division, Hewlett-Packard Company, 1400 Fountaingrove Parkway, Santa Rosa, CA 95403-1799

Dževat Omeragić

Schlumberger-Houston Product Center, 110 Schlumberger Drive, PO Box 2175, Houston, TX 77252-2175

ABSTRACT

For the first time in design optimization of microwave circuits, the aggressive space mapping (SM) optimization technique is applied to automatically align electromagnetic (EM) models based on hybrid mode-matching/network theory simulations with models based on finite-element (FEM) simulations. SM optimization of an H-plane resonator filter with rounded corners illustrates the advantages as well as the challenges of the approach. The parameter extraction phase of SM is given special attention. The impact of selecting responses and error functions on the convergence and uniqueness of parameter extraction is discussed. A statistical approach to parameter extraction involving ℓ_1 and penalty concepts facilitates a key requirement by SM for uniqueness and consistency. A multi-point parameter extraction approach to sharpening the solution uniqueness and improving the SM convergence is also introduced. Once the mapping is established, the effects of manufacturing tolerances are rapidly estimated with the FEM accuracy. SM has also been successfully applied to optimize waveguide transformers using two hybrid mode-matching/network theory models: a coarse one using very few modes and a fine model using many modes to represent discontinuities.

---

* Also affiliated with Bandler Corporation, P.O. Box 8083, Dundas, Ontario, Canada L9H 5E7.

All authors were formerly affiliated with the Simulation Optimization Systems Research Laboratory and the Department of Electrical and Computer Engineering, McMaster University, Hamilton, Ontario, Canada L8S 4L7, and with Optimization Systems Associates Inc., Dundas, Ontario, Canada, before acquisition by HP EEsof.

I. INTRODUCTION

Direct exploitation of electromagnetic (EM) simulators in the optimization of arbitrarily shaped 3D structures at high frequencies is crucial for first-pass success CAD [1,2]. Recently, we reported successful automated design optimization of 3D structures using FEM simulations [1,3].

The objective of space mapping (SM) [3-5] is to avoid direct optimization of computationally intensive models. In this paper, for the first time, the aggressive space mapping (ASM) optimization is applied to automatically align the results of two separate EM simulation systems. The RWGMM library [6,7] of waveguide models based on the mode matching (MM) technique [6-8] is used for fast/coarse simulations in the so-called optimization space X_{os}. The library is linked to the network theory optimizers of OSA90/hope [9]. Ansoft's Maxwell Eminence or HP HFSS [10] (both widely known simply as HFSS) simulations accessed through Empipe3D [9] serve as the "fine" model in the so-called X_{em} space. The SM procedure executes all these systems concurrently.

Both RWGMM and HFSS provide accurate EM analysis. RWGMM is computationally efficient in its treatment of a variety of predefined geometries. It is ideally suited for modeling complex waveguide structures that can be decomposed into the available library building blocks. FEM-based simulators [11,12] such as HFSS [10,12] are able to analyze arbitrary shapes, but they are computationally very intensive.

ASM optimization of an H-plane resonator filter with rounded corners is carried out. These rounded corners make RWGMM simulations somewhat less accurate. Once the mapping is established, subsequent Monte Carlo analysis of manufacturing tolerances exploits the FEM-based space mapped model with the speed of the MM/network theory simulator. To illustrate the flexibility in selecting the X_{em} and X_{os} models, SM is also applied to optimize waveguide transformers using two hybrid MM/network theory models: a coarse one using very few modes and a fine model using many modes to represent the discontinuities.

The parameter extraction phase is the key to effective SM optimization. The methodology, however, is sensitive to nonunique solutions or local minima inconsistent with the aimed solution.

An in-depth study of this phenomenon is presented and ways to overcome such problems are addressed. We show that, at the expense of increased simulations of the fast coarse model, we can satisfy the requirement for uniqueness and consistency. We investigate how the choice of error functions influences the convergence and uniqueness of parameter extraction. We offer a solution based on statistical parameter extraction involving a powerful ℓ_1 algorithm and penalty function concepts. We introduce a multi-point parameter extraction approach to sharpening the solution uniqueness and improving the SM convergence in the automated design of a waveguide transformer.

II. FULLY AUTOMATED SPACE MAPPING OPTIMIZATION

By inspecting the steps involved in SM optimization [4,5], we recognize that the parameter extraction process is explicitly dependent on the specific models involved. In the flow diagram shown in Fig. 1 the MM waveguide library serves as the X_{os} model and the FEM simulator as the X_{em} model. SM optimization starts with conventional design optimization of the coarse model: MM optimization, leading to the optimal parameter values x_{os}^*. Those parameter values determine the starting point for the SM update loop which can be implemented within a generic layer of iterations. Following this guideline, the ASM strategy has been fully automated using a two-level Datapipe architecture [9,13]. Fig. 1 illustrates the two iterative loops involving two different sets of variables. The outer loop updates the optimization variables x_{em} of the X_{em} model based on the latest mapping. Within each SM iteration the inner, dotted block, extracts the parameters x_{os} of the X_{os} model while x_{em} is held constant. The parameter extraction process is carried out through auxiliary optimization iterations performed exclusively within the X_{os} model. The goal of parameter extraction is to match the reference data: the fine model responses $R_{em}(x_{em})$ obtained from FEM simulation. The outer SM iterations terminate when the coarse model parameters x_{os} approach x_{os}^*. The Datapipe techniques allow us to carry out the nested optimization loops in two separate processes while maintaining a functional link between their results (e.g., the next increment to x_{em} is a function of the results of parameter extraction).

Within the inner loop of parameter extraction, we can also utilize the Datapipe technique

to connect external model simulators to the optimization environment (e.g., the Empipe3D system is a specialized Datapipe interface to HFSS). Further details of the parameter extraction step will be elaborated in Sections IV through VII.

III. SPACE MAPPING OPTIMIZATION USING MM/NETWORK THEORY AND FEM

We address the design of the H-plane resonator filter with rounded corners shown in Fig. 2(a). The waveguide cross-section is 15.8 × 7.9 mm, while the thickness of the irises is t = 0.4 mm. The radius of the corners is R = 1 mm. The iris and resonator dimensions d_1, d_2, l_1, l_2 are selected as the optimization variables.

First, minimax optimization of the X_{os} model (Fig. 2(b)) is performed exploring the waveguide MM library with the following specifications provided by Arndt [14]

$$|S_{21}| < -35 \text{ dB} \quad \text{for} \quad 13.5 \text{ GHz} \le f \le 13.6 \text{ GHz}$$

$$|S_{11}| < -20 \text{ dB} \quad \text{for} \quad 14.0 \text{ GHz} \le f \le 14.2 \text{ GHz}$$

$$|S_{21}| < -35 \text{ dB} \quad \text{for} \quad 14.6 \text{ GHz} \le f \le 14.8 \text{ GHz}$$

where f represents the frequency.

The minimax solution x_{os}^* is d_1 = 6.04541, d_2 = 3.21811, l_1 = 13.0688 and l_2 = 13.8841. It yields the target response for SM. At this point, the fine model X_{em} is analyzed by FEM using the x_{os}^* values. The corresponding responses of the FEM model and hybrid mode-matching/network theory models are shown in Fig. 3. Focusing on the passband, we treat responses in the region 13.96 ≤ f ≤ 14.24 GHz. The passband responses of both models at the point x_{os}^* are shown in Fig. 4. Some discrepancy is evident.

Tables I and II summarize the steps of the successful ASM optimization. The solution, corresponding to point d_1 = 6.17557, d_2 = 3.29058, l_1 = 13.0282 and l_2 = 13.8841, shown in Fig. 5 was obtained after only four HFSS simulations, each with only fifteen frequency points. The SM results were verified by directly optimizing the H-plane filter using Empipe3D driving the HFSS solver. Essentially the same solution was found.

IV. ERROR FUNCTIONS FOR PARAMETER EXTRACTION

A natural choice in formulating the objective function for the parameter extraction phase of SM is to use the responses for which the specifications are given. In the case of the H-plane filter they are $|S_{11}|$ in dB at selected passband frequencies, and thus the individual errors could be formed by subtracting $|S_{11}|$ in dB from the corresponding specifications (also in dB). A good choice of the objective function for parameter extraction is the ℓ_1 norm of the error vector. We are, however, free to use any error formulation that could allow us to align the models. The results reported in the preceding section were obtained using $|S_{21}|$. With that formulation the SM iterations proceeded flawlessly. No difficulty in the parameter extraction phase could be noticed.

We also took a close look at the ℓ_1 objective function using some other error formulations. Fig. 6 shows two cases of the ℓ_1 norm for parameter extraction during the second iteration of SM. They are determined in the vicinity of the starting point w.r.t. two selected parameters: the iris openings d_1 and d_2. Fig. 6(a) corresponds to the error definition in terms of $|S_{11}|$ (dB). It exhibits many local minima and provides us with an excellent opportunity to investigate the uniqueness of the parameter extraction phase in SM, as well as to improve its robustness. When the errors are defined in terms of $|S_{21}|$ (as was used to obtain the SM results reported in Section III), the corresponding function surface becomes significantly smoother, as shown in Fig. 6(b).

V. STATISTICAL PARAMETER EXTRACTION

We propose an automated statistical parameter extraction procedure to overcome potential pitfalls arising out of inaccurate or nonunique solutions. First, we perform standard ℓ_1 parameter extraction [15] of the X_{os} model starting from x_{os}^*. If the resulting response matches well the X_{em} model response (the ℓ_1 error is small enough) we continue with the SM iterations. Otherwise we turn to statistical exploration of the X_{os} model.

The key to statistical parameter extraction is to establish the exploration region. Unlike general purpose random/global optimization approaches we want to carry out local statistical exploration as deemed suitable for SM. To this end we take advantage of the fact that during the

SM iterations the desired parameter extraction solutions should rapidly approach x_{os}^{*} in the X_{os} space (see [5,16]).

Consider the kth SM iteration. When the current mapping ($x_{os} = P^{(k-1)}(x_{em})$) is applied to the current point in the X_{em} model space we arrive at x_{os}^{*}, since that point has been determined by the inverse mapping ($x_{em}^{k} = P^{(k-1)^{-1}}(x_{os}^{*})$, see [5]) . The fact that the new point (to be extracted) differs from x_{os}^{*} is not only a basis for modifying the mapping, but also quantitatively establishes the degree of inconsistency w.r.t. the existing mapping. This allows us to define an appropriate exploration region. If, for the kth step, we define the multidimensional interval δ as

$$\delta = x_{os}^{k-1} - x_{os}^{*} \tag{1}$$

the statistical exploration may be limited to the region defined by

$$x_{osi} \in [\ x_{osi}^{*} - 2 \mid \delta_i \mid,\ x_{osi}^{*} + 2 \mid \delta_i \mid\ ] \tag{2}$$

Another choice for the exploration region could be an elliptical multidimensional domain with semiaxes $2 \mid \delta_i \mid$ defined by

$$\sum_{i} (\ x_{osi} - x_{osi}^{*}\ )^2 / \mid \delta_i \mid^2 \leq 4 \tag{3}$$

A set of N_s starting points is then statistically generated within the region (2) or (3) and N_s parameter extraction optimizations are carried out. These parameter extractions are further aided by a penalty function [16] of the form

$$\lambda \parallel x_{os}^{k} - x_{os}^{*} \parallel \tag{4}$$

augmenting the ℓ_1 objective function. In the case of multiple minima this penalty term forces the optimizer to select local minima closer to x_{os}^{*}. The resulting solutions (expected to be multiple) are then categorized into clusters and ranked according to the achieved values of the error function. Finally, the penalty term is removed and the process repeated in order to focus the clustered solution(s). Absence of the penalty term brings the solution point to the "true" local minimum, thus removes "fuzziness" which may occur when the penalty term is used. The aforementioned steps are briefly summarized by the following algorithm and illustrated in the flow chart shown in Fig. 7.

Algorithm

Step 1 Initialize the exploration region. (2) or (3) can be used in the second and all subsequent SM iterations.

Step 2 Generate N_s random starting points.

Step 3 Perform N_s parameter extractions from the N_s starting points including the penalty function (4).

Step 4 Categorize the solutions. Select one or more best clusters of the solutions.

Step 5 Focus the clusters by reoptimizing without the penalty term.

This approach has been automated by adding one more level in the Datapipe architecture described in Section II. Furthermore, it can be parallelized since the N_s parameter extractions considered are carried out independently.

VI. PARAMETER EXTRACTION OF THE H-PLANE FILTER

We use the H-plane filter example to investigate the statistical parameter extraction outlined in the preceding section. To verify the robustness of the approach we have used the ℓ_1 objective function with various definitions of individual errors. The case when the individual errors are defined in terms of $|S_{11}|$ in dB was already illustrated by Fig. 6(a) for the second iteration of ASM.

Fig. 8 presents the variation of the MM/network theory model response in the vicinity of the starting point. Responses are computed along the direction of the first ASM step, defined by points $\boldsymbol{x}_{os}^{*}$ and $\boldsymbol{x}_{os}^{1}$. Although the responses shown in Fig. 8 are all smooth when only one parameter is varied, the ℓ_1 objective function defined in terms of $|S_{11}|$ (dB) has multiple minima, hence the optimizer may terminate at an undesirable solution.

A set of 100 starting points is statistically generated from a uniform distribution within the range (2). The distances between the point $\boldsymbol{x}_{os}^{*}$ and the random starting points are depicted in Fig. 9(a). The corresponding 100 ℓ_1 parameter extraction optimizations with the penalty term (4) are then performed from these points. The distances between $\boldsymbol{x}_{os}^{*}$ and the solutions of parameter extraction optimizations based on the errors defined in terms of $|S_{11}|$ in dB are shown in Fig. 9(b).

The solutions are scattered, confirming our observation that the ℓ_1 objective function has many local minima, as illustrated in Fig. 6(a). Among the 100 solutions a cluster of 15 points is detected. Fig 9(b) provides some insight into the process of cluster selection: all the points within the cluster exhibit a similar distance from x_{os}^*. A deciding factor, however, for a point to belong to the cluster is its distance from other points in the cluster. Therefore, only a subset of all the points with similar bar sizes can actually form the cluster. Furthermore, depending on the cluster "diameter", some points actually selected for the cluster may appear in Fig. 9(b) as outliers. Once the cluster is identified, removing the penalty term and restarting the parameter extraction process from all its points further sharpens the solution. Here, all the points within the cluster converge to the same solution, as depicted in Fig. 9(c). Figs. 10 and 11 show the responses of the X_{os} model at those 100 points before and after parameter extraction, respectively. Fig. 12 displays the responses corresponding to the cluster of 15 points which converged to the same solution, validating successful parameter extraction.

Fig. 13 illustrates the impact of the penalty term. When the penalty term is not used, only 10 parameter extractions lead to the desired solution, as shown in Fig. 13(a). Here $|S_{11}|$ in dB is used to define the errors. Figs. 13(b) and 13(c) present the results when the errors are defined in terms of $|S_{21}|$. Without the penalty term the procedure leads to 52 successful parameter extractions (Fig. 13(a)); adding the penalty term (4) yields 100% success (Fig. 13(c)). The corresponding responses at the solutions are shown in Fig. 14. Note that for this case of using $|S_{21}|$ in error definition, starting from the default point, x_{os}^*, yields the correct result. This explains the flawless SM iterations reported in Section III.

The use of $|S_{11}|$ in dB amplifies errors in the computed parameter S_{11}. The relative error for this case is higher since $|S_{11}|$ is small in the pass-band region. We have shown that even for such numerically sensitive cases our new procedure yields successful parameter extractions.

VII. MULTI-POINT PARAMETER EXTRACTION

We use the two-section waveguide transformer example [17] to further investigate the impact of

parameter extraction uniqueness on the convergence of the SM iterations. We observe symmetrical ℓ_1 contours with respect to the two section lengths L_1 and L_2, as illustrated in Fig. 15, with two local minima. Consequently the result of parameter extraction is not unique. The impact can be seen in the trace depicted in Fig. 16, where the SM steps oscillate around the solution due to the "fuzzy" results of parameter extraction.

We introduce a multi-point parameter extraction approach to sharpen the parameter extraction result. Instead of minimizing

$$\| \boldsymbol{R}_{os}(\boldsymbol{x}_{os}^{i}) - \boldsymbol{R}_{em}(\boldsymbol{x}_{em}^{i}) \| \tag{5}$$

at a single point, we find $\boldsymbol{x}_{os}^{i}$ by minimizing

$$\| \boldsymbol{R}_{os}(\boldsymbol{x}_{os}^{i} + \Delta \boldsymbol{x}) - \boldsymbol{R}_{em}(\boldsymbol{x}_{em}^{i} + \Delta \boldsymbol{x}) \| \tag{6}$$

where $\Delta \boldsymbol{x}$ represents a small perturbation to $\boldsymbol{x}_{os}^{i}$ and $\boldsymbol{x}_{em}^{i}$. By simultaneously minimizing (6) with a selected set of $\Delta \boldsymbol{x}$, we hope to improve the uniqueness of the parameter extraction process. Conceptually, we are attempting to match not only the response, but also a first-order change in the response with respect to small perturbations in the parameter values. We have exploited a similar concept in multi-circuit modeling [18]. Fig. 17 depicts the ℓ_1 contours for multi-point parameter extraction of the two-section transformer, which indicates a unique solution. We used three points (i.e., original $\boldsymbol{x}_{em}^{i}$ and two perturbations in L_1 and L_2 directions) for parameter extraction. The corresponding SM trace is shown in Fig. 18, where the convergence of the SM iterations is dramatically improved. The price we may have to pay for such an improvement might be the increased number of $\boldsymbol{X}_{em}$ simulations required: although more $\boldsymbol{X}_{em}$ model simulations are needed in parameter extraction, the overall number of iterations may be reduced.

VIII. TOLERANCE SIMULATION USING SPACE MAPPING

Once the SM is established, it provides not only the design solution (parameter values), but also an efficient means for modeling the circuit in the vicinity of the solution, in particular for statistical analysis. We can map parameter spreads in the $\boldsymbol{X}_{em}$ space to the corresponding incremental changes in the $\boldsymbol{X}_{os}$ space. Consequently, using the space-mapped $\boldsymbol{X}_{os}$ model we can rapidly estimate the

effects of tolerances, benefitting at the same time from the accuracy of the X_{em} model.

As an illustration, consider Monte Carlo analysis of the H-plane filter using FEM as the X_{em} model and the hybrid MM/network theory simulations as the X_{os} model (Section III). Parameter values are assumed to be normally distributed with a standard deviation of 0.0333% (of the order of 1 μm). The results of Monte Carlo analysis are shown in Fig. 19. For a specification on $|S_{11}|$ < -15 dB in the passband the yield, estimated from 200 outcomes, is 88.5%. When the standard deviations is increased to 0.1% the yield drops to 19% for 200 outcomes. The CPU time required for the entire Monte Carlo analysis with 200 outcomes is comparable to just a single full FEM simulation.

IX. SPACE MAPPING OPTIMIZATION USING COARSE AND FINE MM MODELS

To illustrate the flexibility in selecting the X_{em} and X_{os} models, consider SM between two hybrid MM/network theory models: a coarse one using very few modes and a fine model using many modes to represent the discontinuities. These two models are applied here to optimize waveguide transformers, specifically three-section and seven-section transformers described in [17]. In this application, SM enhances the efficiency of the MM-based optimization.

Sharp corners are assumed here which makes the MM models with large numbers of modes very accurate. The RWGMM library allows the designer to implicitly control the number of higher-order modes which are used to model waveguide transition components. Increasing the number of modes improves accuracy at the expense of higher computational cost.

For the coarse model, we use just one mode. For the fine model, we include all the modes below the cut-off frequency of 50 GHz. The actual number of modes included in the fine model is automatically determined by the RWGMM program. As the lengths and heights of the waveguide sections are optimized, the number of modes included in the fine model varies from 49 to 198 for the three-section and at least 180 for the seven-section transformer. The optimized solutions shown in Figs. 20 and 21 require two and fourteen SM iterations, respectively.

X. CONCLUSIONS

We have presented new applications of aggressive space mapping to filter optimization using network theory, mode-matching and finite element simulation techniques. A statistical approach to parameter extraction incorporating the ℓ_1 error and penalty function concepts has effectively addressed the requirement of a unique and consistent solution. We have introduced a multi-point approach to enhancing the prospect of a unique parameter extraction solution in the space mapping process. SM provides a feasible means for Monte Carlo analysis of microwave circuits that could be carried out with the accuracy of FEM simulations. We have also demonstrated SM optimization based on coarse and fine MM models with different numbers of modes.

ACKNOWLEDGEMENT

The authors would like to thank HP EEsof Division of Santa Rosa, CA, Ansoft Corp. of Pittsburgh, PA, and Prof. Fritz Arndt of the University of Bremen, Germany, for making their respective software available for this work. This work was carried out and supported in part by Optimization Systems Associates Inc. before acquisition by HP EEsof, and supported in part by the Natural Sciences and Engineering Research Council of Canada under Grants OGP0007239, OGP0042444 and STR0167080, through the Micronet Network of Centres of Excellence, and through an Industrial Research Fellowship granted to Dr. Omeragić.

REFERENCES

1. J.W. Bandler, R.M. Biernacki, S.H. Chen, L.W. Hendrick and D. Omeragić, "Electromagnetic optimization of 3D structures," *IEEE Trans. Microwave Theory Tech.*, vol. 45, 1997, pp. 770-779.

2. F. Arndt, S.H. Chen, W.J.R. Hoefer, N. Jain, R.H. Jansen, A.M. Pavio, R.A. Pucel, R. Sorrentino and D.G. Swanson, Jr., *Automated Circuit Design using Electromagnetic Simulators*. Workshop WMFE (J.W. Bandler and R. Sorrentino, Organizers and Chairmen), IEEE MTT-S Int. Microwave Symp., Orlando, FL, May 1995.

3. J.W. Bandler, R.M. Biernacki and S.H. Chen, "Fully automated space mapping optimization of 3D structures," *IEEE MTT-S Int. Microwave Symp. Dig.*, (San Francisco, CA, June 1996), pp. 753-756.

4. J.W. Bandler, R.M. Biernacki, S.H. Chen, P.A. Grobelny and R.H. Hemmers, "Space

mapping technique for electromagnetic optimization," *IEEE Trans. Microwave Theory Tech.*, vol. 42, 1994, pp. 2536-2544.

5. J.W. Bandler, R.M. Biernacki, S.H. Chen, R.H. Hemmers and K. Madsen, "Electromagnetic optimization exploiting aggressive space mapping," *IEEE Trans. Microwave Theory Tech.*, vol. 43, 1995, pp. 2874-2882.

6. T. Sieverding, U. Papziner, T. Wolf and F. Arndt, "New mode-matching building blocks for common circuit CAD programs," *Microwave Journal*, vol. 36, pp. 66-79, July 1993.

7. F. Arndt, T. Sieverding, T. Wolf and U. Papziner, "Optimization-oriented design of rectangular and circular waveguide components using efficient mode-matching simulators in commercial circuit CAD tools," *Int. J. Microwave and Millimeter-Wave Computer-Aided Engineering*, vol. 7, 1997, pp. 37-51.

8. F. Alessandri, M. Dionigi and R. Sorrentino, "A fullwave CAD tool for waveguide components using a high speed direct optimizer," *IEEE Trans. Microwave Theory Tech.*, vol. 43, 1995, pp. 2046-2052.

9. *OSA90/hope*™ and *Empipe3D*™, formerly Optimization Systems Associates Inc., P.O. Box 8083, Dundas, Ontario, Canada L9H 5E7, now HP EEsof Division, Hewlett-Packard Company, 1400 Fountaingrove Parkway, Santa Rosa, CA 95403-1799.

10. *Maxwell Eminence*, Ansoft Corporation, Four Station Square, Suite 660, Pittsburgh, PA 15219, USA. *HFSS Version 4*, HP EEsof Division, Hewlett-Packard Company, 1400 Fountaingrove Parkway, Santa Rosa, CA 95403-1799.

11. P.P. Silvester and G. Pelosi, *Finite elements for wave electromagnetics, methods and techniques*. New York: IEEE Press, 1994.

12. J.-F. Lee, D.-K. Sun and Z.J. Cendes, "Full-wave analysis of dielectric waveguides using tangential vector finite elements," *IEEE Trans. Microwave Theory Tech.*, vol. 39, 1991, pp. 1262-1271.

13. J.W. Bandler, R.M. Biernacki, S.H. Chen and P.A. Grobelny, "Optimization technology for nonlinear microwave circuits integrating electromagnetic simulations," *Int. J. Microwave and Millimeter-Wave Computer-Aided Engineering*, vol. 7, 1997, pp. 6-28.

14. F. Arndt, Microwave Department, University of Bremen, P.O. Box 330 440, Kufsteiner Str., NW1, D-28334 Bremen, Germany, 1996, *private communications.*

15. J.W. Bandler, S.H. Chen and S. Daijavad, "Microwave device modeling using efficient ℓ_1 optimization: a novel approach," *IEEE Trans. Microwave Theory Tech.*, vol. MTT-34, 1986, pp. 1282-1293.

16. J.W. Bandler, R.M. Biernacki, S.H. Chen and Y.F. Huang, "Design optimization of interdigital filters using aggressive space mapping and decomposition," *IEEE Trans. Microwave Theory Tech.*, 1997, vol. 45, pp. 761-769.

17. J.W. Bandler, "Computer optimization of inhomogeneous waveguide transformers," *IEEE Trans. Microwave Theory Tech.*, vol. MTT-17, 1969, pp. 563-571.

18. J.W. Bandler and S.H. Chen, "Circuit optimization: the state of the art," *IEEE Trans. Microwave Theory Tech.*, vol. 36, 1988, pp. 424-443.

TABLE I

SPACE MAPPING OPTIMIZATION OF THE H-PLANE FILTER

Point	d_1	d_2	l_1	l_2
x_{em}^1	6.04541	3.21811	13.0688	13.8841
x_{em}^2	6.19267	3.32269	12.9876	13.8752
x_{em}^3	6.17017	3.29692	13.0536	13.8812
x_{em}^4	6.17557	3.29058	13.0282	13.8841

Values of all optimization variables are in mm.

TABLE II

PARAMETER EXTRACTION RESULTS FOR SPACE MAPPING OPTIMIZATION

Point	d_1	d_2	l_1	l_2	$\| x_{os}^* - x_{os}^i \|$
x_{os}^1	5.89815	3.11353	13.1500	13.8930	0.19823
x_{os}^2	6.07714	3.25445	12.9757	13.8757	0.10519
x_{os}^3	6.03531	3.22421	13.1119	13.8806	0.04482
x_{os}^4	6.04634	3.22042	13.0618	13.8831	0.00750

Values of all optimization variables are in mm.

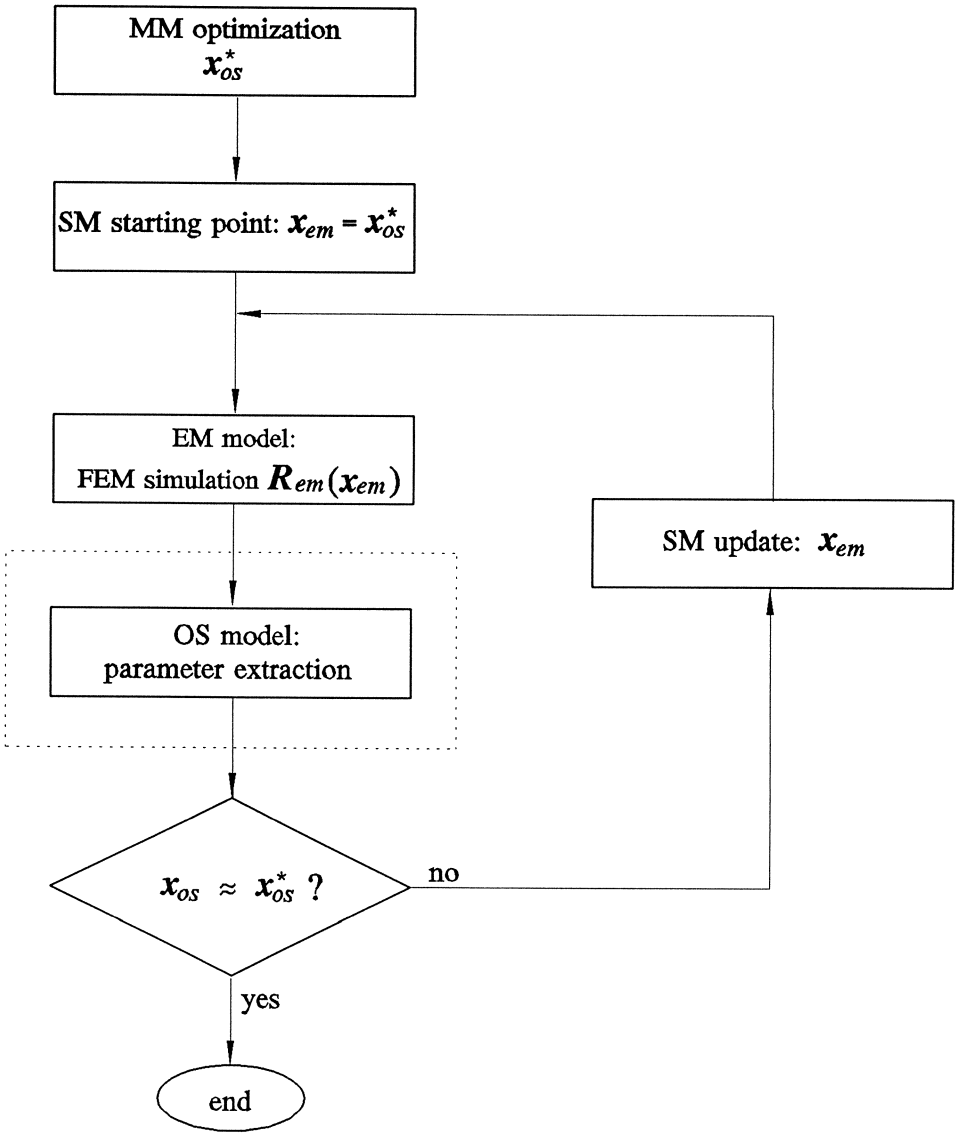

Fig. 1. Flow diagram of the SM optimization procedure concurrently exploiting the hybrid MM/network theory and FEM techniques and statistical parameter extraction.

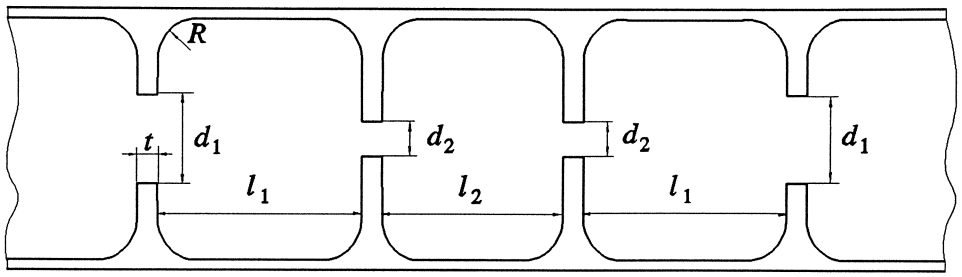

(*a*)

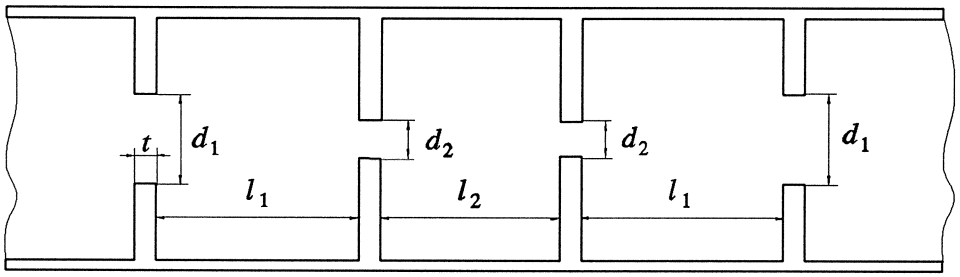

(*b*)

Fig. 2. Structures for SM optimization: (*a*) X_{em} model, for analysis by FEM; (*b*) X_{os} model, for hybrid MM/network theory. The waveguide cross-section is 15.8 × 7.9 mm, the thickness of the irises is t = 0.4 mm. Optimization variables are iris openings d_1, d_2 and resonator lengths l_1, l_2.

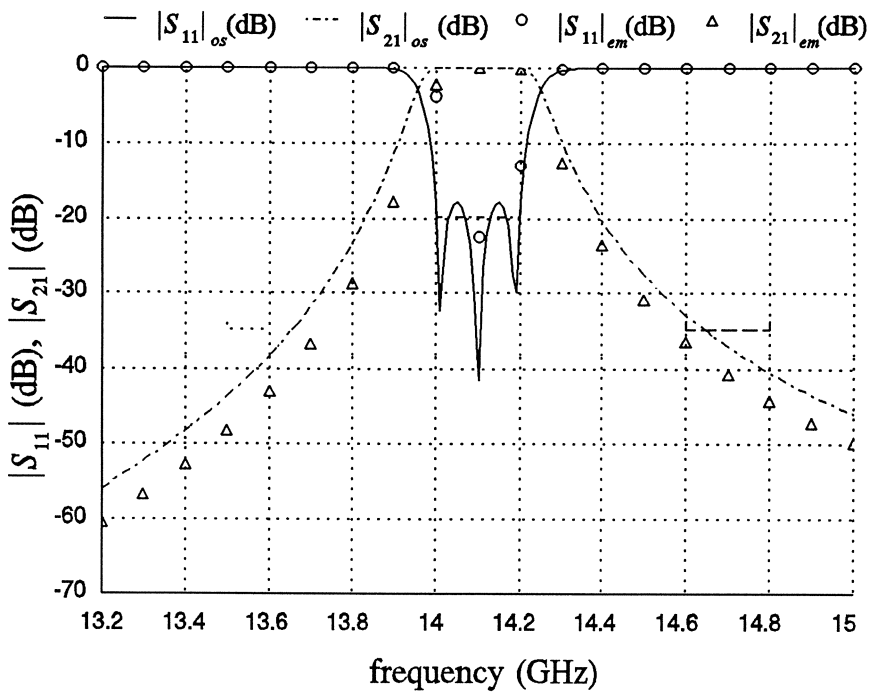

Fig. 3. Magnitudes of S_{11} and S_{21} of the H-plane filter before SM optimization, as simulated using RWGMM (curves) and by HFSS (points).

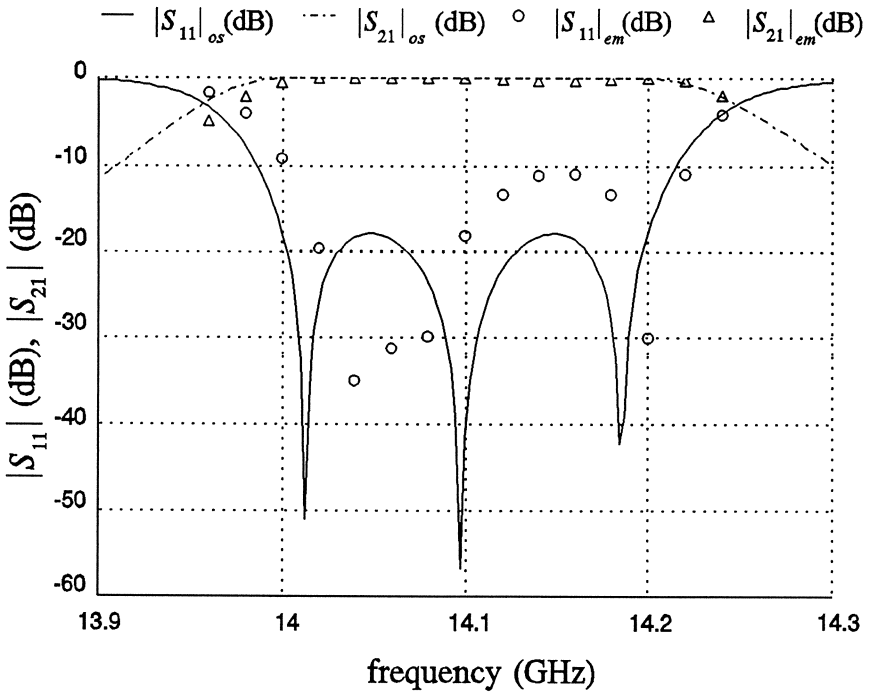

Fig. 4. Magnitudes of S_{11} and S_{21} of the H-plane filter before SM optimization, as simulated using RWGMM (curves) and by HFSS (points); passband detail.

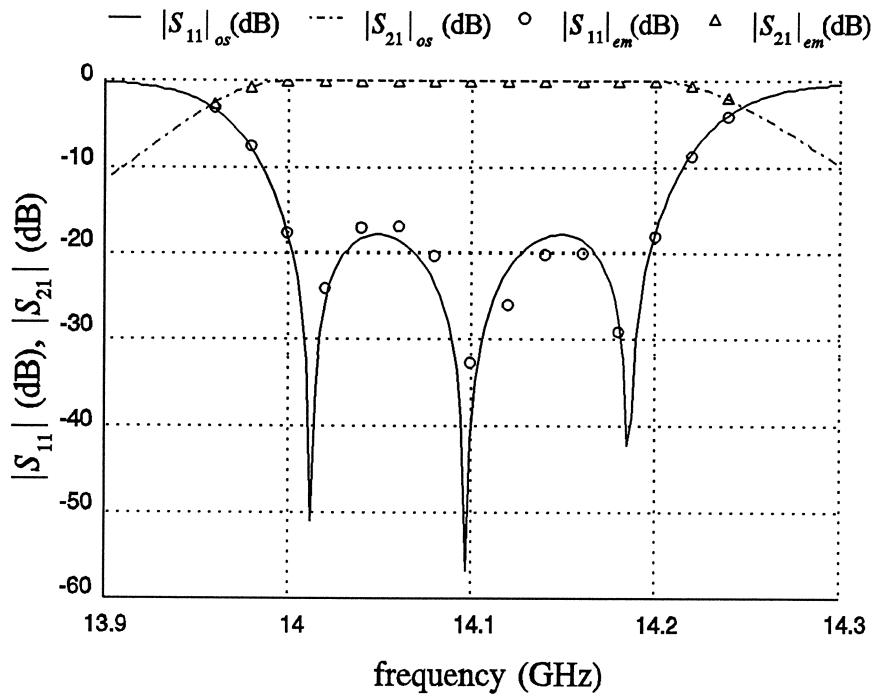

Fig. 5. FEM responses (points) of the H-plane filter at the SM solution compared with optimal X_{os} target responses (curves). The results have been obtained after only four simulations by HFSS.

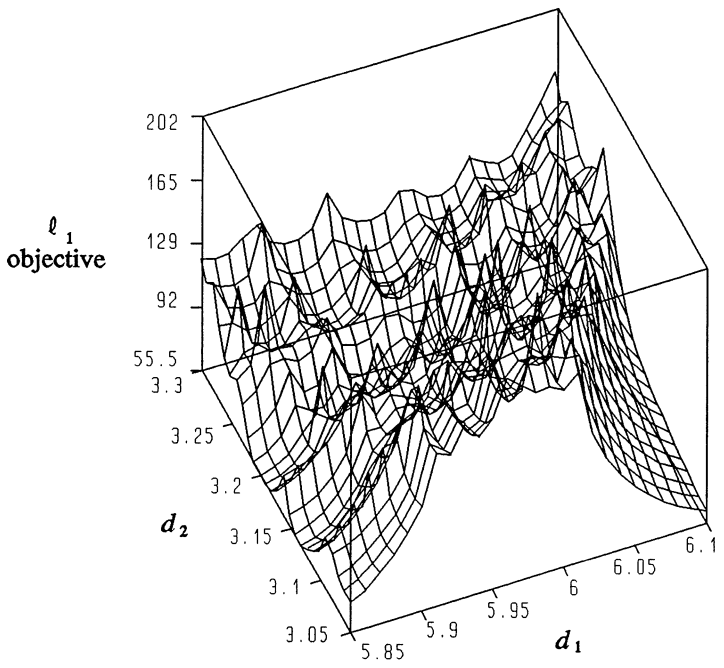

(*a*)

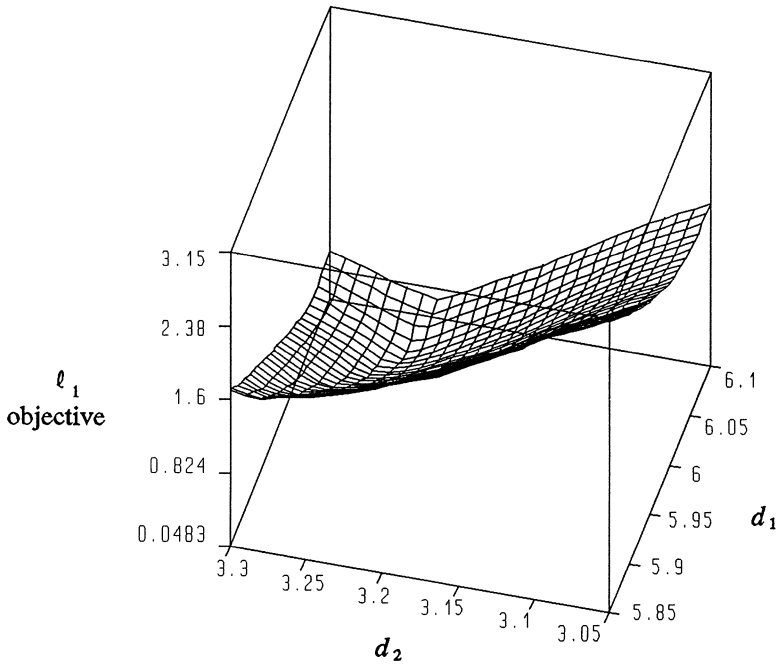

(*b*)

Fig. 6. Variation of the ℓ_1 objective w.r.t. iris openings d_1 and d_2. Other parameters are held fixed at values corresponding to $\boldsymbol{x}_{os}^*$. Individual errors defined in terms of: (*a*) $|S_{11}|$ (dB); (*b*) $|S_{21}|$.

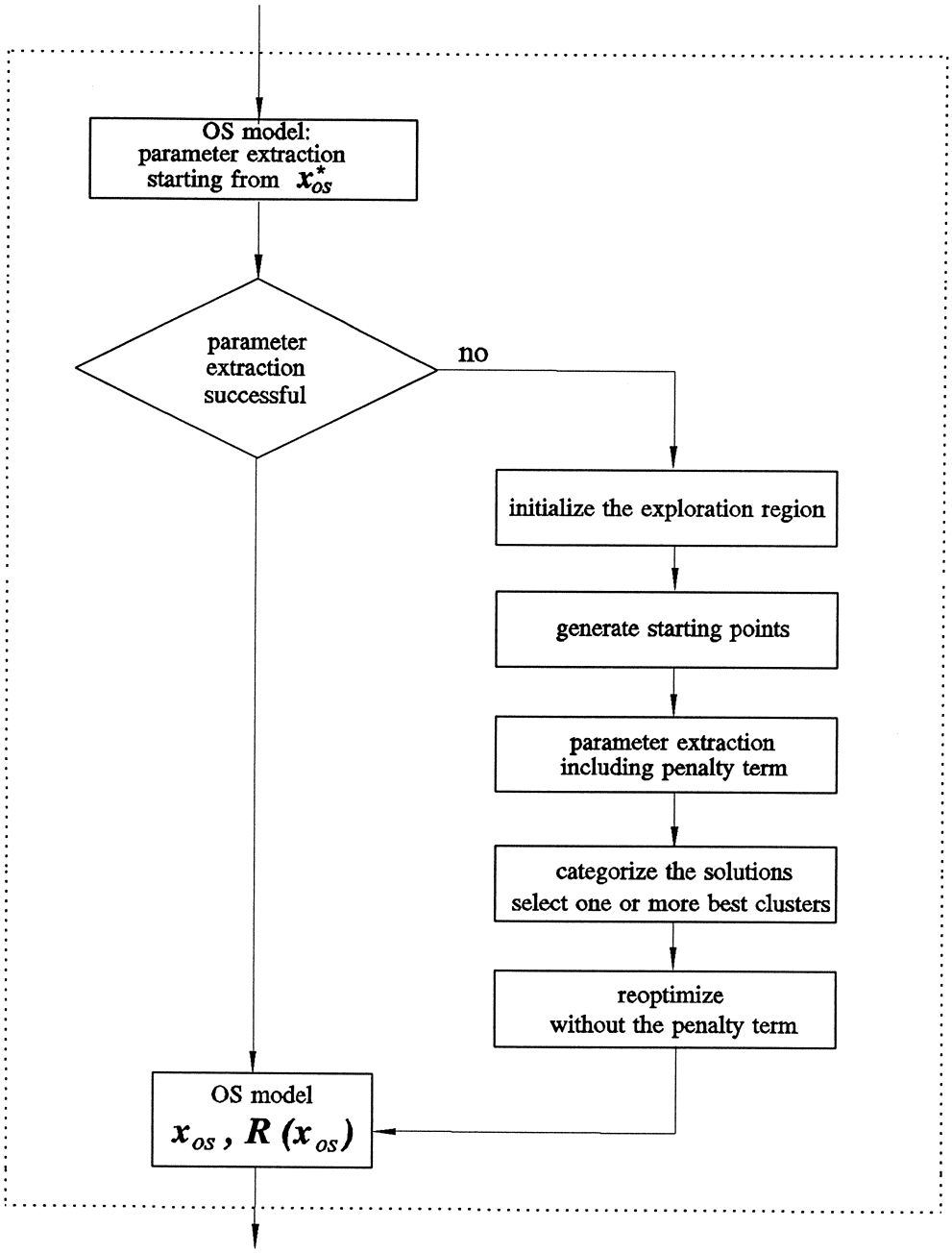

Fig. 7. Flow diagram of the statistical parameter extraction procedure.

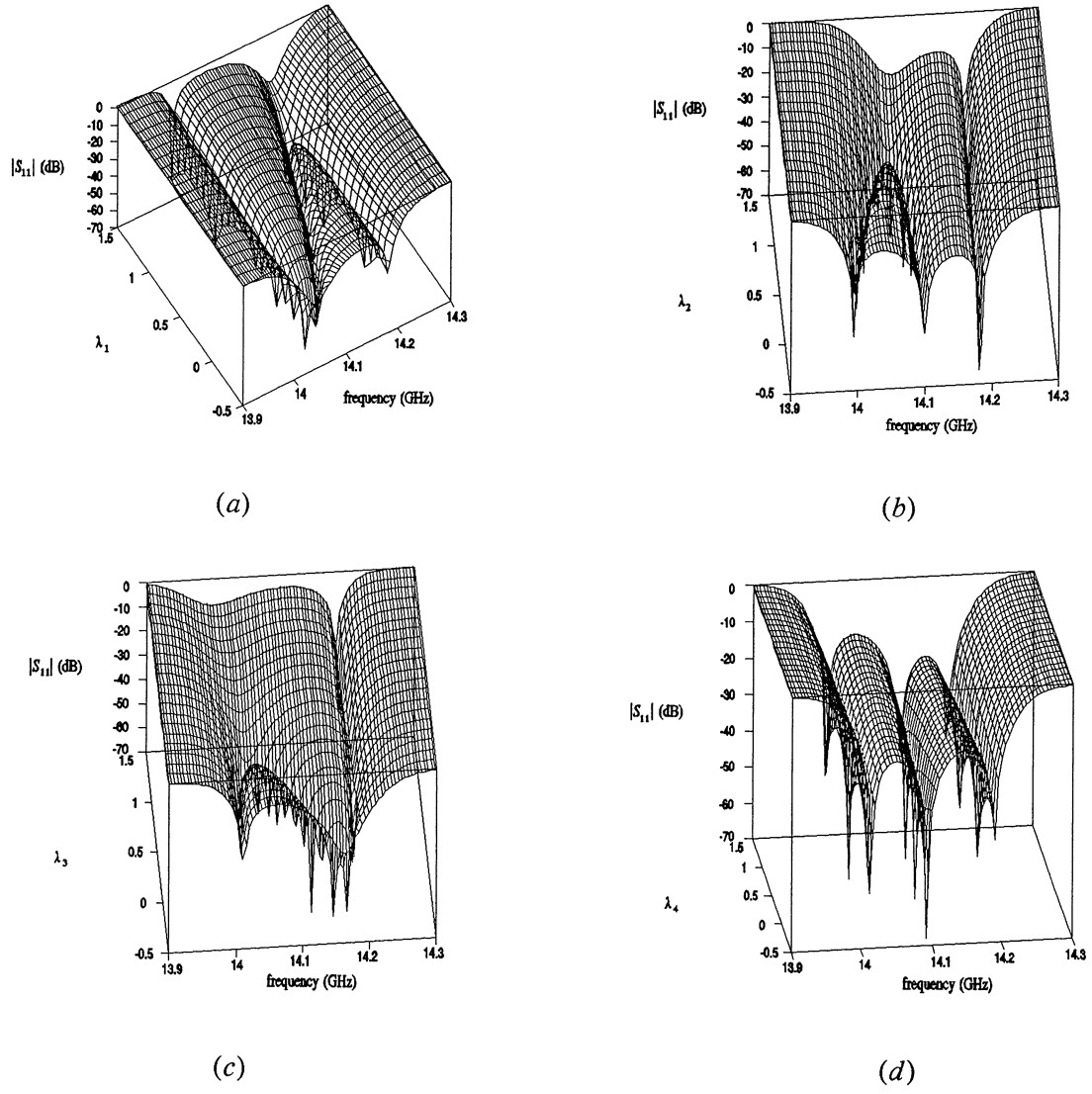

Fig. 8. 3D plots of $|S_{11}|$ in dB vs. frequency and filter parameters: (*a*) opening of the first iris d_1; (*b*) opening of the second iris, d_2; (*c*) length of the first resonator; (*d*) length of the second resonator. The range of parameter changes is defined by the first SM step: λ_i = 0 at x_{os}^* and λ_i = 1 at x_{os}^1.

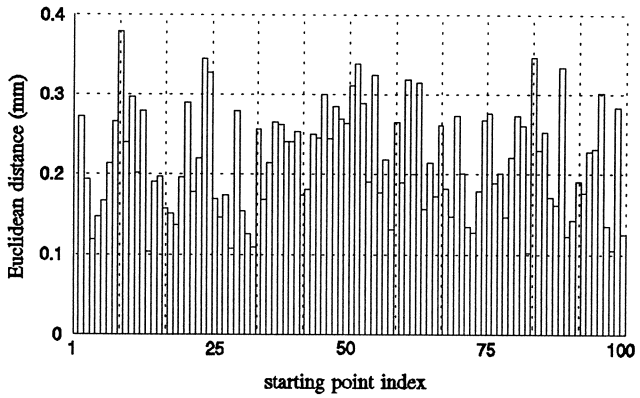

(*a*)

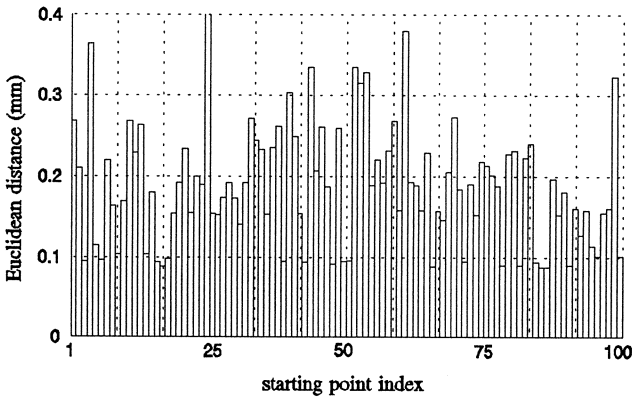

(*b*)

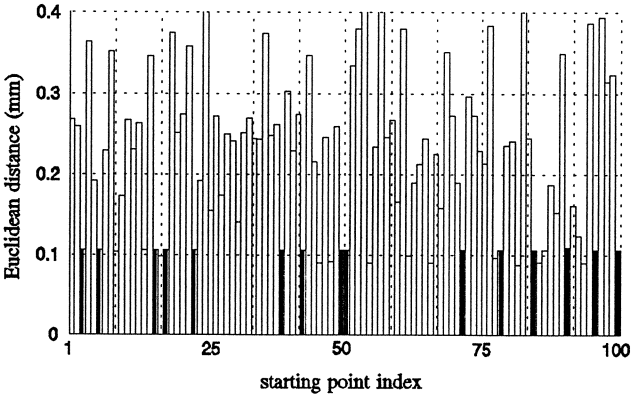

(*c*)

Fig. 9. Euclidean distances measured from x_{os}^{*} to: (*a*) the randomly generated starting points for statistical exploration, (*b*) the converged points after the first stage; (*c*) the converged points after the second stage of statistical parameter extraction. Individual errors defined in terms of $|S_{11}|$ in dB.

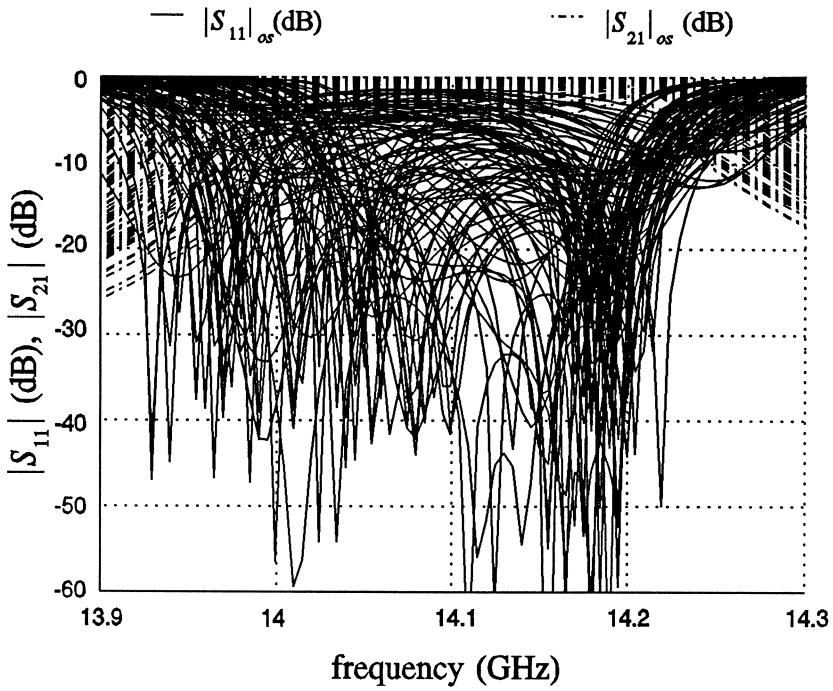

Fig. 10. Statistical parameter extraction: responses at 100 randomly generated starting points.

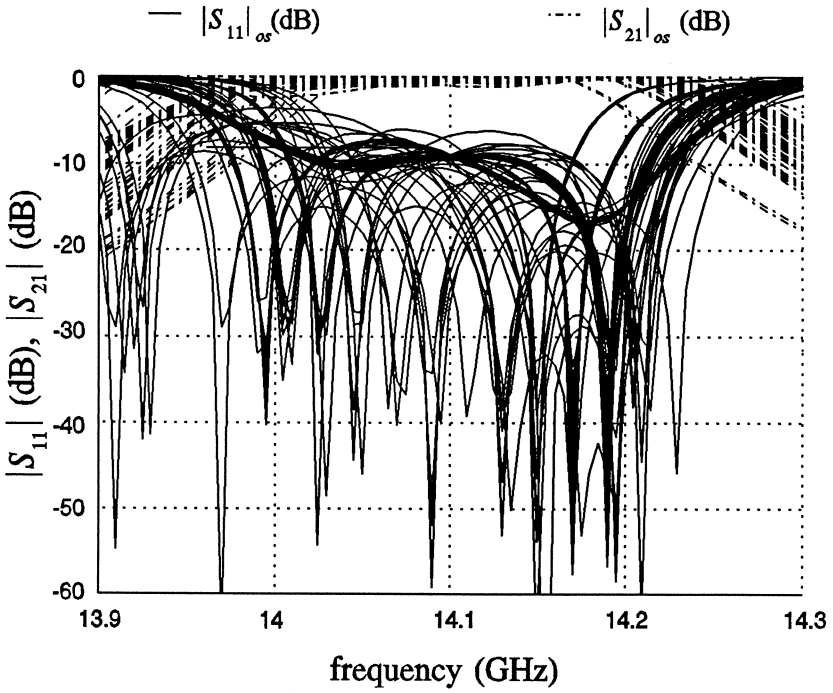

Fig. 11. Statistical parameter extraction: responses at 100 solution points (after two stages).

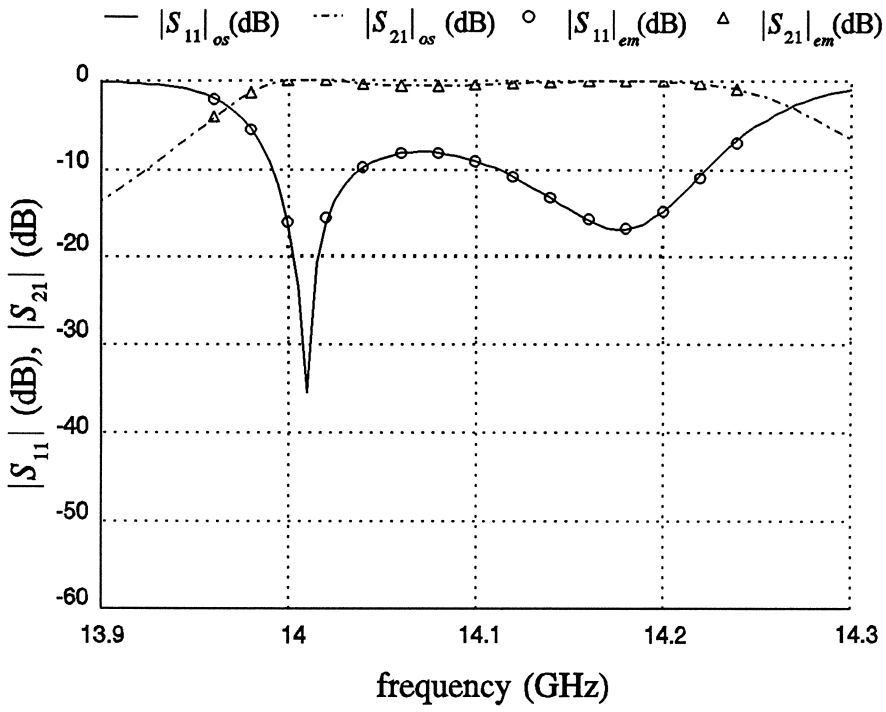

Fig. 12. MM responses corresponding to a cluster of 15 points obtained after statistical parameter extraction. The 15 responses are indistinguishable from each other. The match to the FEM response is very good.

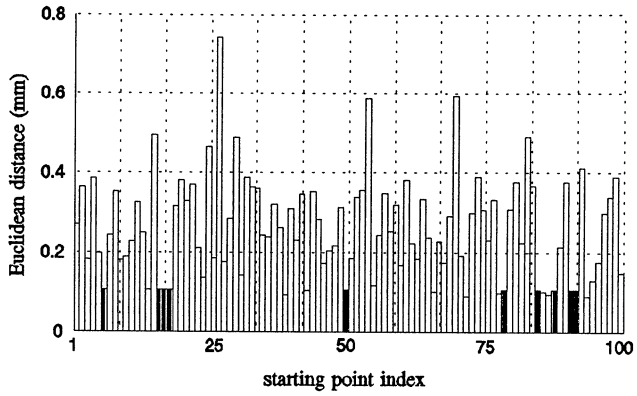

(*a*)

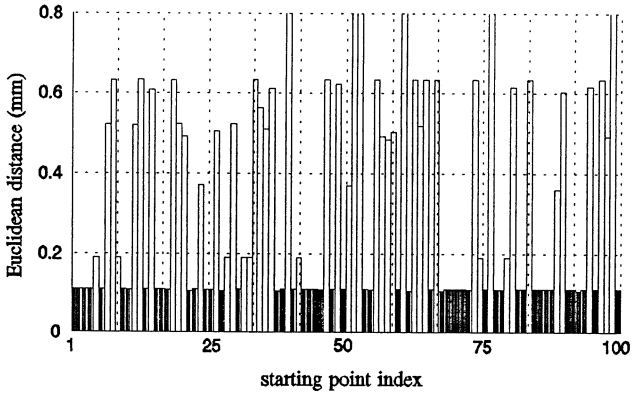

(*b*)

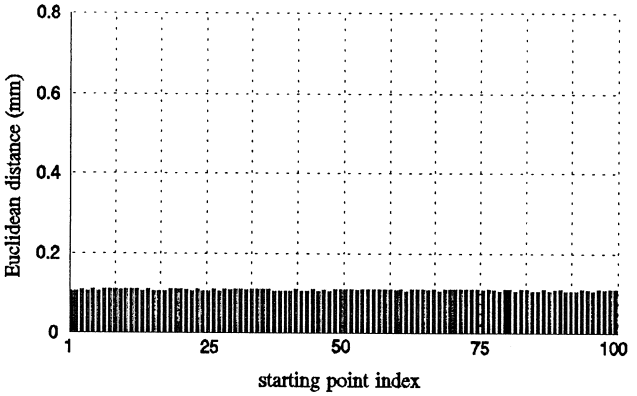

(*c*)

Fig. 13. Euclidean distances measured from $\boldsymbol{x}_{os}^{*}$ to the solution points after the second stage of statistical parameter extraction. (*a*) Errors defined in terms of $|S_{11}|$ in dB, no penalty term used. (*b*) Errors defined in terms of $|S_{21}|$, no penalty term used. (*c*) Errors defined in terms of $|S_{21}|$, the penalty term (4) used.

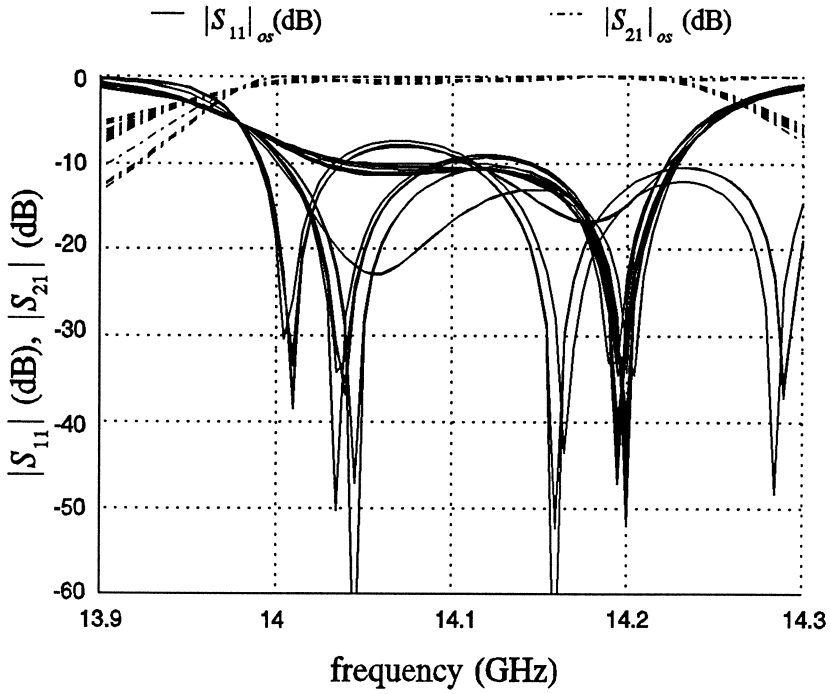

Fig. 14. Statistical parameter extraction: responses at 100 solution points (after two stages) corresponding to Fig. 13(b) when no penalty term is used and individual errors are defined in terms of $|S_{21}|$.

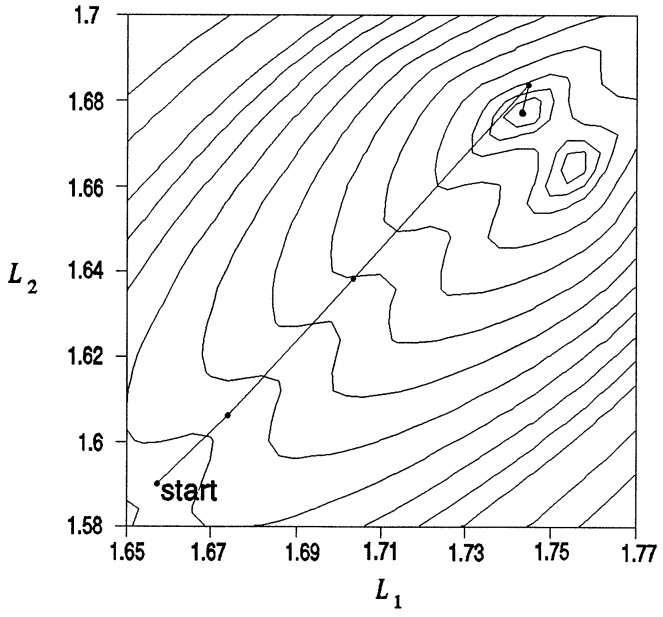

Fig. 15. The ℓ_1 contours of the parameter extraction problem for the two-section waveguide transformer. The symmetry between the variables L_1 and L_2 produces two local minima. Consequently the result of parameter extraction is not unique.

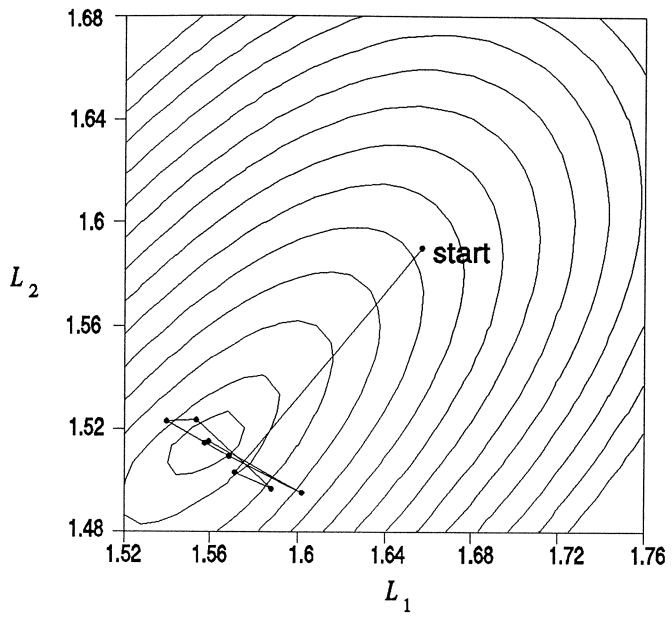

Fig. 16. Trace of the SM steps of the two-section waveguide transformer projected onto the minimax contours in the L_1-L_2 plane. The non-unique parameter extraction results lead to the SM steps oscillating around the solution.

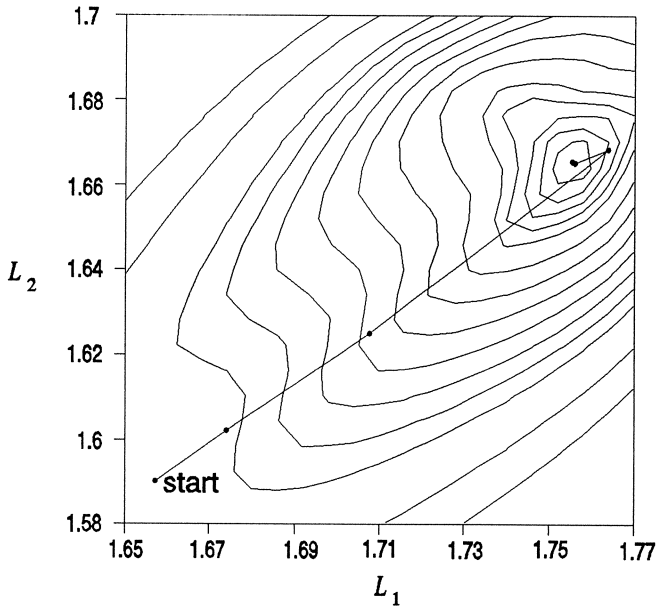

Fig. 17. The ℓ_1 contours of multi-point parameter extraction of the two-section waveguide transformer. The parameter extraction has a unique solution.

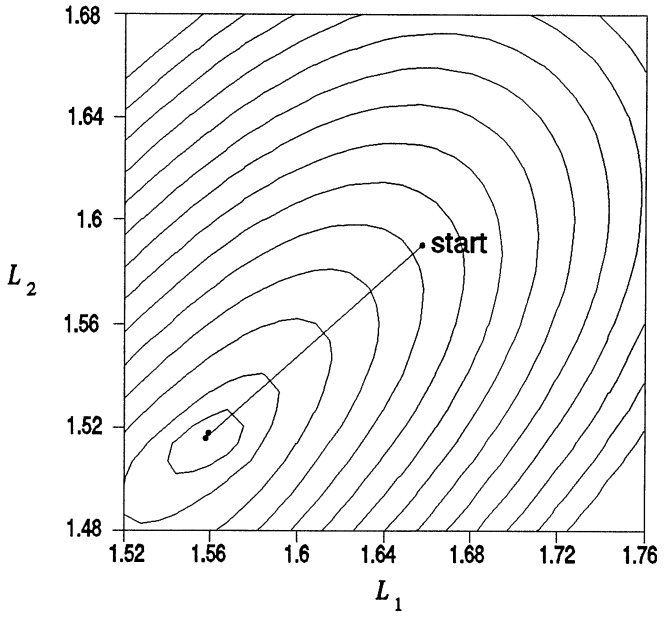

Fig. 18. Trace of the SM optimization with multi-point parameter extraction of the two-section transformer projected onto the minimax contours in the L_1-L_2 plane. The convergence is dramatically improved when compared with Fig. 16.

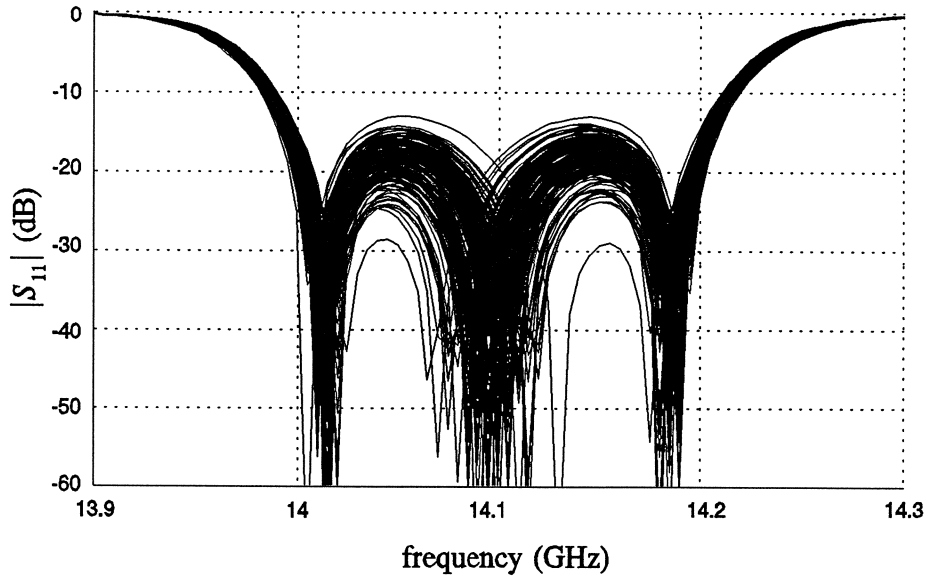

Fig. 19. Monte Carlo analysis of the H-plane filter. The parameter values are randomly generated from a normal distribution with a standard deviation of 0.0333%. The yield, estimated from 200 outcomes, is 88.5%.

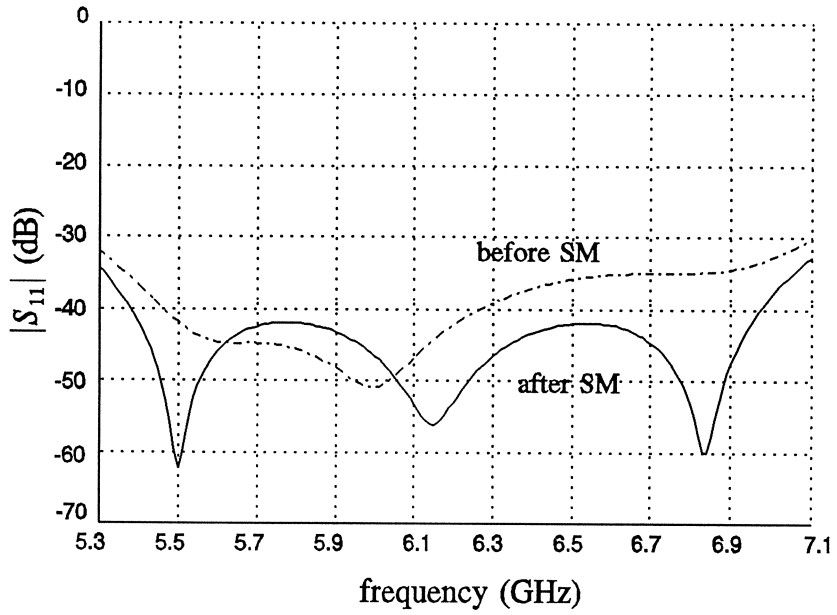

Fig. 20. $|S_{11}|$ (in dB) of a three-section waveguide transformer simulated by RWGMM library before and after two SM iterations. The solution is indistinguishable from the optimal coarse model response.

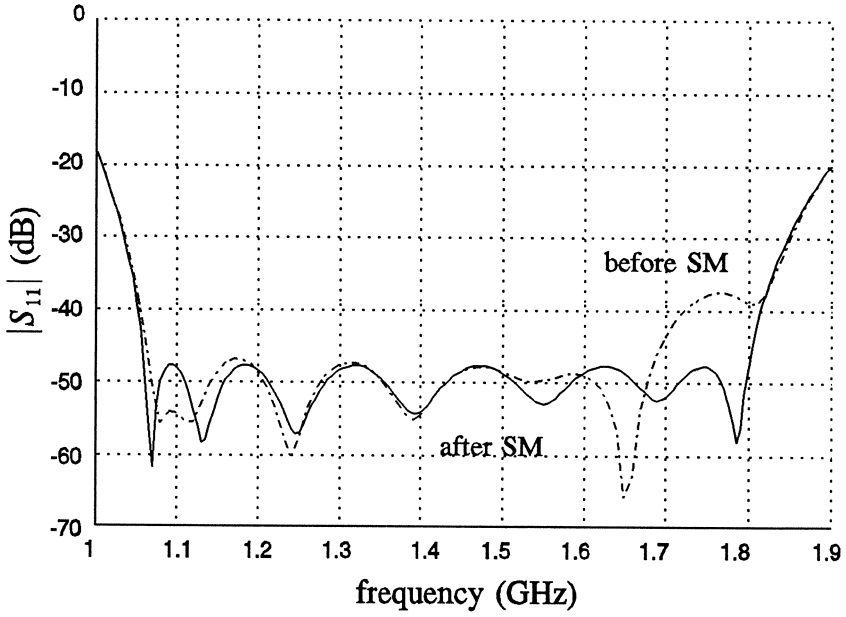

Fig. 21. $|S_{11}|$ (in dB) of a seven-section waveguide transformer simulated by RWGMM library before and after 14 SM iterations. The solution is indistinguishable from the optimal coarse model response.

The Electromagnetic Analysis and Optimization of a Broad Class of Problems Using Companion Models

Anthony M. Pavio

Motorola Communications Semiconductor Products Division
5005 East McDowell Rd., E108
Phoenix, AZ 85008
602-244-3422

OVERVIEW

- METHOD OUTLINE AND ADVANTAGES
- NOTCH FILTER EXAMPLE
- DELAY LINE ANALYSIS AND OPTIMIZATION
- HIGH "Q" FILTER DESIGN
- CONCLUSION

METHOD OUTLINE

- THE CIRCUIT IS ANALYZED USING STANDARD LINEAR/ NONLINEAR SIMULATION TECHNIQUES.
- THE OPTIMIZED CIRCUIT VALUES (COMPANION MODEL) ARE MAPPED TO THE EM SIMULATOR.
- THE CIRCUIT MODEL VALUES ARE THEN ADJUSTED SO THAT THE SIMULATED PERFORMANCE MATCHES THAT OF THE FIRST PASS EM SIMULATION.
- THE CHANGE IN VALUES FROM THE COMPANION CIRCUIT MODEL ARE THEN USED TO UPDATE THE EM SIMULATOR FOR THE NEXT ITERATION STEP.

SIMPLIFIED EXAMPLE

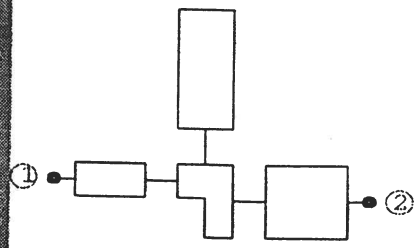

COMPANION MODEL

MAP

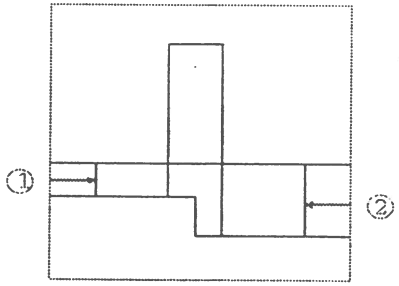

EM

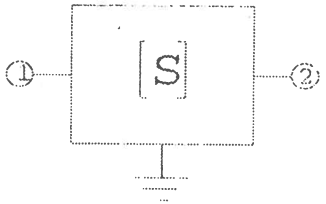

INITIAL SIMULATION

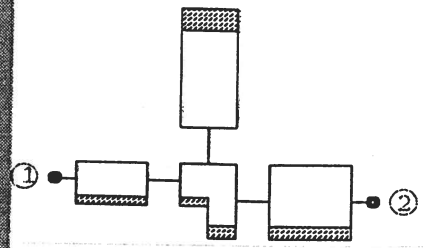

ADJUSTED MODEL
(FIRST FIT)

MAP

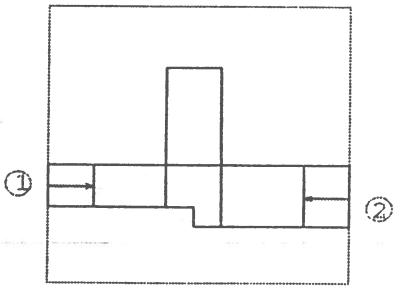

EM

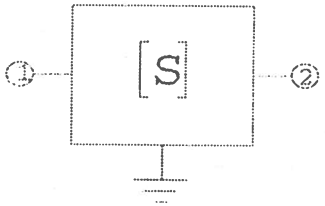

SECOND PASS

COMPANION CIRCUIT MODEL

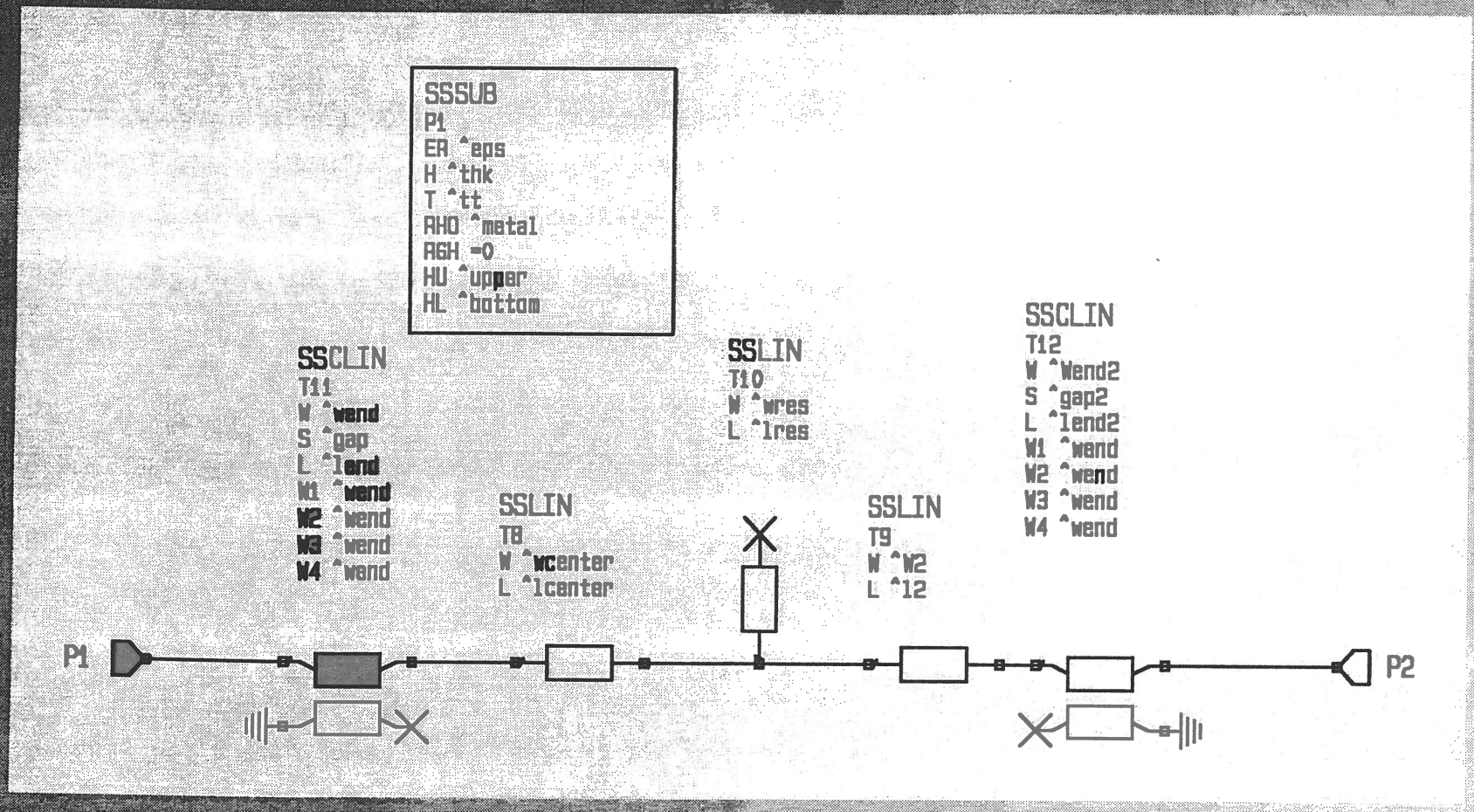

SUSPENDED SUBSTRATE NOTCH FILTER

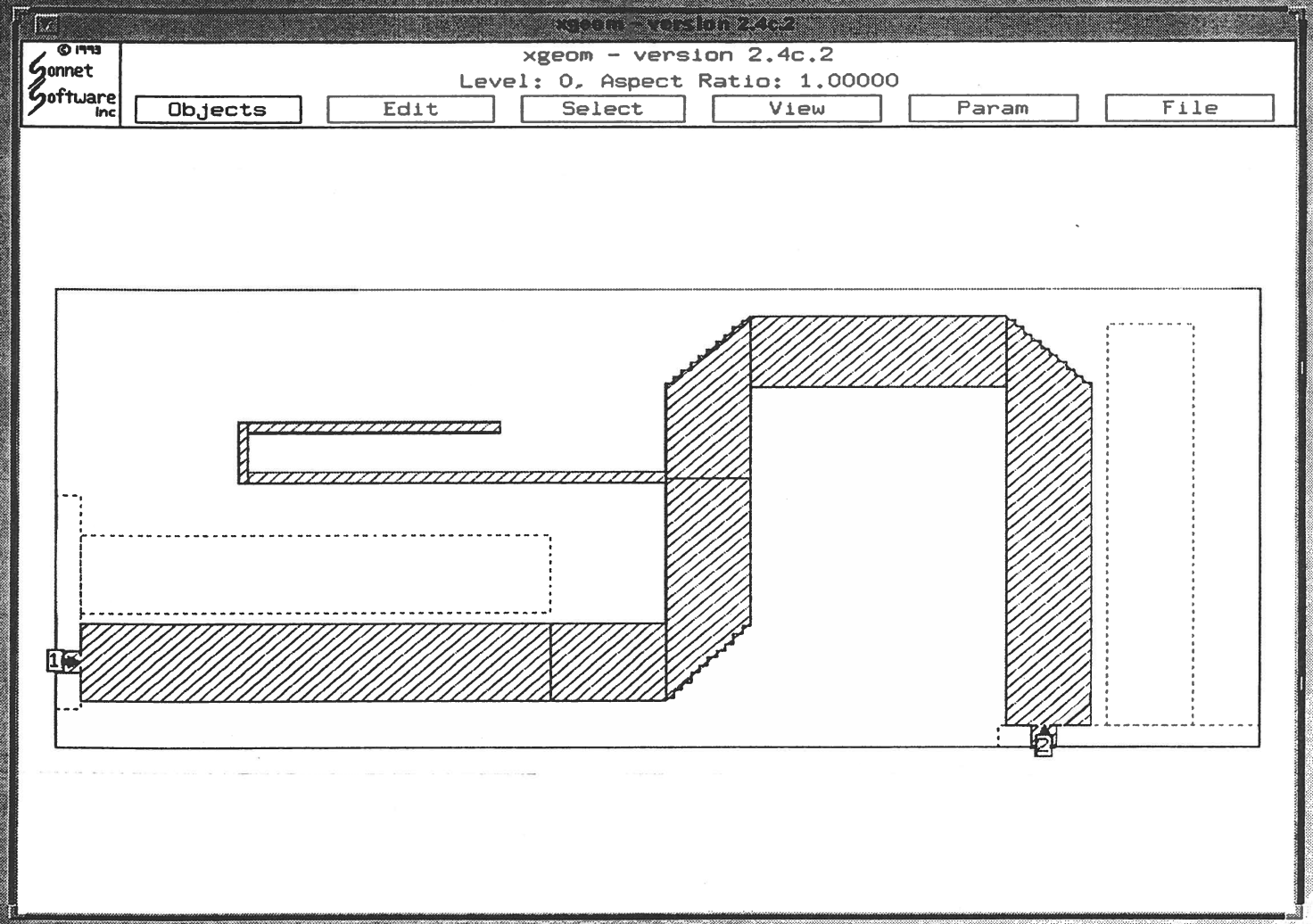

MODEL VERSUS EM SIMULATION FOR NOTCH FILTER

ANALYSIS # 1

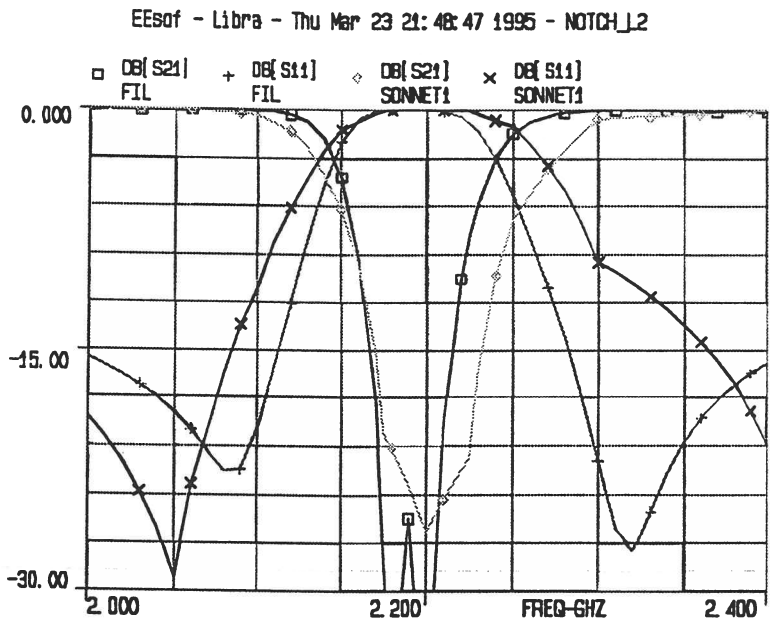

ANALYSIS # 2

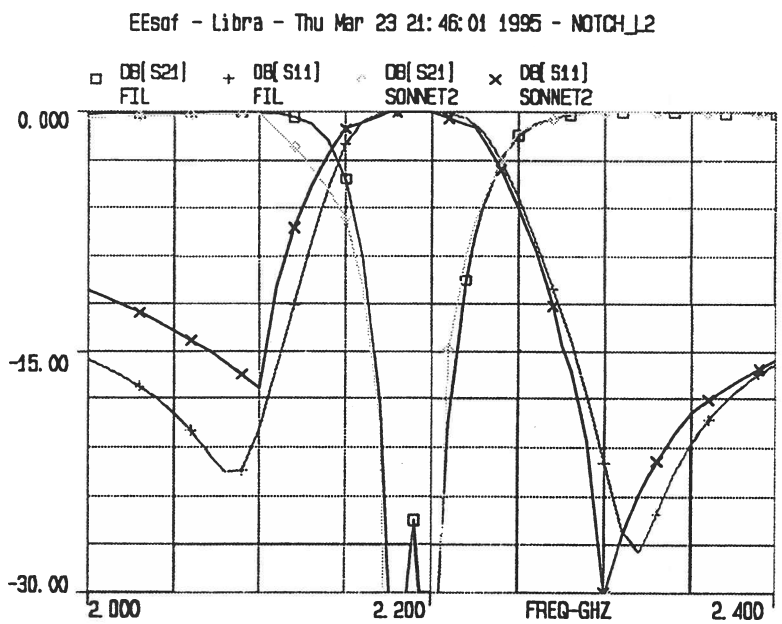

ITERATION MATRIX

	MODEL	FIT # 1	DELTA1	FIT # 2	DELTA2
WEND	220	220	0	220	0
LEND	1185	1160	25	1187	-2
GAP	29	23	6	29	0
WEND2	200	200	0	200	0
LEND2	1200	1192	8	1201	-1
GAP2	38	28	10	38	0
LCENTER	975	1008	-33	979	-4
LRES	1770	1754	16	1770	0
L2	960	957	13	958	2

DELAY LINE - COMPANION MODEL

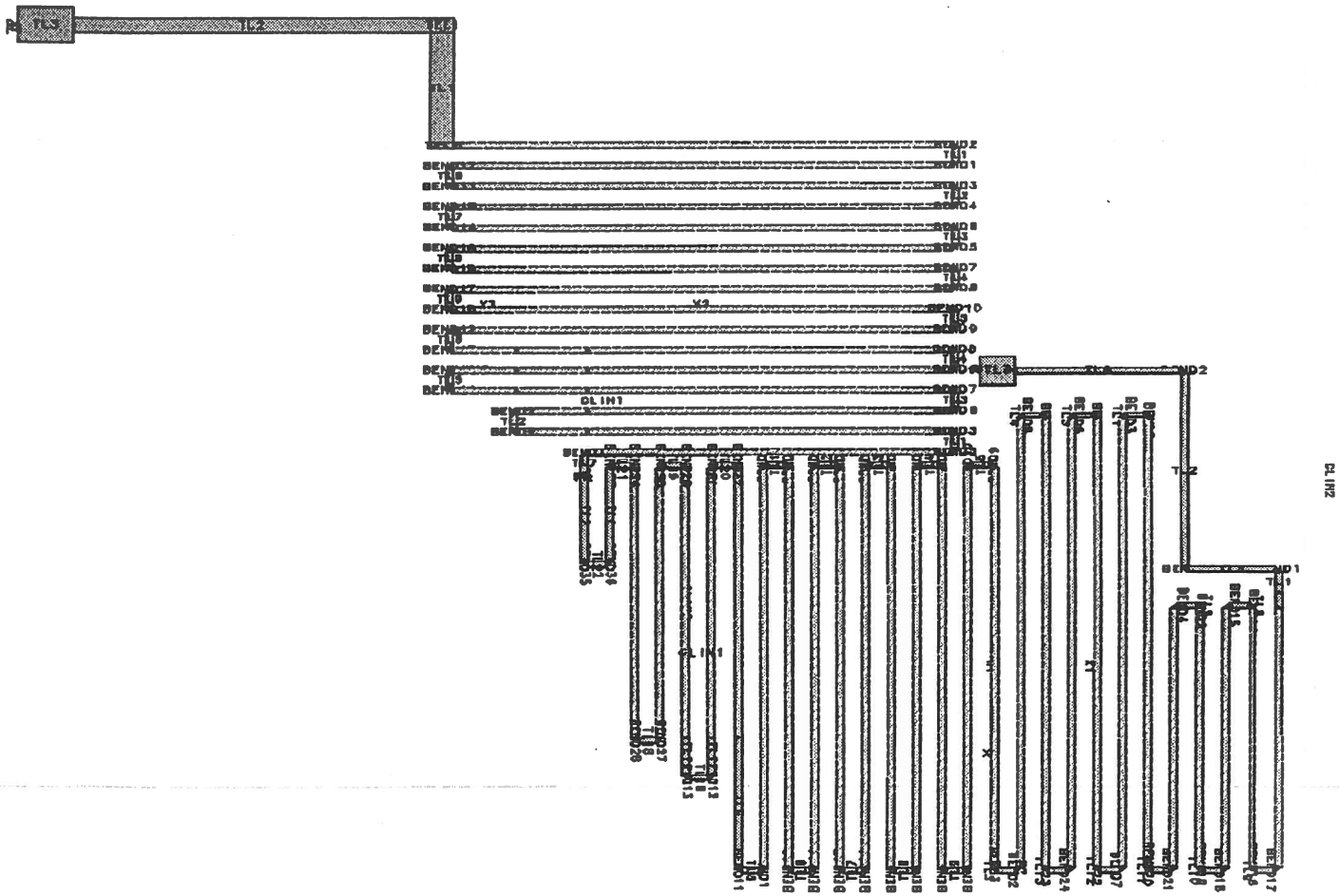

1995 MTTS

STRUCTURES FOR EM ANALYSIS

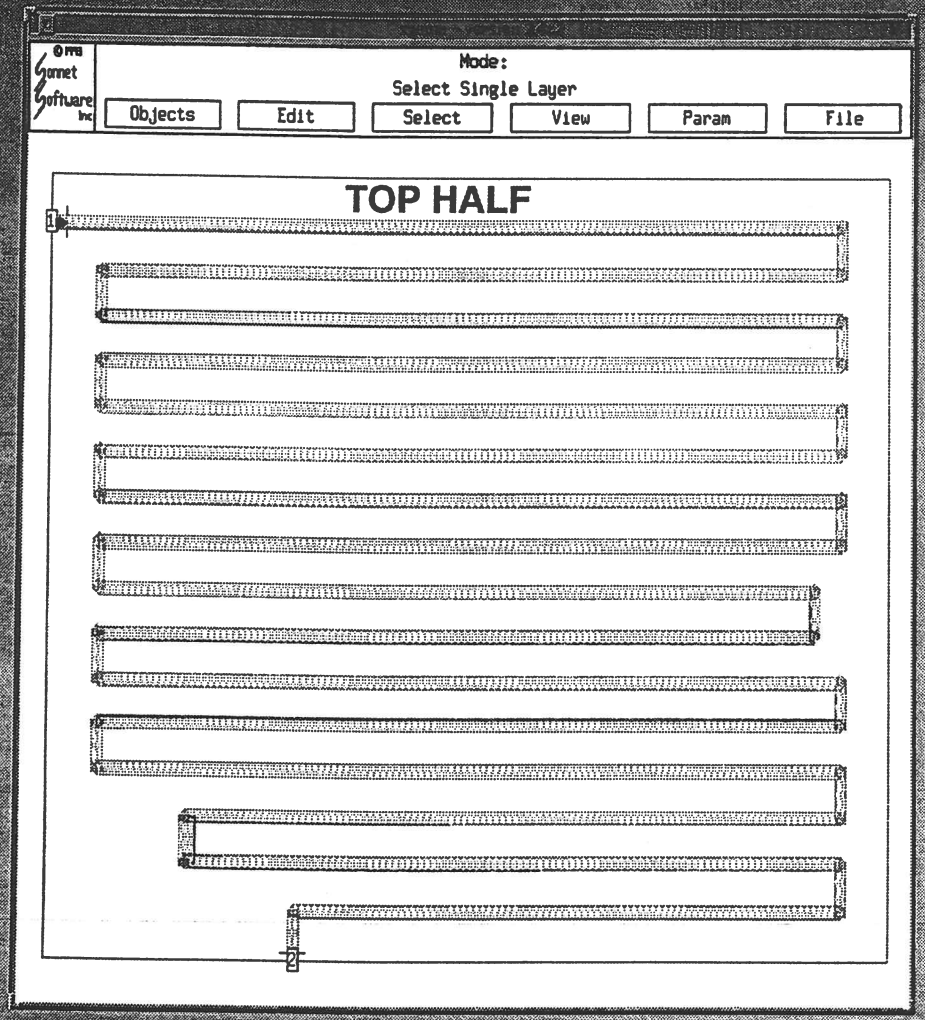

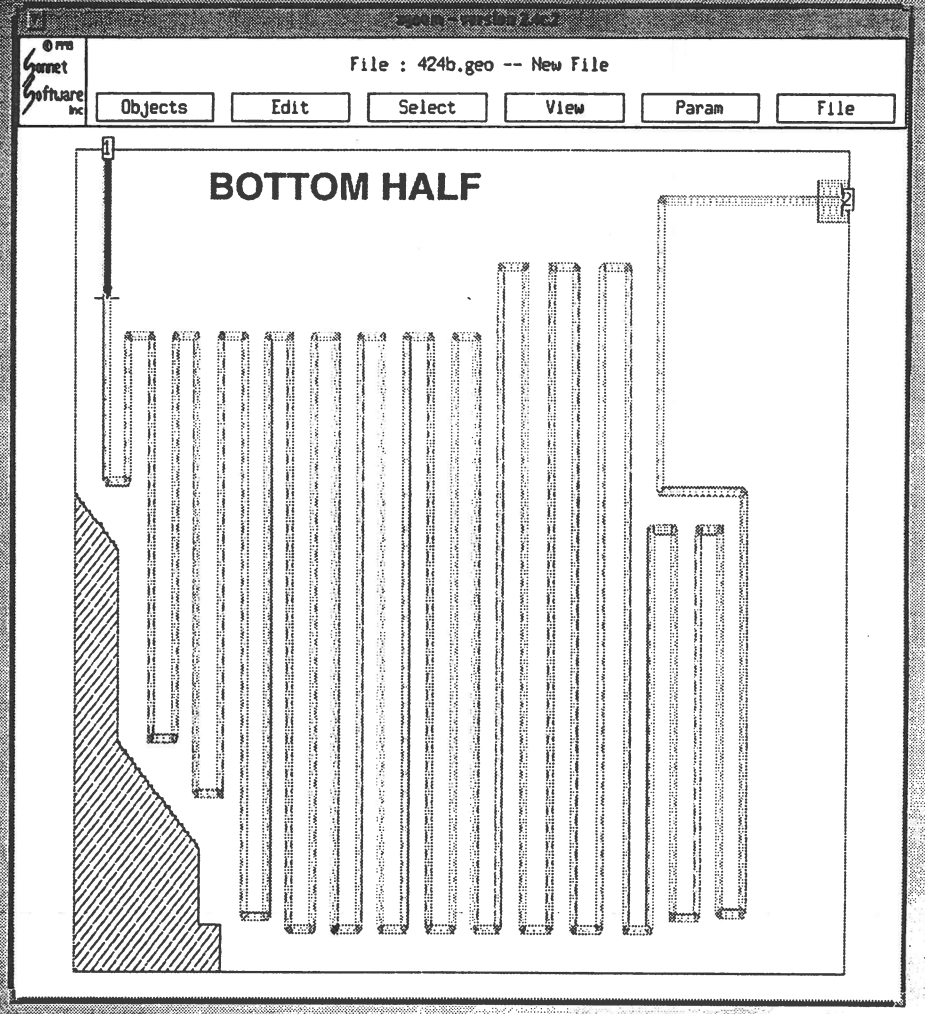

DELAY-LINE PHASE RESPONSE

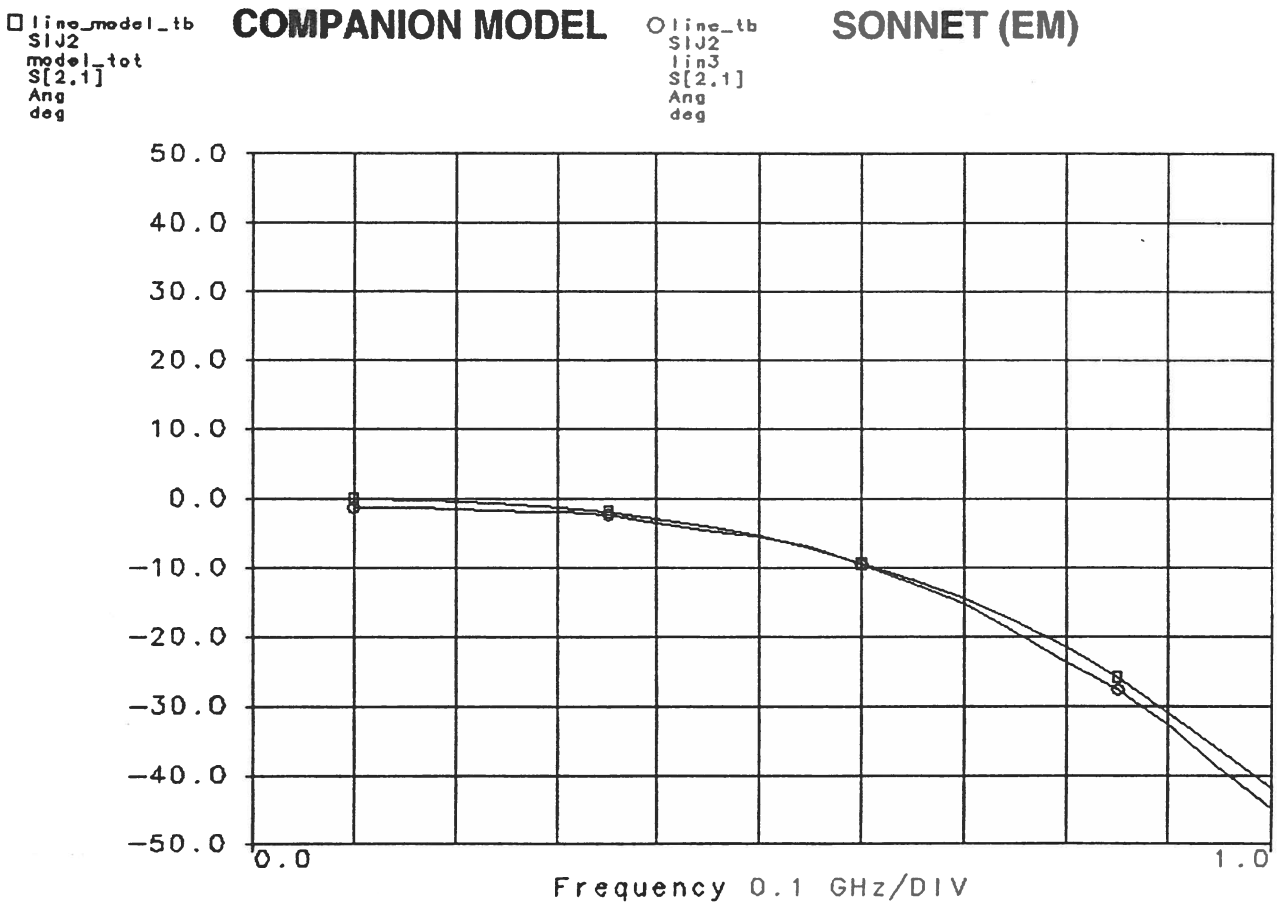

MITER OPTIMIZATION

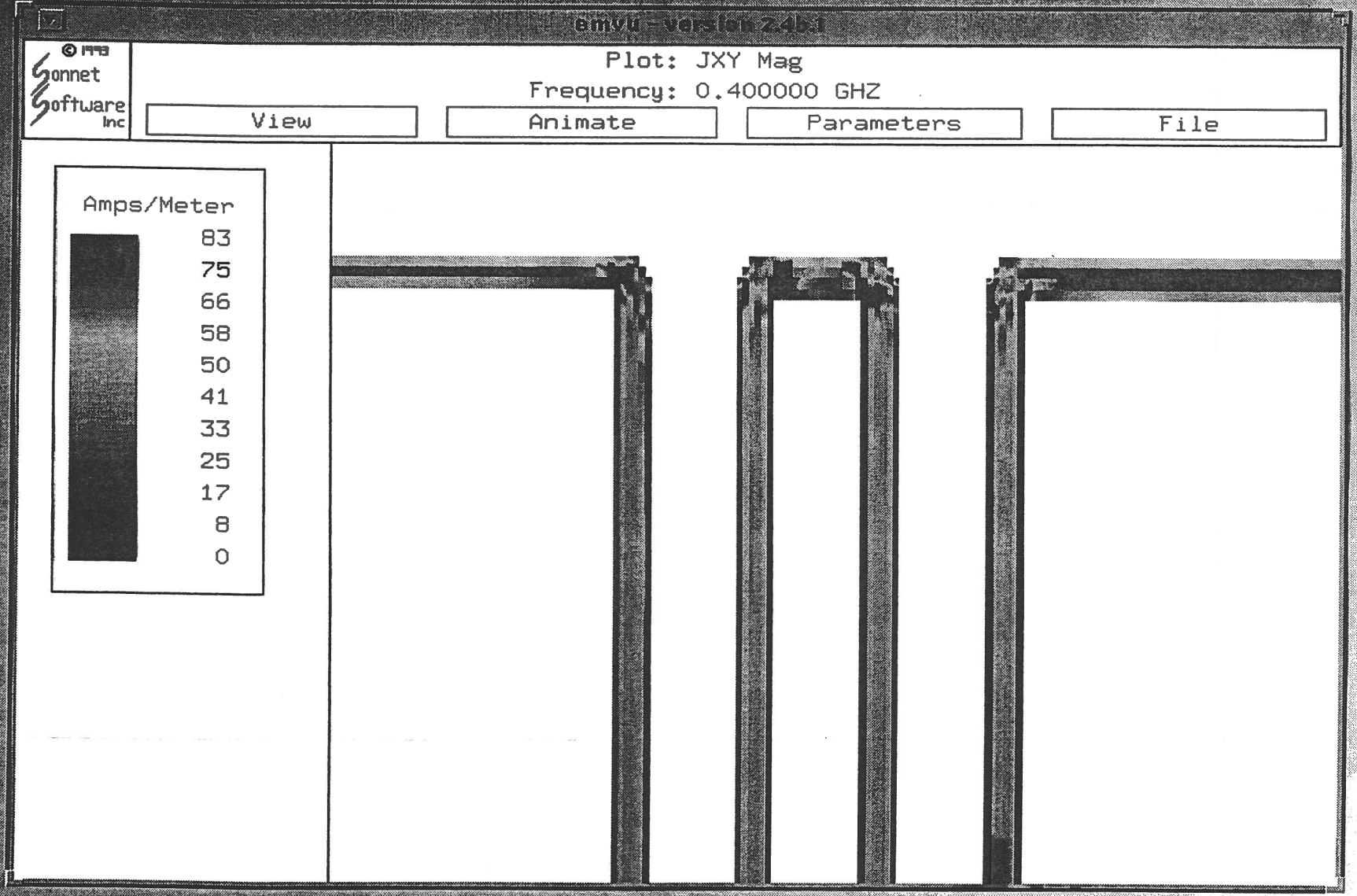

CLASSICAL INTERDIGITAL FILTER ANALYSIS

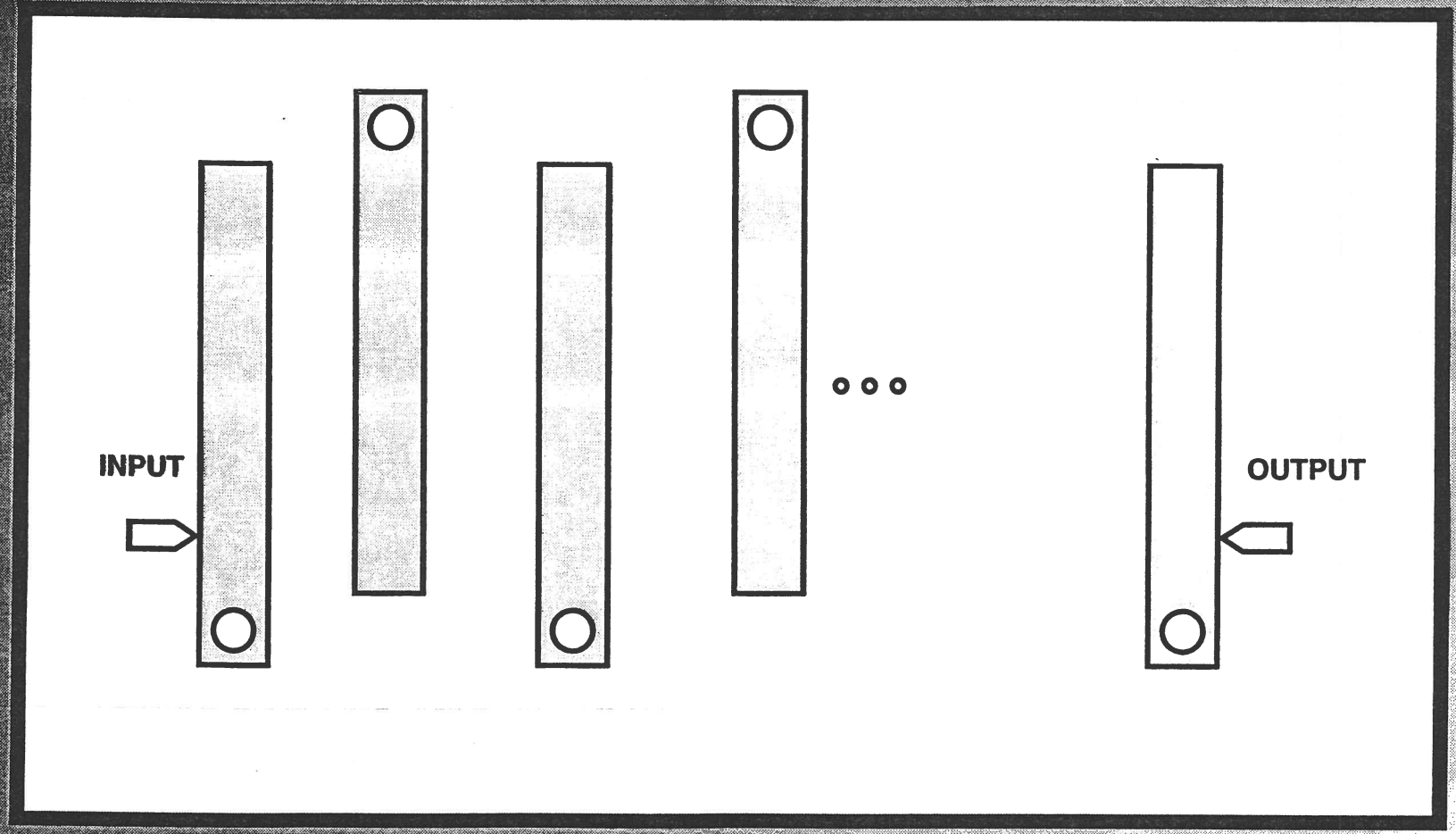

ALTERNATE FILTER ANALYSIS

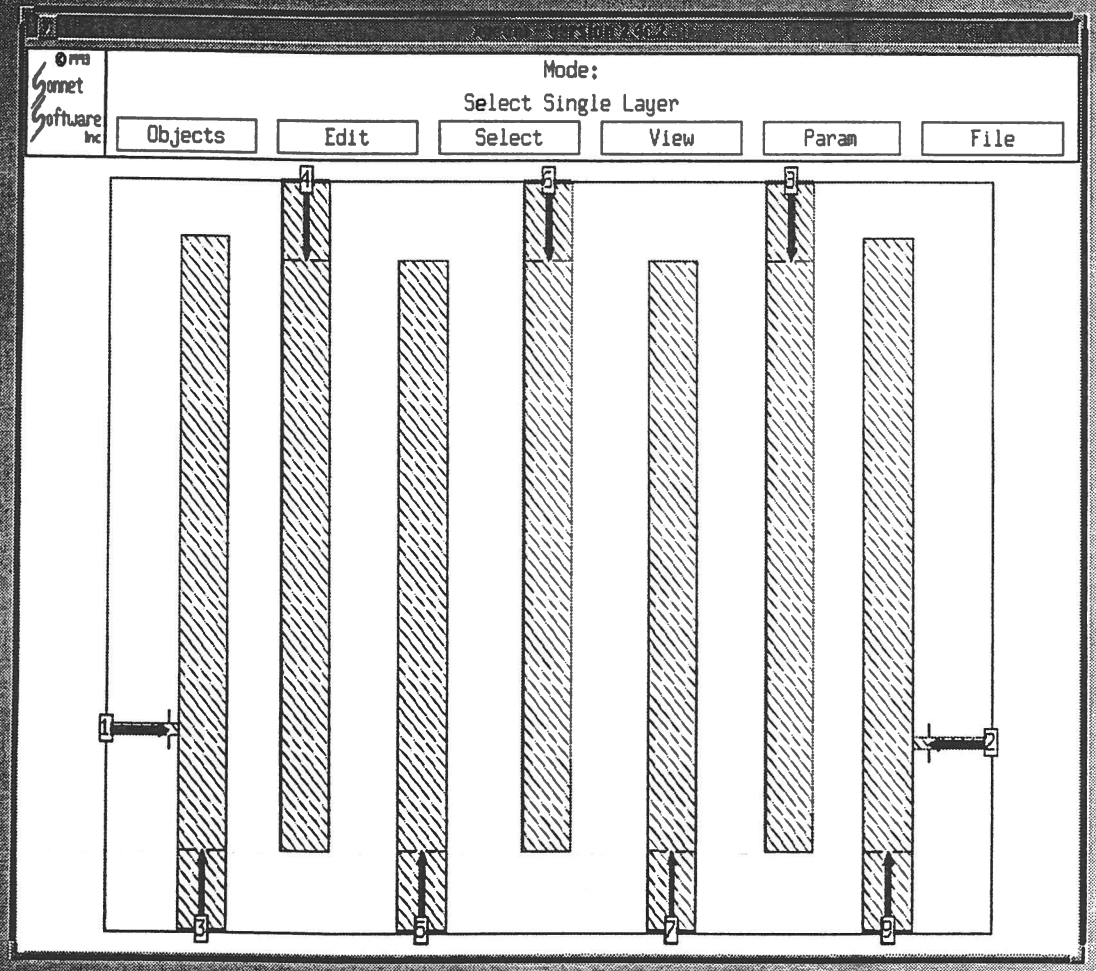

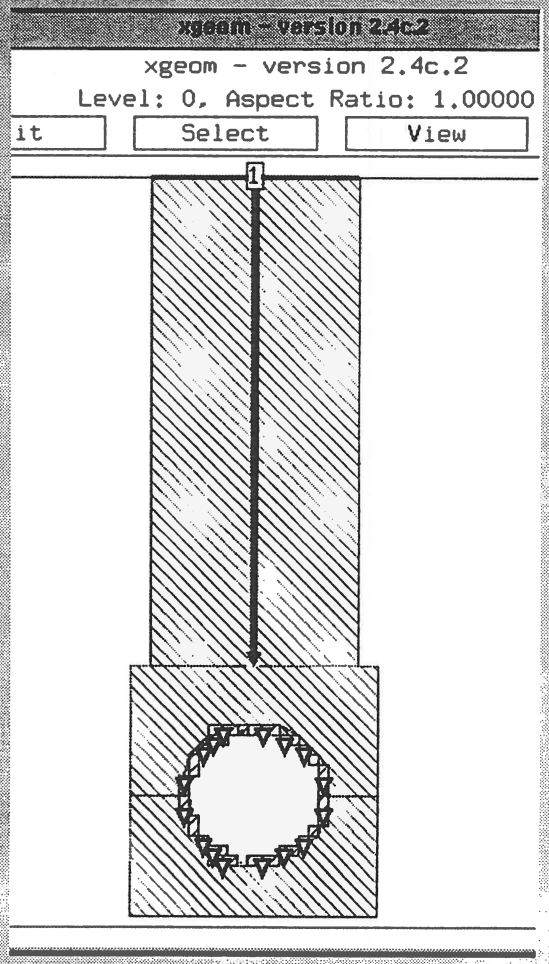

INTERDIGITAL 5 POLE FILTER COMPANION MODEL

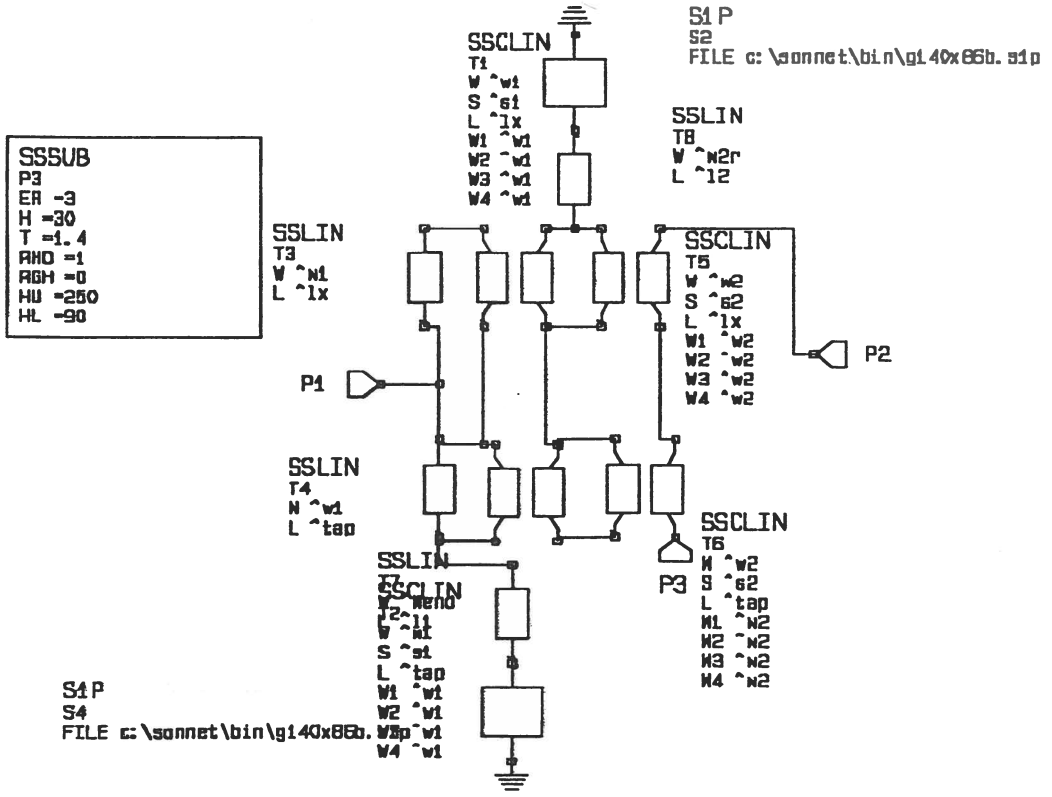

MODEL & EM ANALYSIS of 5 POLE INTERDIGITAL FILTER

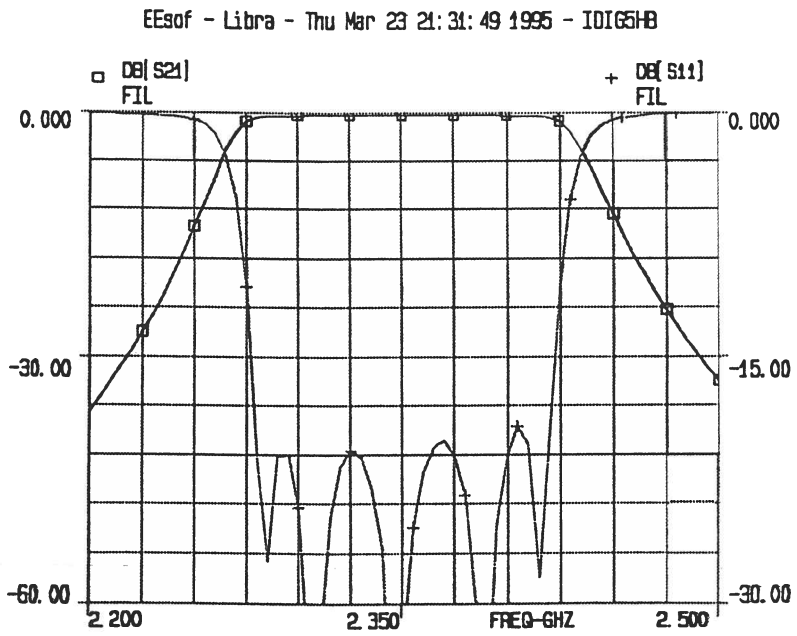

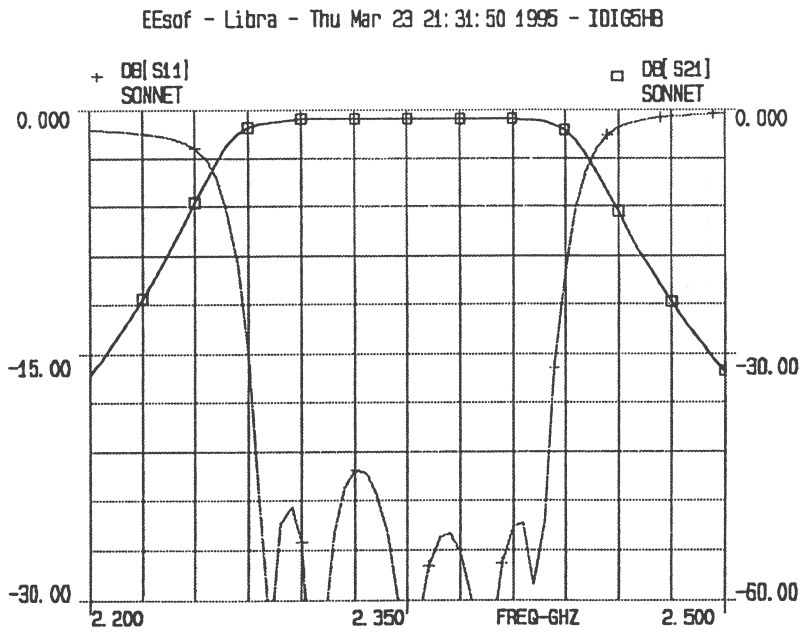

SUMMARY

- METHOD IS EASY TO APPLY USING MANUAL TECHNIQUES.
- SPECIAL STRUCTURES SUCH AS HIGH "Q" FILTERS AND DELAY LINES CAN BE RAPIDLY OPTIMIZED.
- ACTIVE DEVICES CAN BE ADDED TO SIMULATION.
- METHOD CAN BE EASILY AUTOMATED AND EXTENDED FOR ARBITRARY STRUCTURES.
- LARGE CIRCUITS SHOULD BE SEGMENTED AND SOLVED USING MULTIPLE PROCESSORS.